4-2015

Priming for Supereruption: the hot pre-Peach Spring Tuff lavas and Peach Spring Tuff magmatic enclaves, Black Mountains, Arizona

Megan E. Flansburg
College of William and Mary

Priming for Supereruption: the hot pre-Peach Spring Tuff lavas and Peach Spring Tuff magmatic enclaves, Black Mountains, Arizona

A thesis submitted in partial fulfillment
of the requirements for the degree of Bachelor of Science in Geology
from The College of William and Mary in Virginia

by

Megan E. Flansburg

Accepted for High Honors

Dr. Christopher M. Bailey, Department Chair

Dr. Brent E. Owens

Dr. Douglass A. DeBerry

Williamsburg, Virginia
April 28, 2015

Table of Contents

List of Figures....3

List of Tables……....5

Abstract....6

Introduction....7

Geologic Setting and Past Research....15
- *The Peach Spring Tuff*....15
- *The Source Caldera and Basin & Range Extension*....17
- *Pre-Peach Spring Tuff Volcanic Activity*....19
- *Post-Peach Spring Tuff Volcanic Activity*....20
- *Magma Mixing and Eruption Triggers*....20

Methods....26

Results....32
- *Field Observations—Stratigraphy and Hand Sample Petrography*....32
- *Petrography*....44
- *Whole Rock Geochemistry*....55
- *Full Elemental Analyses with ICP-MS*....63
- *Scanning Electron Microscope Analyses*....64
- *Temperature Modeling*....68

Discussion....84
- *Interpretations*....87

Future Work....89

Conclusions....90

Acknowledgements....91

References Cited....92

Appendices....97
- A. *Sample Location and Hand Sample Petrography*....97
- B. *Whole Rock Geochemistry*....99
- C. *Temperature Modeling*....100
- D. *Full Elemental Analyses*....102
- E. *Scanning Electron Microscope Analyses*....103

List of Figures

Figure 1. Volcanic Explosivity Index....8

Figure 2. Distribution of the Peach Spring Tuff....10

Figure 3. Volcanic stratigraphy (% phenocrysts)....12

Figure 4. Volcanic stratigraphy....12

Figure 5. Geology around Silver Creek caldera....18

Figure 6. Crenulate margins on a magmatic enclave....23

Figure 7. Satellite imagery of the Black Mountains....27

Figure 8. Flux melter at MTSU....28

Figure 9. Cartoon of pyroxene and plagioclase zoning....30

Figure 10a. Shaded relief of the study area....35

Figure 10b. Generalized geology of the study area....35

Figure 11a. Field photo: MBF-1....36

Figure 11b. Field photos: SPF-1A, SPF-1B, SPF-2....37

Figure 11c. Field photo: WSWF-1 and PST....38

Figure 11d. Field photo: McHeffy Butte....38

Figure 12. Geologic map with sample locations....39

Figure 13a. Volcanic stratigraphy: Southern Black Mountains....40

Figure 13b. Volcanic stratigraphy: PST unconformity....40

Figure 14a. Photos: magmatic enclaves at Warm Springs West....42

Figure 14b. Photos: magmatic enclaves at Kingman....43

Figure 15a-15j. Thin section micrographs: Esperanza Trachyte and mafic lavas....46-50

Figure 16a-16d. Thin section micrographs: magmatic enclaves................................52-54

Figure 17. TAS diagram with samples...55

Figure 18a. Major element plots: CaO, K_2O, P_2O_5...58

Figure 18b. Major element plots: Fe_2O_3, MgO, Mg #..59

Figure 18c. Major element plots: Al2O3, Na2O, TiO2…………………………………...60

Figure 19. Minor element plots: Zr, Sr, Ba, Y, Nb, Rb..62

Figure 20. Rare earth elements plot...63

Figure 21a-21d. Scanning electron microscope images...65-67

Figure 22. Excel-MELTS temperatures at varying H_2O %...70

Figure 23a-23c. Excel-MELTS outputs at 1% H2O...71-73

Figure 24a-24c. Excel-MELTS outputs at 2% H2O...74-76

Figure 25a-25c. Excel-MELTS outputs at 3% H2O...77-79

Figure 26. Excel-MELTS temperatures with trend-lines...80

Figure 27. Apatite-saturation and zircon-saturation...82

Figure 28. Apatite-saturation, zircon-saturation, and Excel-MELTS temperatures……83

List of Tables

Table 1. Whole rock geochemistry: mafic lavas, major elements..................................56

Table 2. Whole rock geochemistry: magmatic enclaves, major elements.......................56

Table 3. Whole rock geochemistry: mafic lavas, minor elements..................................61

Table 4. Whole rock geochemistry: magmatic enclaves, minor elements.......................61

Table 5. Excel-MELTS temperatures: mafic lavas..69

Table 6. Excel-MELTS temperatures: magmatic enclaves...69

Abstract

Supereruptions are some of the most cataclysmic events on Earth, ejecting greater than 450 km^3 of material during eruption. The 18.8 Ma Peach Spring Tuff (PST) erupted in what is now the southern Black Mountains, Arizona, with outflow covering an area greater than 35,000 km^2. The volcanic deposits erupted prior to PST supereruption provide important insights on pre-supereruption magmatic conditions in the region. The pre-PST volcanic sequence consists of a ~1 km thick suite of trachyte lavas and a relatively thin sequence of more mafic lavas. We sampled pre-PST mafic lavas, one trachyte lava, and magmatic enclaves within the PST. Bulk analyses of samples were obtained with XRF, full elemental analyses determined through ICP-MS, and phenocryst compositions determined by SEM. Magmatic temperatures were estimated with Excel-MELTS and mineral-saturation thermometry. An atypically hot (~1025°C) aphyric lava, last of the trachyte sequence, contrasts with the rest of the sequence near 850°C (Rice et al., 2014), and is followed by the eruption of mafic lavas. Mafic lavas range from trachy-basalts to trachy-andesites (5-15% pheno.) and estimated temperatures range from 980-1095°C. Magmatic enclaves within the PST are basaltic trachy-andesite to trachy-andesite (5-20% pheno.), and are similar geochemically to the mafic lavas. Estimated temperatures of enclave magmas range from 1000-1070°C, similar to the mafic lavas and the only definitive enclave identified previously (Pamukcu et al., 2013). Full elemental analyses of three enclaves and two lavas further imply relation between the two sample types. The hot trachyte flow, followed by mafic lavas and related enclaves within the PST, indicate heat input into the Black Mountains magmatic system preceding PST supereruption and are possible evidence of the eruption trigger.

Introduction

Supereruptions are some of the most dramatic events that occur on Earth: they have both the power to change climate and drive biotic extinction events. Supereruptions are eruptions that eject greater than 400 km^3 dense rock equivalent, or DRE, and greater than 1000 km^3 tephra volume (USGS, 2012; Wark and Miller, 2008). Four hundred cubic kilometers of DRE is approximately equivalent to the volume of magma within the chamber that generates the volcano and registers as a magnitude 8 eruption on the Volcanic Explosivity Index (Figure 1), the highest magnitude on the scale. By comparison, the 1980 eruption of Mt. St. Helens was a magnitude 5 and ejected only 1 km^3 of material (Wark and Miller, 2008), while still disrupting airline traffic and devastating a large area from the lateral blast of the eruption, resulting in over 50 deaths. The study of supereruptions, their products, and volcanic deposits representing activity before and after the event, can reveal how large-scale magmatic systems work. In particular, volcanic material from before a supereruption can help to identify possible eruption trigger mechanisms and their comparability to smaller-scale volcanic eruptions.

In the past few decades, geologists have gained a better understanding of eruption trigger mechanisms, both for supereruptions and their smaller counterparts (see Sparks and Wilson, 1977; Gregg et al., 2012; Pamukcu et al., 2013). One subject area of recent focus is that of mafic magma injection. Mafic magmas derived from the mantle are an important source of heat for magmatic systems as lower silica magmas correlate with hotter temperatures. The input of a mafic magma into an existing felsic one can lead to an increase in pressure, causing fractures in the overlying roof and triggering a maximum-caldera forming eruption (Sparks and Wilson, 1977; Gregg et al., 2012). This process is described in detail below in **Geologic Setting and Past Research:** *Mafic mingling and eruption triggers*.

VOLCANIC EXPLOSIVITY INDEX (VEI)

VEI	Plume height (km)	Ejected volume (km^3)	Frequency on Earth	Example
0	<0.1	$>\sim 10^{-6}$	daily	Kilauea, Hawai'i
1	0.1–1	$>\sim 10^{-5}$	daily	Stromboli, Italy
2	1–5	$>\sim 10^{-3}$	weekly	Galeras, Colombia, 1993
3	3–15	$>\sim 10^{-2}$	yearly	Nevado del Ruiz, Colombia, 1985
4	10–25	$>\sim 10^{-1}$	~every 10 y	Soufrière Hills, West Indies, 1995
5	>25	>~1	~every 50 y	Mount St. Helens, USA, 1980
6	>25	>~10	~every 100 y	Pinatubo, Philippines, 1991
7	>25	>~100	~every 1000 y	Tambora, Indonesia, 1815
8	**>25**	**>~1000**	**~every 10,000–100,000 y**	***Supereruptions:* Toba, 74 ka**

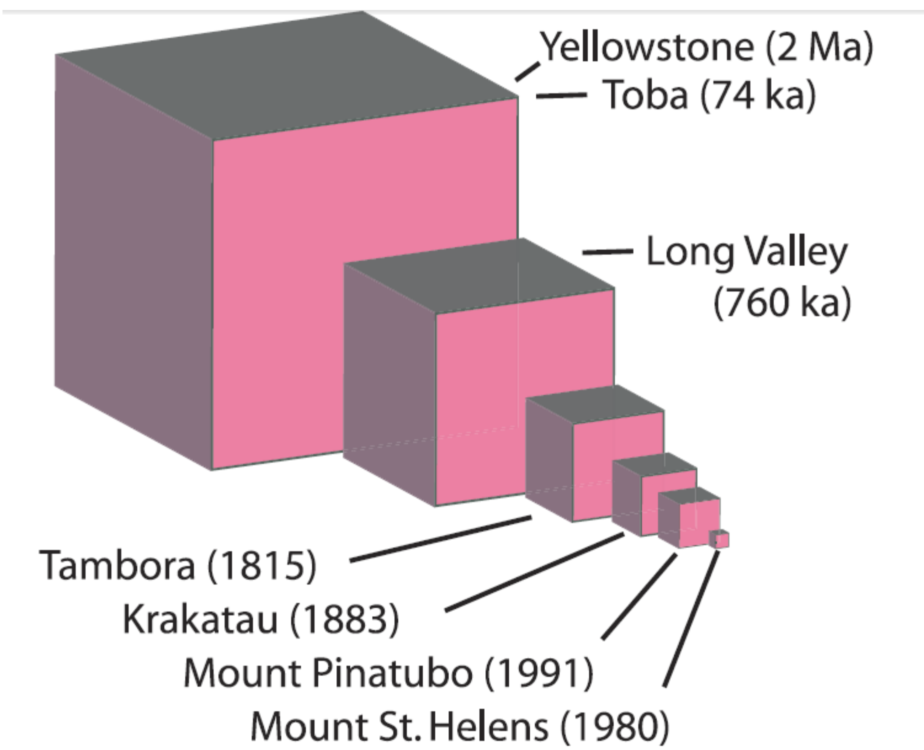

Figure 1. The VEI scale. Long Valley and larger are VEI 8 eruptions. From Wark and Miller (2008), modified from Newhall and Self (1982).

Supereruptions are known to have occurred all around the globe and most of the general public in the United States knows of the supervolcano underneath Yellowstone National Park in Wyoming. However, the western United States has a long history of supereruptions. In the southwestern U.S., along the Arizona-Nevada-California border, the Peach Spring Tuff erupted 18.8 million years ago (Ferguson et al, 2013). The Peach Spring Tuff is an ash-flow deposit with little associated fallout that has been equated to roughly 640 km^3 DRE (Pamukcu et al., 2013). The Peach Spring Tuff has been correlated for 35,000 km^2 over parts of Arizona, Nevada, and California, post-extension (Figure 2) (Glazner et al., 1986 and Gusa et al., 1987). The source caldera for this massive ignimbrite was recently identified near the old mining town of Oatman, Arizona by Ferguson et al. (2013) and was named the Silver Creek caldera. Silver Creek caldera exists within the Colorado River extensional corridor and since the Peach Spring eruption, the caldera has been dismembered northeast-southwest by extension associated with the development of the southern Basin & Range region in the mid-Cenozoic. To the south, rapid extension began before supereruption at Silver Creek, approximately 1-2 My after supereruption at the caldera location, and 2-3 My after eruption to the north (Faulds et al., 2001).

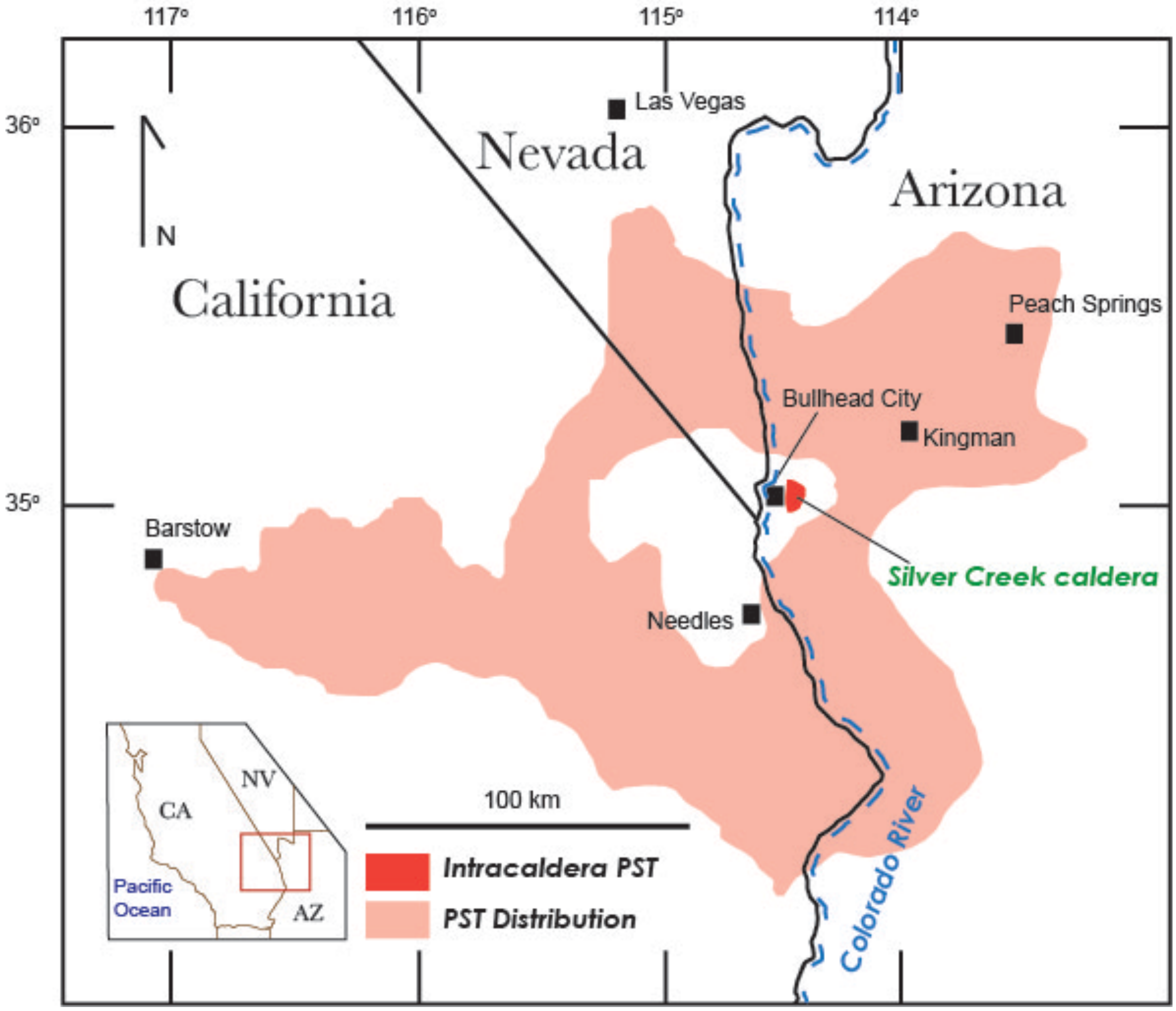

Figure 2. Distribution of the Peach Spring Tuff (PST). A region with no PST deposits exists around Silver Creek caldera, creating the "bulls-eye" effect. This unconformity is possibly due to the swollen surface of the supervolcano. Modified from Pamukcu et al. (2013) and Glazner et al. (1986).

Preceding the Peach Spring supereruption, lava flows extruded onto the surface. These lava flows are not well studied, but the flows can be grouped into two units or sequences. The first, and older, sequence is an approximately 1 km thick trachytic sequence that has been dated to 19.0 Ma (Lang et al., 2008; McDowell et al., 2014). Above the trachyte sequence is a relatively thin mafic lava sequence (Figure 3 and Figure 4). Combined, these lavas were extruded over a period of several hundred thousand years prior to the Peach Spring supereruption. Because dating mafic igneous bodies is difficult, the age of the mafic lava sequence is determined relatively, based on the 19 Ma trachyte flows below and the 18.8 Ma Peach Spring Tuff above. This brackets the mafic lavas into a 0.2 My time range. The lavas focused on in this study have been previously categorized as basaltic trachy-andesites, trachy-basalts, and near-aphyric trachytes. Due to the closeness in age of the mafic and trachytic pre-Peach Spring lava flows, they presumably represent the same broad magma system in the Black Mountains (McDowell et al., 2014). It is reasonable to speculate that the younger mafic flows represent the hot, juvenile mantle input that was a key part to generating the volcanic sequence as a whole. A goal of this research is to determine the petrologic and geochemical characteristics of these little-studied lava flows and to determine their possible relation to the Peach Spring Tuff supereruption. I speculate that these lava flows, being so close in age to the Peach Spring Tuff, may represent the heat input to the magmatic system prior to and perhaps triggering the Peach Spring supereruption.

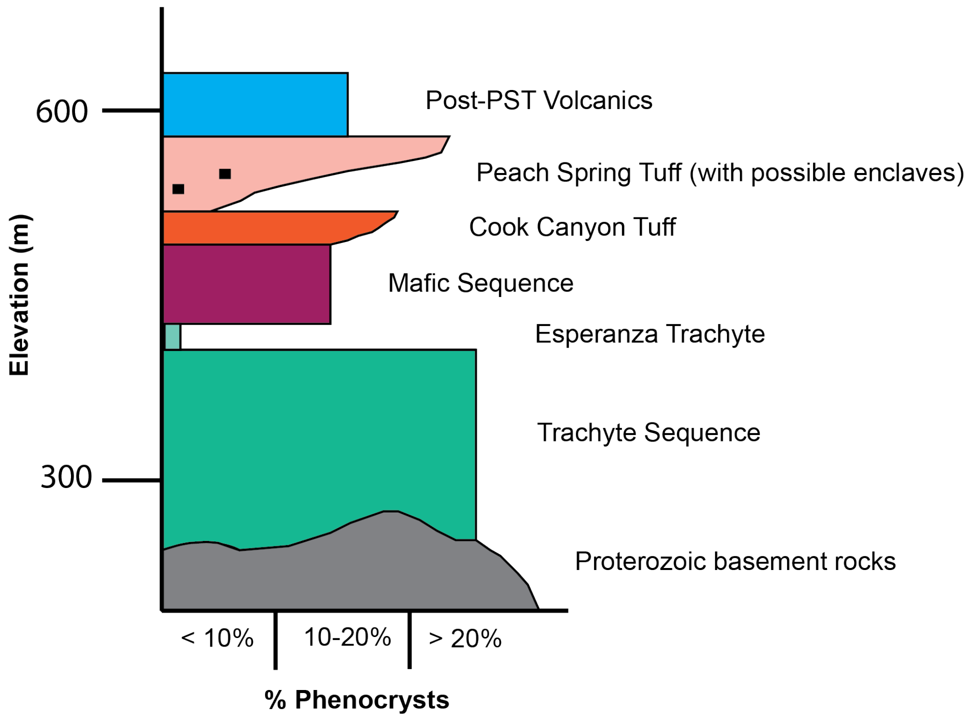

Figure 3. Volcanic stratigraphy of the southern Black Mountains, with % phenoncrysts rather than resistance to erosion on the bottom axis. The Cook Canyon Tuff is an ignimbrite older than and distinct from the Peach Spring Tuff. Data from Spencer et al. (2007) and Pamukcu et al. (2013).

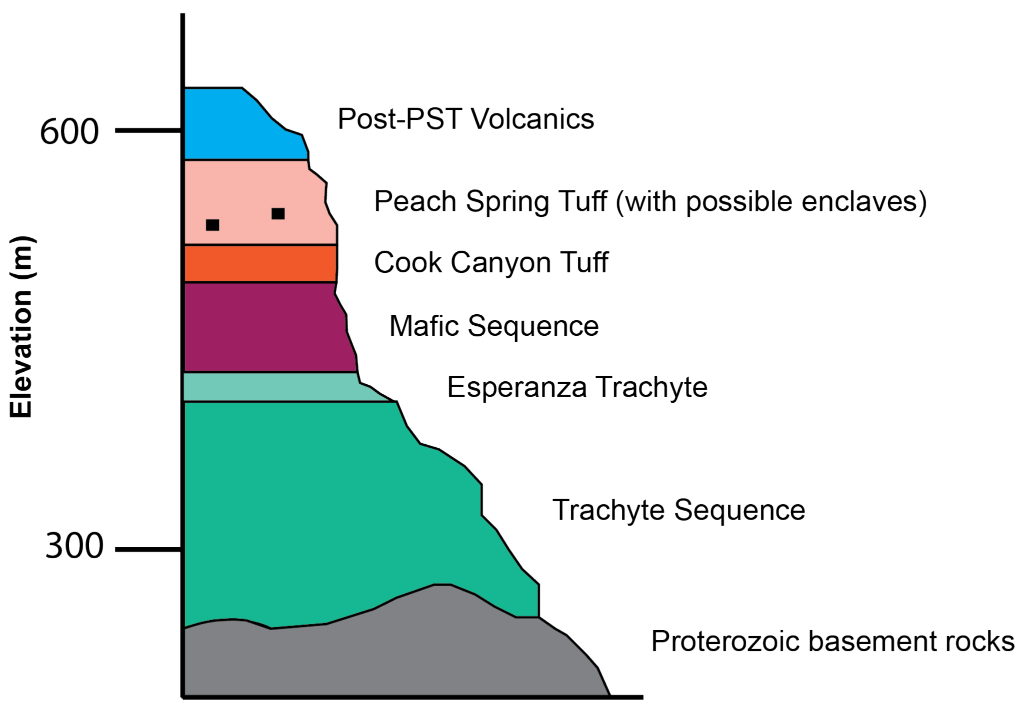

Figure 4. Volcanic stratigraphy of the southern Black Mountains in cross-section. The lava sequences are typified by both cliff-forming units and slope-forming units. The tuffs are mostly cliff-formers. Created from preliminary field work in January 2014.

Curiously, these mafic and trachytic lava flows are commonly present where the Peach Spring Tuff itself is missing, possibly due to the region's existence as an erosional highland during the middle Cenozoic like the Nevadaplano described by Henry et al. (2012). However, this topographic high would have to have been very localized since there is evidence of depositional basins surrounding the caldera where the Peach Spring Tuff, sediments, and post-Peach Spring Tuff units were deposited. A "bulls-eye" pattern surrounds the Peach Spring Tuff unconformity (Figure 2), centered on Silver Creek caldera. More plausibly, the "bulls-eye" may be related to the swollen surface above the supervolcano and by subsequent caldera collapse (Ferguson et al., 2013).

While mafic, hotter lavas are indeed evidence of hot magma in the region, alone they are not proof of a hotter magma existing within a cooler, silicic, supereruptive chamber. At the macroscopic level, evidence of magma mingling takes the form of magmatic enclaves, of a different composition than the host ignimbrite, within an ignimbrite deposit (Pamukcu et al., 2013). At the microscopic level, reverse zoning of phenocrysts is evidence of possible magma mingling or mixing (Nakagawa et al., 2012).

This study aims to examine the petrology and geochemistry of the last trachyte lava flow and the mafic lava flows that erupted before the Peach Spring supereruption. Additionally, magmatic enclaves discovered within the Peach Spring Tuff were similarly analyzed and compositionally compared to the pre-Peach Spring lavas. Understanding the characteristics of these lavas and enclaves allows us to conclude if there was heat input into the Black Mountains volcanic system preceding the Peach Spring supereruption and the possibility of mafic magma injection as an eruption trigger mechanism. In addition to understanding the geochemical and petrographic properties of these two sample types (lavas and enclaves), we identified localities where each sample type existed, with the furthest distance between sampling locations being 40 km. We were also curious about the stratigraphic relationship between these more mafic lavas and the Peach Spring Tuff unconformity (the “bull’s eye” map pattern) and its implications for the dynamic Black Mountains volcanic center in the middle-Miocene.

Geologic Setting and Past Research

The Peach Spring Tuff erupted within what is now the state of Arizona close to the borders of Nevada and California. The source caldera resides within the current Basin & Range province of the United States, specifically within the Colorado River extensional corridor. To the east of the study region, the Colorado Plateau rises up to elevations greater than 2000 m. The Peach Spring Tuff spans current elevations of 300 m near the caldera to over 1400 m near Peach Springs, AZ on the Colorado Plateau. To the west of the study region, the topographic elevation rises gradually to just over 900 m in the Mojave Desert, where the Peach Spring Tuff has also been correlated.

The geology of the Black Mountains was first examined and mapped from the late 19^{th} through early 20^{th} centuries after several gold veins were discovered in the area. Though their motive was an economic one and the gold was discovered in granite porphyries younger than the Peach Spring Tuff, the U.S. Geological Survey's *Geology of the Oatman Gold District, Arizona: A Preliminary Report* (Ransome, 1923) also describes some of the pre-Peach Spring Tuff lava flows that are of interest in this study.

The Peach Spring Tuff

Young and Brennan (1974) first defined the Peach Spring Tuff and used it as a marker unit to study the geomorphological and structural changes on the Colorado Plateau since the middle-Miocene. Named after the type locality in the town of Peach Springs, Arizona (Figure 2), it was initially referred to as the Peach Springs Tuff, but is now referred to as the Peach Spring Tuff due to nomenclature conflicts with a previously named unit (see Billingsley et al., 1999).

The unit is characterized by its light gray to tan color and its phenocryst assemblage suggests the Peach Spring Tuff outflow is trachytic to rhyolitic in composition, while the intracaldera deposits and some proximal outflow are trachytic. The unit ranges from phenocryst-poor (~10%) in the main outflow body to phenocryst-rich (>30%) at the top of the outflow and in the intracaldera ignimbrite (Figure 3). Mineralogically, the Peach Spring Tuff consists of sanidine (often blue in color and in quantities much greater than plagioclase), plagioclase, "biotite, hornblende, pyroxene, and rare quartz" (Pamukcu et al., 2013). Primary accessory minerals include titanite, zircon, and chevkinite. Miller et al. (1998) reported an isochron age of the Peach Spring Tuff at 18.42 +/- 0.07 Ma. Ferguson et al. (2013) reported an age of 18.78 +/- 0.02 Ma, using the Fish Canyon Tuff standard of the $^{40}Ar/^{39}Ar$ system on sanidine.

The Peach Spring Tuff has been correlated over a large area in the southwestern United States since it was first described. Glazner et al. (1986) were the first to report that previously described Tertiary welded tuffs, discontinuously cropping out from Peach Springs, Arizona on the Colorado Plateau to Barstow, California, were in fact the same outflow sheet. Most mountain ranges and stratigraphic sections in the study, spanning western Arizona, southern Nevada, and southeastern California, only contained one large Tertiary ignimbrite and were of the same phenocryst composition as the Peach Spring Tuff. Notably, all of the outcrops throughout western Arizona and the Mohave Desert were identified by the presence of chatoyant sanidine phenocrysts. The outflow sheet was correlated over 35,000 km^2 (Figure 2). The broad extent of the tuff suggested it was not the product of an ordinary-sized volcanic eruption and must have erupted hundreds of cubic kilometers of material (Glazner et al., 1986; Gusa et al., 1987).

The Source Caldera and Basin & Range Extension

Both Young and Brennan (1977) and Glazner et al. (1986) suggested that the source for the Peach Spring Tuff was likely in or near the southern Black Mountains near the borders of Arizona, California, and Nevada, though no caldera had been identified at the time of their studies. These and other previous studies suggested that the source caldera had been so dismembered and buried by younger volcanic deposits and basin sediments that it would never be found. Thorson (1971) speculated on the presence of an existing caldera in the Oatman mining district.

However, Ferguson et al. (2013) recently mapped the southern Black Mountains and revealed the location of the Peach Spring Tuff source caldera. The presence of a densely welded, trachytic, intra-caldera ignimbrite within part of the formerly named Alcyone caldera (Thorson, 1971), with the same phenocryst assemblage and age, 18.78 +/- 0.02 Ma, as the Peach Spring Tuff (Figure 5), has led to the identification of the Peach Spring source caldera (Ferguson et al., 2013). The Alcyone caldera has been renamed as the Silver Creek caldera for the purpose of uniquely distinguishing the Peach Spring Tuff source location.

The Silver Creek caldera and the Black Mountains reside in the Colorado River extensional corridor (CREC). The CREC is 70-100 km wide in the eastern extent of the Basin & Range province. Extension in the region began during and after regional calc-alkaline magmatism swept through the region between 22 Ma and 12 Ma. This included the activity associated with the Peach Spring Tuff as the magmatism swept from south to north (Faulds et al., 2001; Miller et al., 1998). The period of extension, so soon after the eruption at Silver Creek caldera, led to the geologically rapid dismemberment of the caldera structure. The caldera identified as the source is in fact just the eastern rim of the inner caldera: the structure has been extended northeast and southwest of its original position. Another large fragment exists 40 km to the southwest of Silver Creek (Ferguson et al., 2013).

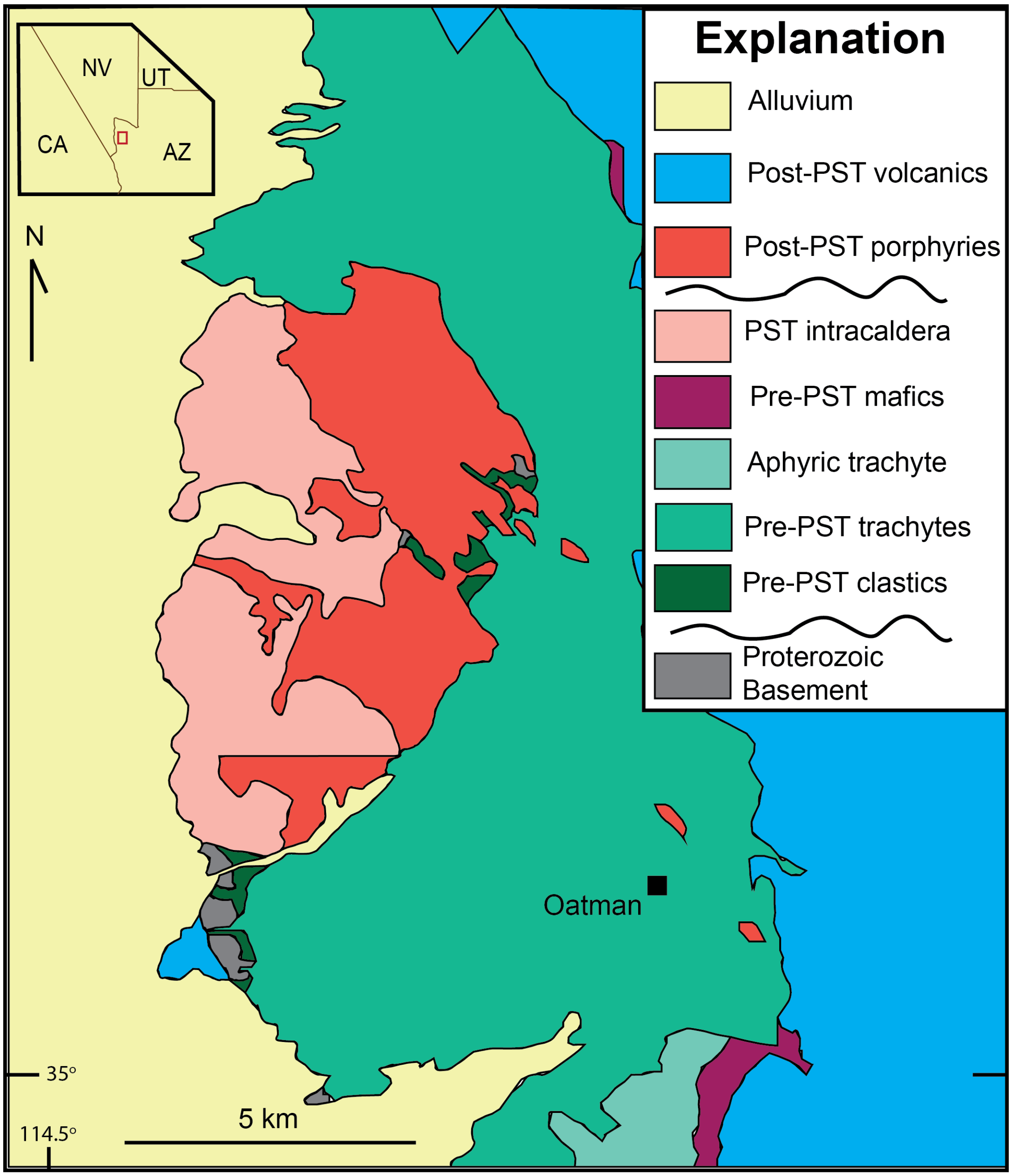

Figure 5. The intracaldera ignimbrite, shown in pink, was identified by Ferguson et al. (2013) as Peach Spring Tuff (PST). The aphyric trachyte and the pre-PST mafics were examined in this study. Modified from Ferguson et al. (2013).

Pre-Peach Spring Tuff Volcanic Activity

The pre-Peach Spring Tuff lava flows in this study are lumped into two general sequences: 1) a >1 km thick, older trachytic sequence; and 2) a thinner, close-to-supereruption mafic sequence. Lang (2001) interpreted the trachyte sequence to be either lava flows or sills with interjected fingers of volcanogenic sediments. The nature of this trachyte sequence (as sills versus lava flows) was unclear because the sequence dips in the same direction as the volcanogenic sedimentary layers but lacks clear brecciated flow tops and bottoms. Lang et al. (2008) dated these trachytes to 18.55 Ma using $^{40}Ar/^{39}Ar$ in biotite. McDowell et al. (2014) reported a weighted mean $^{206}Pb/^{238}U$ zircon age of 19.01 +/- 0.26 Ma.

The last of the trachyte sequence, referred to as the Esperanza Trachyte (Ransome, 1923), was the only section of the trachyte sequence we examined closely. The trachyte sequence as a whole is characterized by its phenocryst-rich nature, typically with 25-35% phenocrysts (Rice et al., 2014). The Esperanza Trachyte is distinct from the trachyte lava flows below it in that it is nearly aphyric, with less than 1% phenocrysts. Because the Esperanza Trachyte is aphyric, it suggests that the melt did not have much time to cool slowly and grow more crystals and indicates possible evidence of heat in the magmatic system.

Above the Esperanza and the top of the trachyte lava flows is a relatively thin suite of mafic lava flows. Previous geochemical work revealed that these lavas were alkalic in nature, consistent with the other volcanic deposits in the region (Pearthree et al., 2009). Spencer et al. (2007) and Pearthree et al. (2009) mapped these lavas as a series of basaltic trachy-andesites and trachy-basalts.

Post-Peach Spring Tuff Volcanic Activity

The region was far from inactive after the Peach Spring supereruption. Rhyolite lava flows were extruded in abundance, as well as trachytic lava flows, and granitic plutons. The 18.63 +/- 0.08 Ma Times and 18.76 +/- 0.11 Ma Moss porphyries shallowly intruded into the region shortly after supereruption (Figure 5) (McDowell et al., 2014). Analysis of both plutons indicates that they originated from a magma body different from that of the Peach Spring ignimbrite. Most buttes in the region are capped in post-Peach Spring Tuff basalt lava flows. The last active volcanism in the region around the Silver Creek caldera is recorded in a thin, discontinuous, ash-fall tephra from the early Pliocene (Spencer et al., 2007).

Magma Mixing and Eruption Triggers

Understanding eruption trigger mechanisms is important for elucidating magma chamber dynamics. Recent studies have examined the longevity of large silicic magma bodies, much like the Peach Spring giant magma body. Bachmann and Bergantz (2003) used the Fish Canyon magmatic system in Colorado as the foundation for a computer model that tested the injection of gases into the base of a large silicic magma body as a rejuvenation mechanism. In their model, volatiles are released from a hotter, mafic magma as it comes in contact with a cooler, silicic magma. The volatile gases were found to generate flux melting: water-rich fluids flow into a dry rock and dramatically lower the solidus, the temperature at which the rock begins to melt. Flux melting results in the reheating of the chilled magma body on the scale of approximately 100 thousand years, a relatively short amount of time, though current work suggests even shorter time scales (McDowell et al., 2014). This model suggests that large volume eruptions of silicic mushes may be triggered by the input of gases, but other processes are likely at work as well (Bachmann and Bergantz, 2003).

One prevailing thought is that the introduction of a more mafic magma into a pre-existing magma could be a source of both heat and volatiles into the system, though controversial ideas about crystallization at the pseudo-invariant point have also been suggested (Fowler and Spera, 2010). Bachmann and Bergantz (2003) suggest with their model that volatiles injected with mafic magma lead to increased pressure within the pre-existing felsic chamber. Increased pressure is often released in small-scale eruptions, but one eruption often triggers others. We can presume that the mafic magma is initially undersaturated in volatiles, because it is juvenile (from the mantle), but as it comes in contact with the cooler felsic magma, it crystallizes. As a result of crystallization, the volatile content in the mafic melt increases, eventually reaches saturation, and results in the release of a fluid phase into the surrounding melt. Because the magma in the chamber is presumably felsic, or at least more silicic than the mafic input, it is very viscous and the added volatiles from the input magma cannot escape, leading to over-pressurization and an explosive eruption. After the initial eruption (whether it is one large event or a small one that triggers other small events), the chamber is partially evacuated and the pressure decreases dramatically, resulting in ground collapse and the creation of a caldera. Caldera formation, in large systems, has been found to be dependent on the brittle threshold of the host rock in which the chamber resides and through-going faults typically develop and subsequently generate collapse of the chamber roof (Gregg et al., 2012).

Magma mixing through the injection of a mafic magma into a silicic one is cited as causing rapid convection and explosive eruptions in Iceland and Greece (Sparks and Wilson, 1977), and dike injection is cited as preceding eruption in Alaska (Eichelberger and Izbekov, 2000). Eichelberger and Izbekov (2000) state that considerable extension occurred north and south of the two volcanic vents of Academy Nauk and Karymsky in Kamchatka, Russia and coincided with heightened thermal output at local hot springs, suggesting dike injection along existing fault structures. The dike, composed of basaltic, denser magma, pooled at the base of the Karymsky andesitic chamber, forcing the andesite to rapidly effusively erupt out of the top of the chamber. Eichelberger and Izbekov (2000) also examined Mt. Katmai in Alaska, United States. Katmai, a large silicic explosive eruption in 1912, is likely to have been caused by the injection of a silicic dike.

Evidence of magma mingling can be seen at both the micro- and macroscopic scales. At the macroscopic scale, magmatic enclaves are direct evidence of two magma types coexisting in a chamber. Magmatic enclaves are identified in the field by the presence of crenulate margins. These "bumpy" margins occur between the enclave and the host-rock because of temperature differences (hot enclave melt and cooler host melt) and are an easy-to-identify characteristic (Figure 7). These enclaves can be identified as magmatic in nature, rather than xenolithic or lithic, because a hotter melt existing within the cooler Peach Spring Tuff melt (the host) creates the characteristic crenulate margin structure as the two melts mingle with one another, often coinciding with chilled margins. Xenoliths or lithic clasts have sharp edges since they were solid before interacting with the host melt.

Figure 6. Crenulate margins around a magmatic enclave at West Kingman (WK in Figure 7 and KPF in Figure 12). Pencil is 15 cm long.

On a microscopic scale, magma mingling can be illuminated through the use of a scanning electron microscope (SEM). SEM analyses provide insight on zoning characteristics of individual phenocryst and reverse zoning is known to be evidence of magma mingling before explosive eruption in some modern day volcanoes (Nakagawa et al., 2012). Analysis with SEM also allows for comparison among samples and sample types (such as enclaves versus lavas). In addition, elemental differences within phenocrysts, reaction zones, and groundmass among samples provide information on the composition of the magma(s). Characterizing magma composition among the pre-Peach Spring Tuff lavas and the Peach Spring Tuff magmatic enclaves helped us understand the changes occurring in the broad Black Mountains volcanic system preceding Peach Spring supereruption. Furthermore, the SEM was used to search for microphenocrysts in samples, particularly zircon and apatite. The presence of these two minerals within a sample determined whether or not temperatures generated through mineral-saturation thermometry calculations were reliable or if they were minima.

Geochemical data is another important tool for comparison between magmatic enclave samples and lava samples. Magmas and lavas are classified based on their SiO_2 weight percent and their alkali content on a Total Alkali Silica (TAS) diagram. TAS diagrams are an easy way to display some important chemical differences among magma compositions. If magmatic enclaves and lavas classify similarly, it is likely they are from similar magmas.

Finally, the temperatures of the magmas, which produced these samples, can be modeled with the use of the MELTS program. The program is used to model magmatic evolution under different temperature and composition conditions, as well as magma mixing and input. However, even as the program advanced with technology, it had some severe limitations when used to model silicic magma systems (see Gualda et al., 2012, p.876-878 for more information). In 2012, a new version of MELTS, dubbed Rhyolite-MELTS, was created in order to address magmatic evolution within silicic magmatic systems. The Bishop Tuff was used to calibrate Rhyolite-MELTS, but the Peach Spring Tuff was used as an example to test the program's effectiveness (Gualda et al., 2012). Pumukcu et al. (2013) used Rhyolite-MELTS to model the temperature of the Peach Spring Tuff. This project used a free, downloadable version of the program usable in Microsoft Excel, known as Excel-MELTS.

The purpose of this research was to understand the petrologic and geochemical characteristics of the lava flows that closely preceded the supereruption of the Peach Spring Tuff at the Silver Creek caldera. The geochemical and mineralogical nature of these flows provides information on dynamics within the Black Mountains volcanic system, including the possibility of magma mingling and triggering mechanisms if they are compared to magmatic enclaves found within the Peach Spring Tuff itself. More broadly, this research helps us better understand processes within large magma bodies and may help identify future instability in modern-day supereruptive bodies, such as the one below Yellowstone National Park in Wyoming, United States.

The Peach Spring supereruption volcanic deposits are trachytic to rhyolitic and as such are intermediate to felsic, although we understand the Peach Spring Tuff trachyte is cumulate from the rhyolitic magma. We speculate that the introduction of more mafic magmas before eruption is possibly recorded in the basaltic trachy-andesite, trachy-basalt, and aphyric trachyte lava flows just below the Peach Spring Tuff in the volcanic stratigraphy of the Black Mountains. Further, the presence of mafic, magmatic enclaves with the Peach Spring Tuff would be conclusive evidence of mafic magma existing within the Peach Spring magma chamber. Together, the pre-Peach Spring Tuff lava flows and any magmatic enclaves found within the Peach Spring Tuff would elucidate the dynamics of the southern Black Mountains volcanic system and may suggest heat input prior to the Peach Spring supereruption.

Methods

The field work for this study involved obtaining samples of both pre-Peach Spring lavas and Peach Spring Tuff magmatic enclaves for a week in January 2014 and for two weeks in late May 2014. The lavas (including the mafic sequence and the Esperanza Trachyte) were sampled at the locations of McHeffy Butte, Warm Springs West, Caliche Springs, and Secret Pass (Figure 7). We recorded stratigraphic relationships in the field, such as the proximity to the Peach Spring Tuff itself and the thickness of the unit. We discovered magmatic enclaves in the locations of Warm Springs West, West Kingman, and North Homestead, within the Boundary Cone, Warm Springs West, and Kingman quadrangles (Figure 7). The last of the trachyte sequence, referred to as the Esperanza Trachyte (Ransome, 1923), was the only section of the trachyte sequence we examined closely.

To understand the relationship between volcanic deposits below and above the Peach Spring Tuff unconformity, and therefore the nature of the unconformity itself, Lee et al. (2014) and Williams et al. (2014) mapped along a 4 km north-south transect approximately 5 km northeast of the Silver Creek caldera rim within the Union Pass quadrangle (location SPW in Figure 7). Samples we collected from parts of this transect, both sedimentary units and volcanic units, were analyzed with the same laboratory methods as the main group of lava and enclave samples, as described below.

The samples were prepared in the laboratories at Vanderbilt University in Nashville, Tennessee and at Middle Tennessee State University (MTSU) in Murfreesboro, Tennessee. Samples were cut with a standard rock saw to make billets for thin sections and to make small pieces which could then be powdered in a shatter-box in preparation for analysis with by x-ray fluorescence spectrometry (XRF) at MTSU.

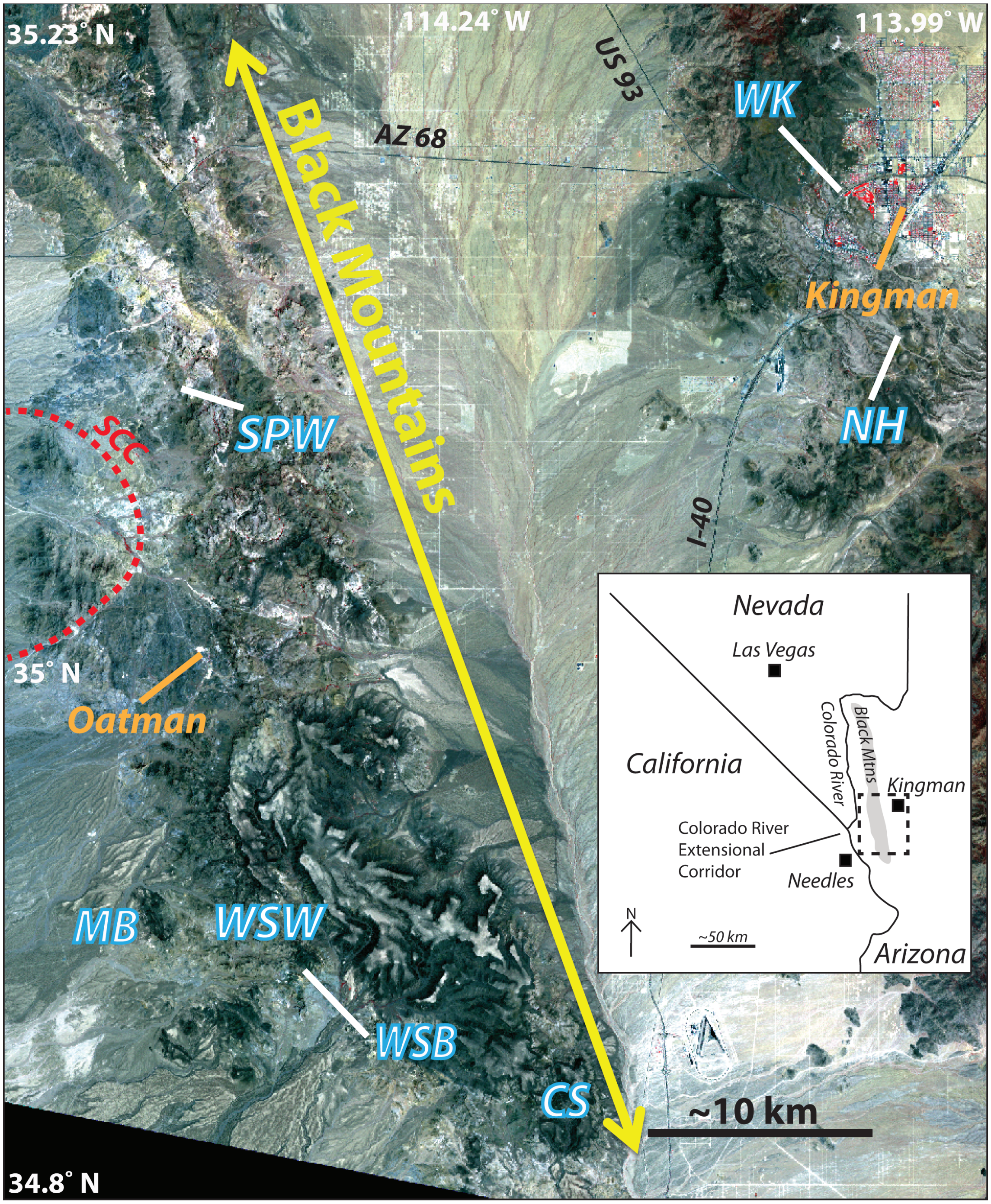

Figure 7. Imagery of the southern Black Mountains. The blue highlighted abbreviations are the sample locations (MB = McHeffy Butte, WSW = Warm Springs West, WSB = Warm Springs Butte, CS = Caliche Springs, NH = North Homestead, WK = West Kingman, SPW = Secret Pass Wash, and SCC = the Silver Creek caldera. Kingman to MB = ~ 40 km).

Petrographic analysis of the 13 samples made into thin sections (both lavas and enclaves) was done to identify phenocryst assemblage and evidence of unique characteristics such as zoning or reaction rims. A Leica petrographic microscope was used at Vanderbilt University and photos of the thin sections were taken using the DP Manager program on an Olympus petrographic microscope at William & Mary.

To obtain whole rock geochemistry, 0.8 g of each powdered sample was flux melted by fusing with1.9 g of lithium tetraborate, 4.3 g of lithium metaborate, and two eye drops of lithium bromide in the flux melter at Middle Tennessee State University (Figure 8). The fused glasses produced were placed in the XRF for minor elemental analyses. To obtain major elements, powdered samples were compressed into pellets through the use of a hydraulic press and were also analyzed with the XRF at MTSU.

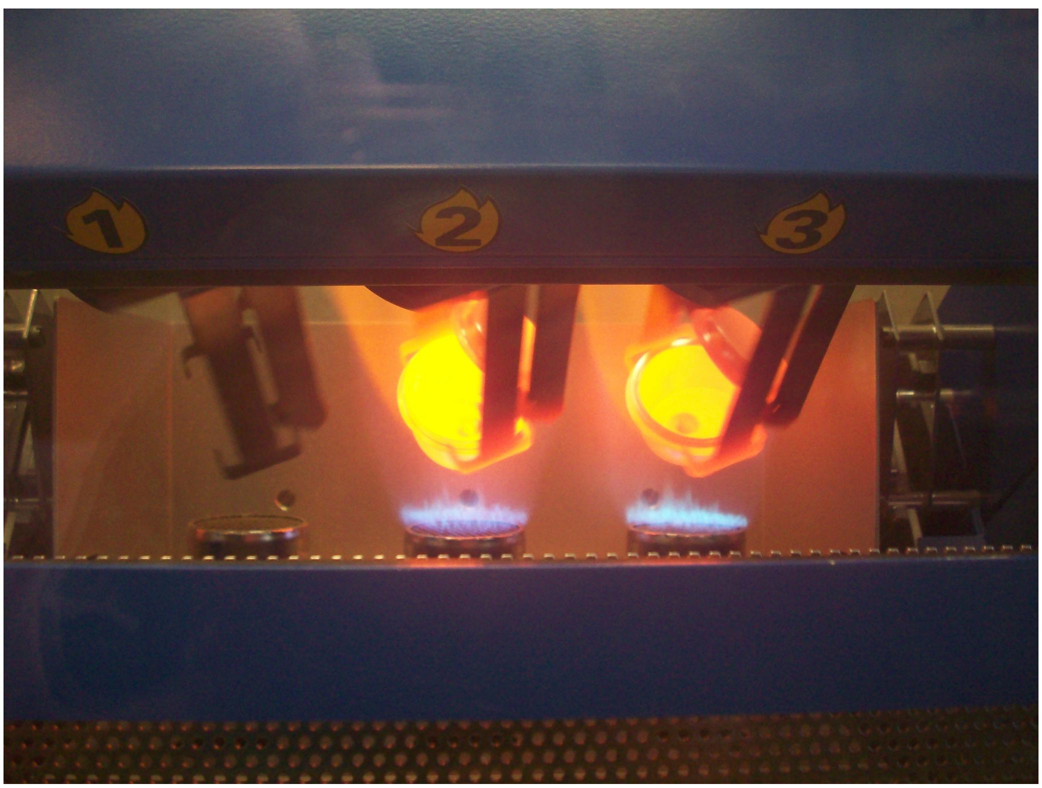

Figure 8. The flux melter at MTSU. Crucibles were made out of platinum to withstand the high temperature of the melter and to avoid reaction with and partial dissolution of the melt.

The geochemical data obtained through the use of the XRF were then plotted on the TAS diagram to determine the rock type of both the lava samples and the enclaves. Aside from the classification of the samples based on their total alkali and silica content, the samples were also plotted on Harker diagrams to determine if there were similar ranges in major element and selected minor element (Zr, Sr, Ba, Nb, Y, Rb) compositions between the lava samples and the magmatic enclave samples.

Full elemental analyses of three enclaves (WSWF-3, WSWF-5, and KPF-5) and two lavas (WSWF-1 AND CS-MF1) were done. The samples were analyzed using Inductively Coupled Plasma Mass Spectrometry (ICP-MS) at ActLabs. These ICP-MS analyses allowed us to compare more than just whole rock major and selected minor element compositions, such as trace elements, including rare-earth elements (REE). Additionally, full elemental analyses allowed for comparison of major element data between ICP-MS and XRF methods.

The scanning electron microscope (SEM) at Vanderbilt University was used to obtain major element concentrations for phenocrysts in most samples. Samples first had to be mounted in epoxy and then polished to as smooth and flat a surface as possible so as to minimize excessive backscatter to the SEM. Polishing was first done at the mm scale and was finalized at the micrometer scale. Mounts were made of the following samples: MBF-1, MBF-4, MBF-5, WSWF-1, WSWF-3, WSWF-5, SPF-1A, SPF-1B, and KPF-5. To analyze zones within phenocrysts, darker and lighter rims were searched for within individual phenocrysts. Denser elements appear lighter in SEM imagery, while less dense elements appear darker. This illuminates normal and reversed zoning (Figure 9).

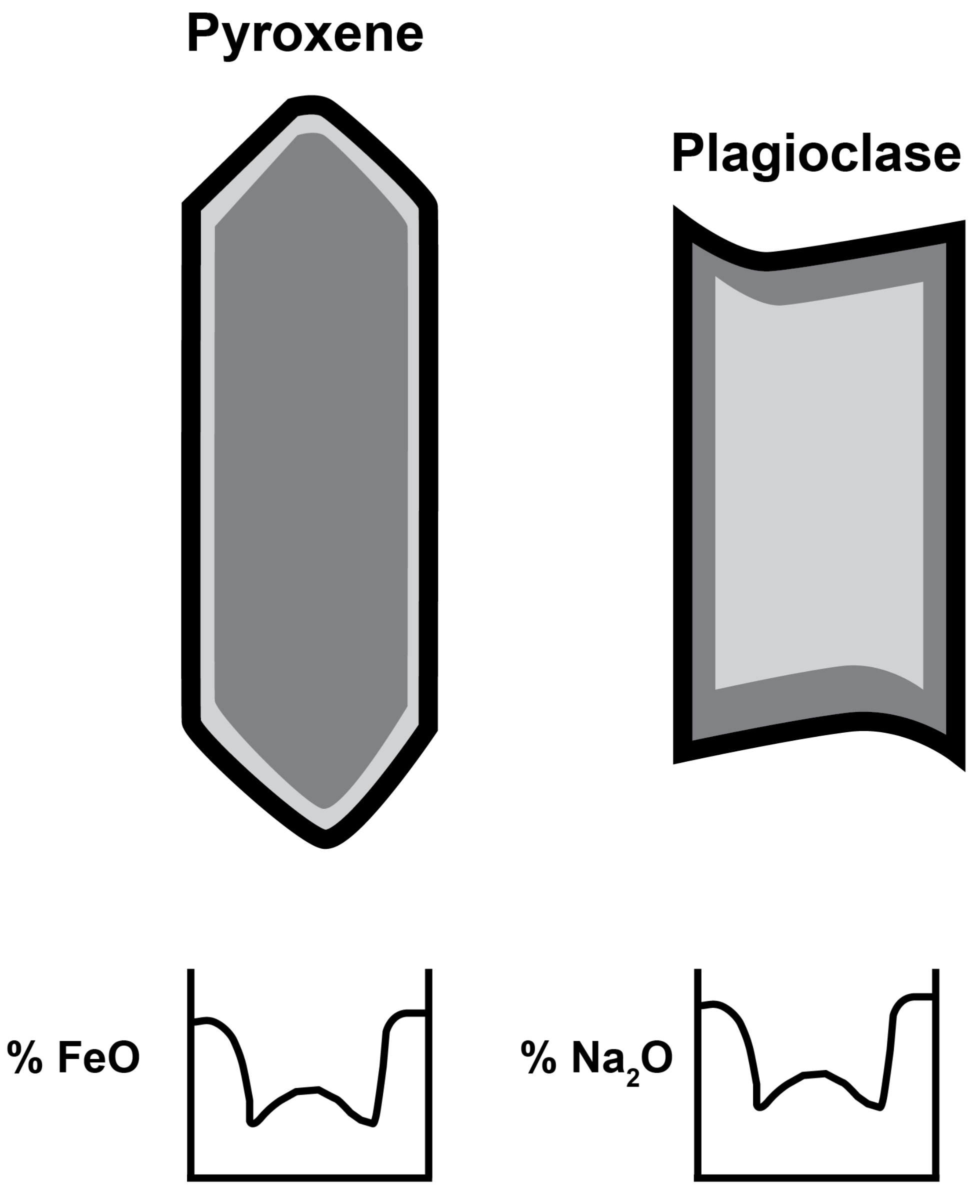

Figure 9. A simple schematic with euhedral crystals depicting the iron-rich outer layer of normally zoned pyroxenes and the sodium-rich outer layer (sodium-rich core) of normally zoned plagioclase phenocrysts.   Reverse zoning would be evidenced by a reversal in dark/light patterns. Based on Nelson (2012).

To model the temperature of these lavas (and their magmas), the XRF data was used with the Excel-MELTS program, a modified version of MELTS, first designed by Ghiorso and Sack (1995), described above. The Excel-MELTS version was used in this study, at the following constant pressure, varying water weight percent, and other constraints, to model the temperatures of the lava flows and the Peach Spring Tuff magmatic enclaves:

- Constant 200 MPa pressure. This is reasonable if we assume these magma bodies are shallow, at 10 km depth.
- Water weight percent: each sample normalized with 1% H_2O, 2% H_20, and 3% H_20 and run through the program.
- ΔNNO used for the log fO2 constraint
- XRF data: FeO determined by multiplying 0.7 by the Fe_2O_3 determined by XRF and Fe_2O_3 was determined by multiplying 0.3 by the Fe_2O_3 determined by XRF.

Mineral saturation thermometry was also used to determine temperatures of melts that generated both lava and enclave samples. For apatite-saturation thermometry, the temperatures can be considered minima for samples in which apatite phenocrysts do not exist or only exist as quench crystals. However, for those samples in which apatite microphenocrysts do exist the temperatures are understood to be reliable. Likewise, the presence of zircon within a sample determines whether temperatures calculated with zircon-saturation thermometry are reliable. The temperature generated through these calculations is the temperature at which apatite or zircon phenocrysts would form, so the lack of the mineral in some samples suggests the lava had not yet reached this temperature. Calculations used in these two methods are detailed in Appendix C. These temperatures were also used to test the validity of those obtained through the Excel-MELTS program.

Results

Field Observations—Stratigraphy and Hand Sample Petrography

The pre-Peach Spring Tuff mafic lava sequence is discontinuous in the southern Black Mountains. We collected 14 samples from lava flows in the study area and sample locations ranged from the southern-most extent at Caliche Springs to the northern-most extent just southeast of the town of Kingman, Arizona (Figure 7). Although these lavas were likely separate events, they are very localized in the southern Black Mountains and exist at the same location within the volcanic stratigraphy. Therefore, it is safe to assume that they are likely related to one another. The general geology of the study area and the extent of the main units observed in this study (Figure 10) helped to illustrate the intensity and dynamic history of magmatism in the southern Black Mountains during the middle-Miocene. The pre-Peach Spring Tuff units are sparse near and around the caldera itself.

The observed units in this study were lumped into the broad units shown on Figure 11. The units were described as follows, from oldest to youngest:

Yg: Proterozoic basement complex consisting of weathered granites and granitoids. This is the oldest unit in the study area.

Td: A thick (~1 km) Tertiary trachyte sequence. The rocks range from 25-35% phenocrysts, dominantly plagioclase and biotite. The sequence is dark gray to green in color and has been dated to ~19 Ma (Lang et al., 2008). The lava sequence is laterally extensive, covering a large area around Silver Creek caldera and has eroded into a hummocky landscape with some dramatic slot canyons.

Tde: Esperanza Trachyte. It is characterized by its near-aphyric (<1% phenocrysts) nature. Those phenocrysts that do exist are elongate 2-5mm plagioclase crystals in the fine-grained matrix. The Esperanza is purple to gray in color and crops out substantially at McHeffy Butte, overlying *Td* and underlying *Tm*.

Tm: The pre-Peach Spring Tuff mafic lava sequence, sometimes referred to as part of the Wrigley Mine volcanics (Spencer et al., 2007). These lava flows range from < 5%-20% phenocrysts, with phenocryst assemblage consisting of both blocky and elongate plagioclase crystals (~60%), clinopyroxene (~35%), rare olivine (< 2%), and secondary minerals (~5%). The sequence is gray to purple in color and typically crops out as relatively thin units above *Td* and/or *Tde*, depending on location. Some lavas are heavily vesiculated and have subsequent amygdules (Figure 11a). Unique mafic units are interbedded with sedimentary units near the Peach Spring Tuff unconformity (Figure 11b) within Secret Pass Wash. At Warm Spring West *Tm* lays directly below *Tt* (Figure 11c) and at McHeffy Butte *Tm* lays above *Tde* and below *Tt* (Figure 11d).

Tc : Cook Canyon Tuff, consisting of 25% phenocrysts, dominantly plagioclase and biotite. This ignimbrite is smaller than and distinct from the Peach Spring Tuff and is trachytic in composition.

Tt: Peach Spring Tuff. Contains 5-25% phenocrysts consisting of sanidine, biotite, and rare quartz and has been dated to 18.8 Ma (Ferguson et al., 2013). This unit is the product of the supereruption at Silver Creek caldera and is laterally extensive over the study area, but is absent around the Silver Creek caldera proper. The PST is trachytic in intra-caldera deposits and is rhyolitic in outflow deposits.

Tg: The Moss and Times granite porphyries that intruded after PST supereruption in the region in and around the caldera itself.

Tv: Post-PST volcanic units ranging from basalt to rhyolite flows, dikes, and plugs.

Ts: Tertiary sedimentary layers, mostly on the western edge of the study area, though some sedimentary units are interbedded with *Tm* near the Peach Spring Tuff unconformity, sourced from basement complex and the trachytes that lay below and likely volcanogenic in nature.

Qal: Quaternary alluvium that covers the valleys in the study area.

Lava samples were collected from McHeffy Butte, Warm Springs West, Caliche Springs, Secret Pass Wash, and Northwest Homestead (Figure 12). Figure 13a shows the general stratigraphic relationships among units across the southern Black Mountains while Figure 13b shows the stratigraphy at the Peach Spring Tuff unconformity within Secret Pass Wash. Near the Peach Spring Tuff unconformity, we noted that the Esperanza Trachyte is not within the sequence. Additionally, the mafic lavas within Secret Pass Wash, while generally similar to those found elsewhere in the study, are interbedded with sandstones, and overlain by post-Peach Spring Tuff rhyolites. Sample locations, including those of magmatic enclaves, in UTM coordinates and descriptions, are in Table 1 of Appendix A.

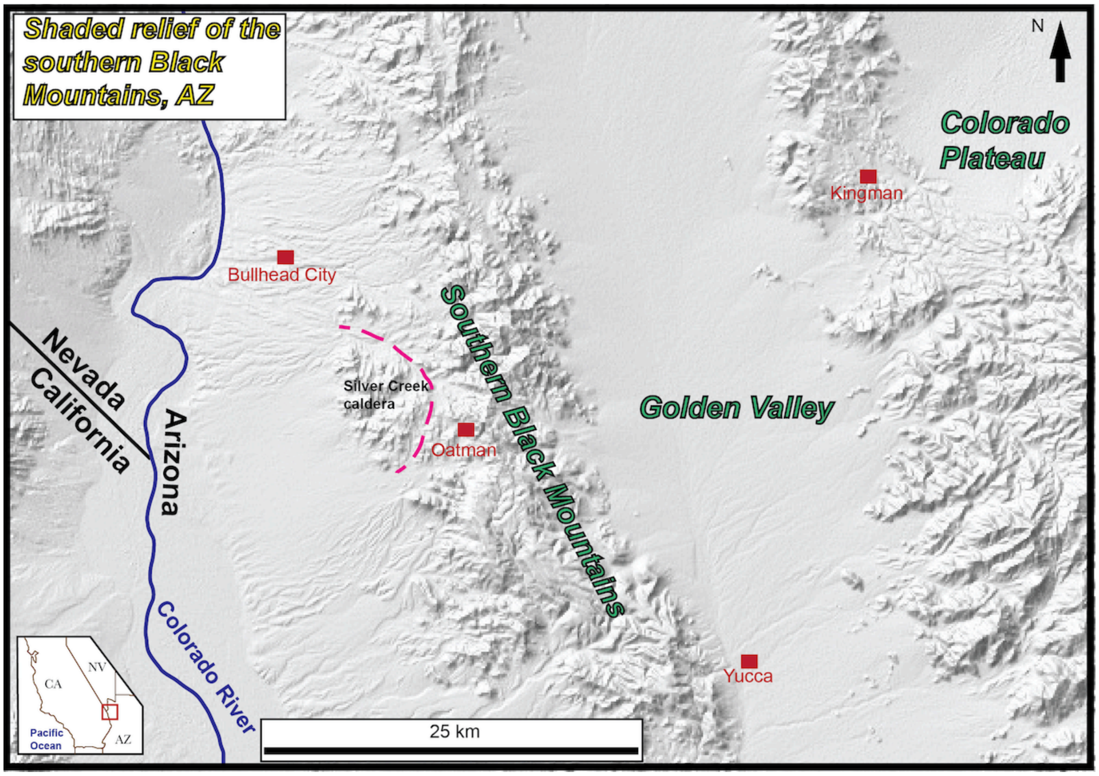

Figure 10a. Shaded relief map of the study area.

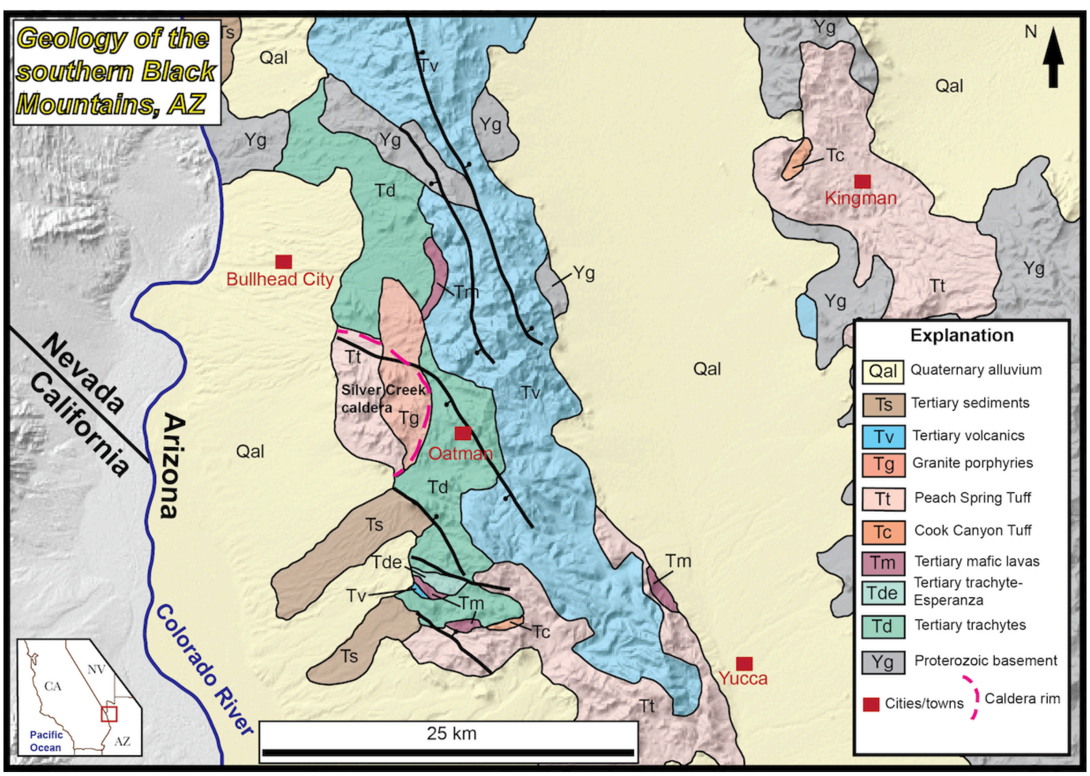

Figure 10b. Generalized geologic map that shows the broad units within the study area. Sample locations are shown in Figure 13.

Figure 11a. Vesicular mafic lava with amygdules at McHeffy Butte (MBF-1). Pencil is 15 cm.

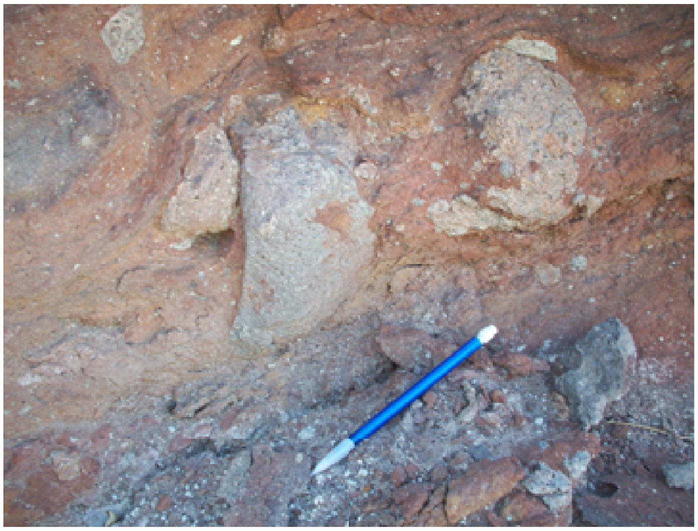

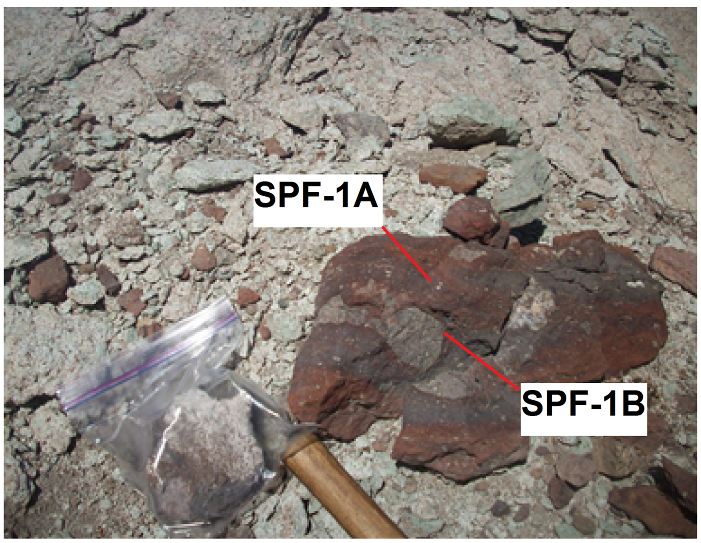

Figure 11b. The top image shows two rocks: a gray lava mingled in with a red volcanogenic sedimentary unit. SPF-1A was taken from the red "host" in the middle image. SPF-1B contained the contact between the gray unit and the red unit. SPF-2 was a mafic lava interbedded with sandstones in Secret Pass Wash just below the Peach Spring Tuff unconformity with flow banding. Pencil is 15 cm.

Figure 11c. Vantage point: standing on top of mafic lava flow (WSWF-1). The Peach Spring Tuff is approximately 15 meters above the vantage point. Photo from Warm Springs West (WSWF-1 on Figure 13, below).

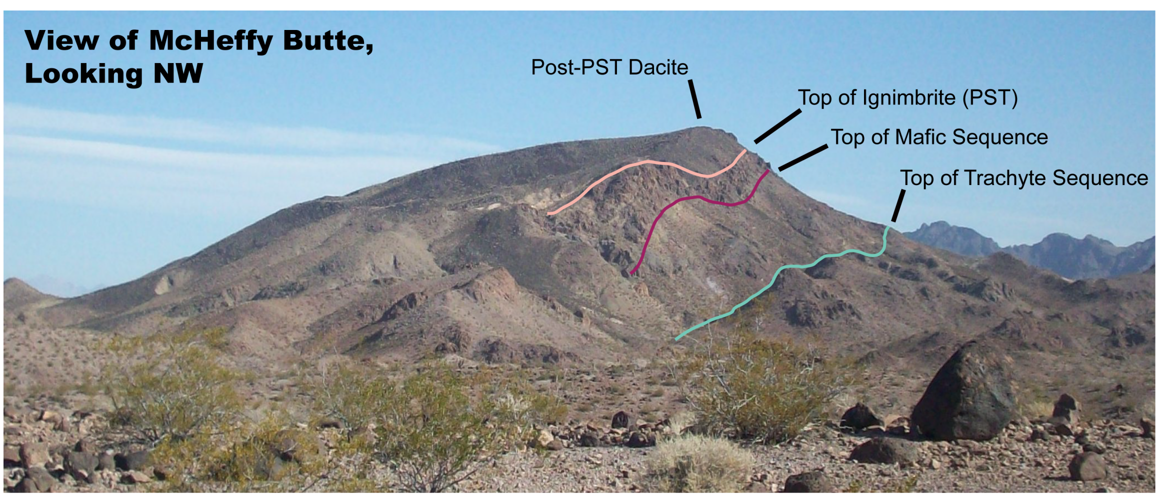

Figure 11d. View to northwest at McHeffy Butte. The relief of the butte is approximately 300 m. Samples MBF-1, MBF-2, MBF-3, MBF-4, and MBF-5 collected on the slope on the right (NE) side of the image.

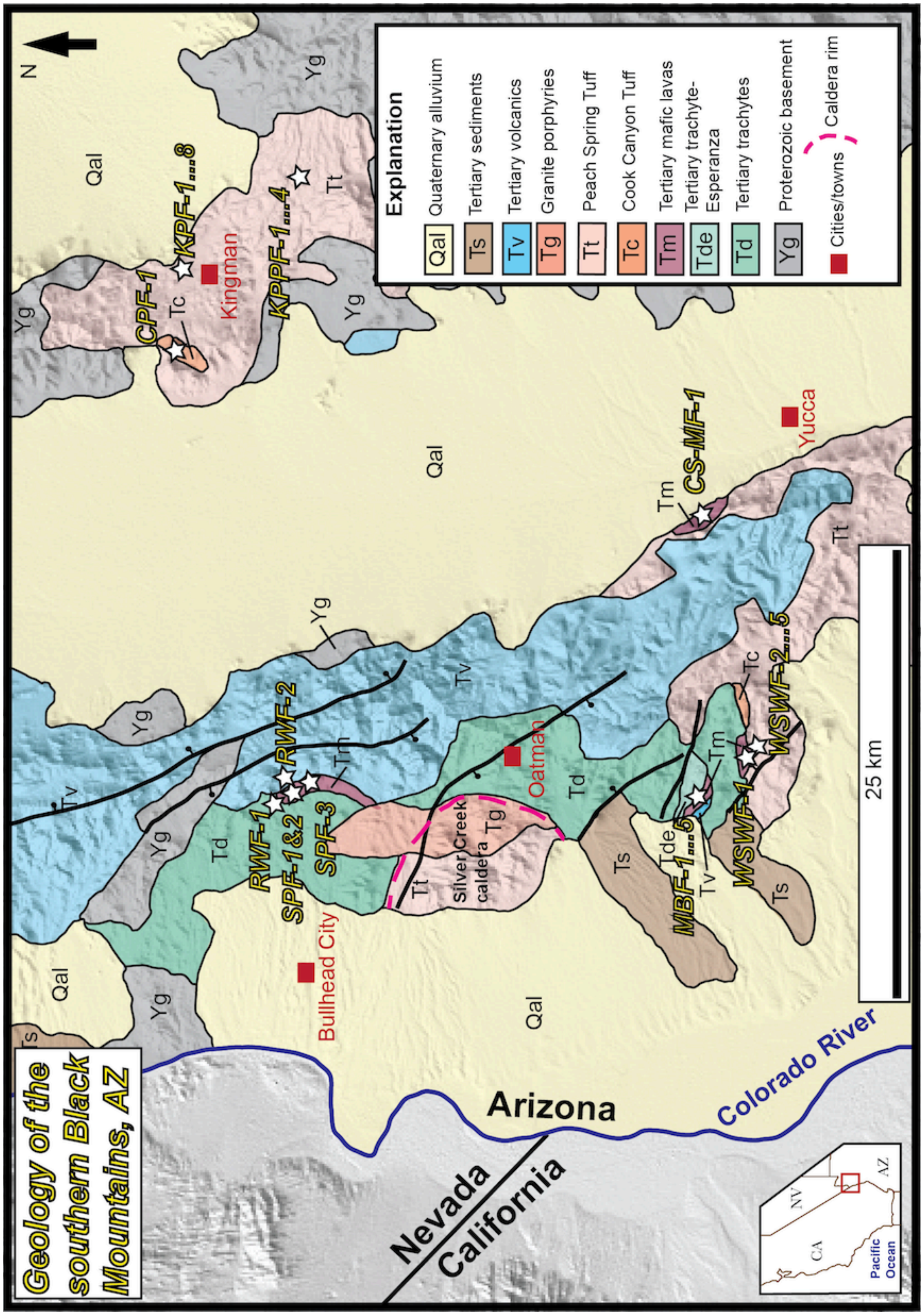

Figure 12. Sample locations underlain by the general geology.

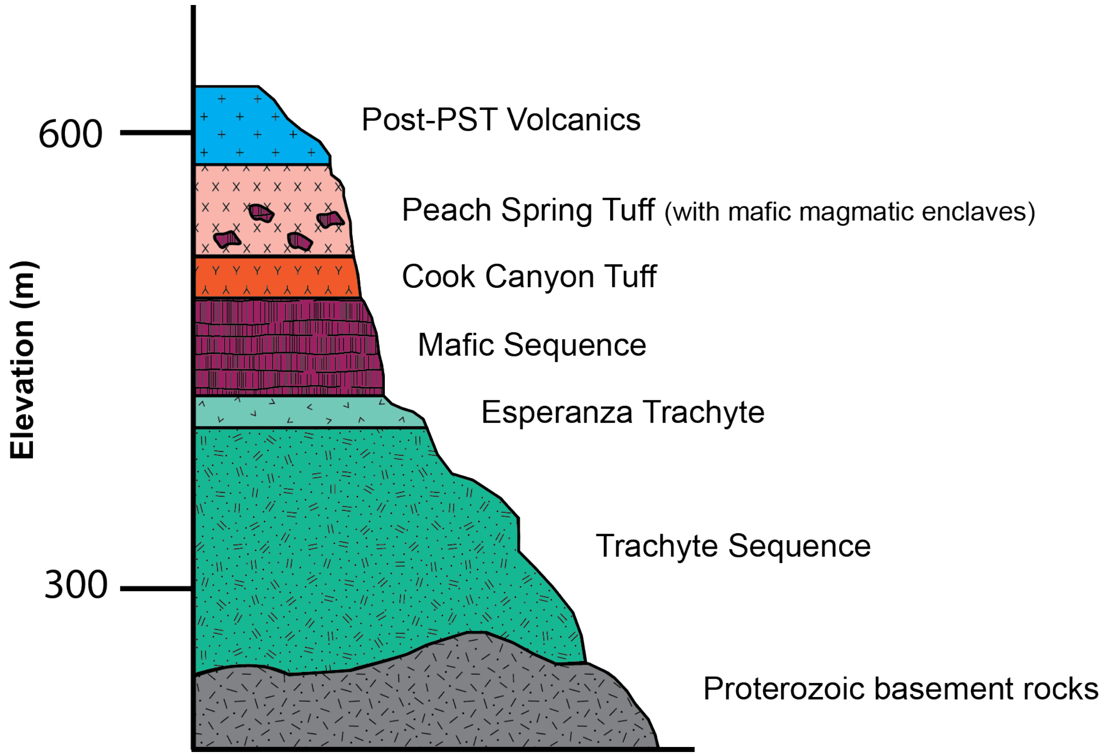

Figure 13a. General Miocene volcanic stratigraphy of the southern Black Mountains.

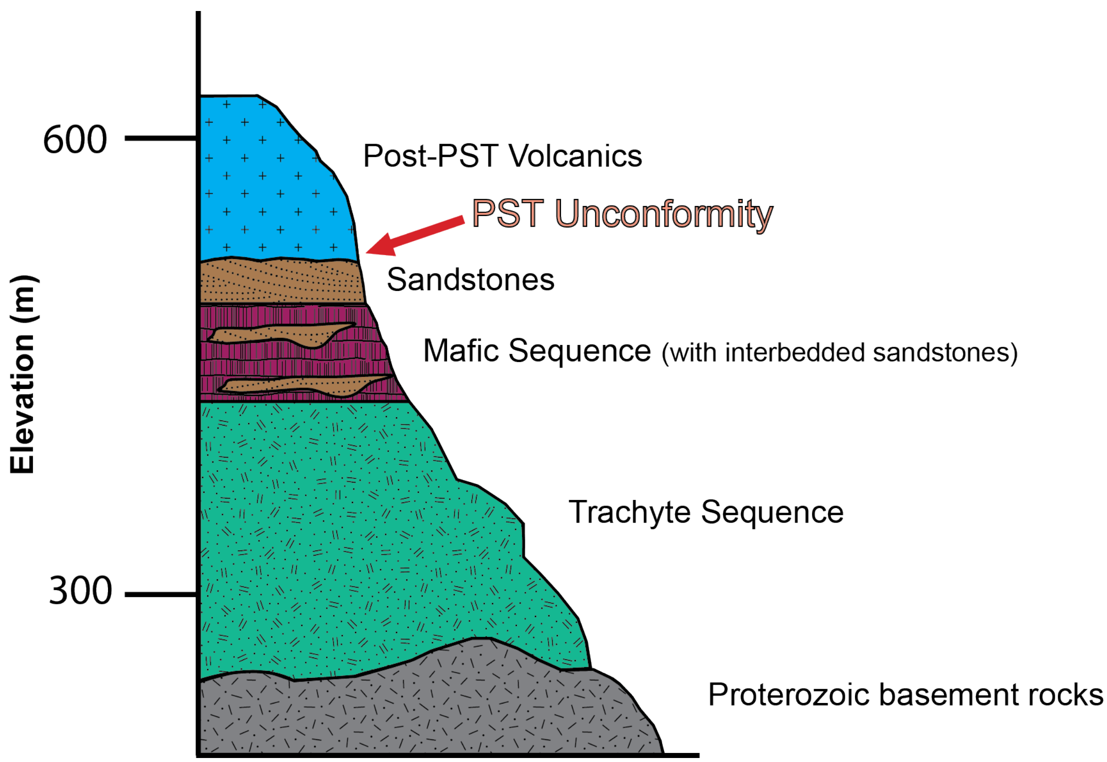

Figure 13b. General Miocene volcanic stratigraphy at the Peach Spring Tuff unconformity within Secret Pass Wash. Note that the Esperanza Trachyte is not within the sequence and that the mafic lavas are interbedded with sandstones.

We discovered over 20 magmatic enclaves within the Peach Spring Tuff itself and sampled 16 of them. These enclaves were collected from the locations of Warm Springs West and from northwest and southeast of Kingman, Arizona (Figure 12). The enclaves were placed into two groups:

Warm Springs West: Samples consist of three large enclaves of 25-50 cm across (WSWF-3, WSWF-4, and WSWF-5) excavated from the cliff of Peach Spring Tuff; several smaller enclaves (WSWF-2A—F); range in size from a few centimeters to greater than 0.5 meter across (Figure 14a); 10-15% phenocrysts (elongate plagioclase and small pyroxenes are dominant with secondary minerals ~5%); smaller enclaves often vesicular.

Kingman: Most enclaves (KPF-1—KPF-8, KPPF-1, and KPPF-2) range from 10-20 cm across (Figure 14b); 5-20% phenocrysts (blocky plagioclase, some pyroxene, and coppery biotite); more weathered than the Warm Springs West enclaves.

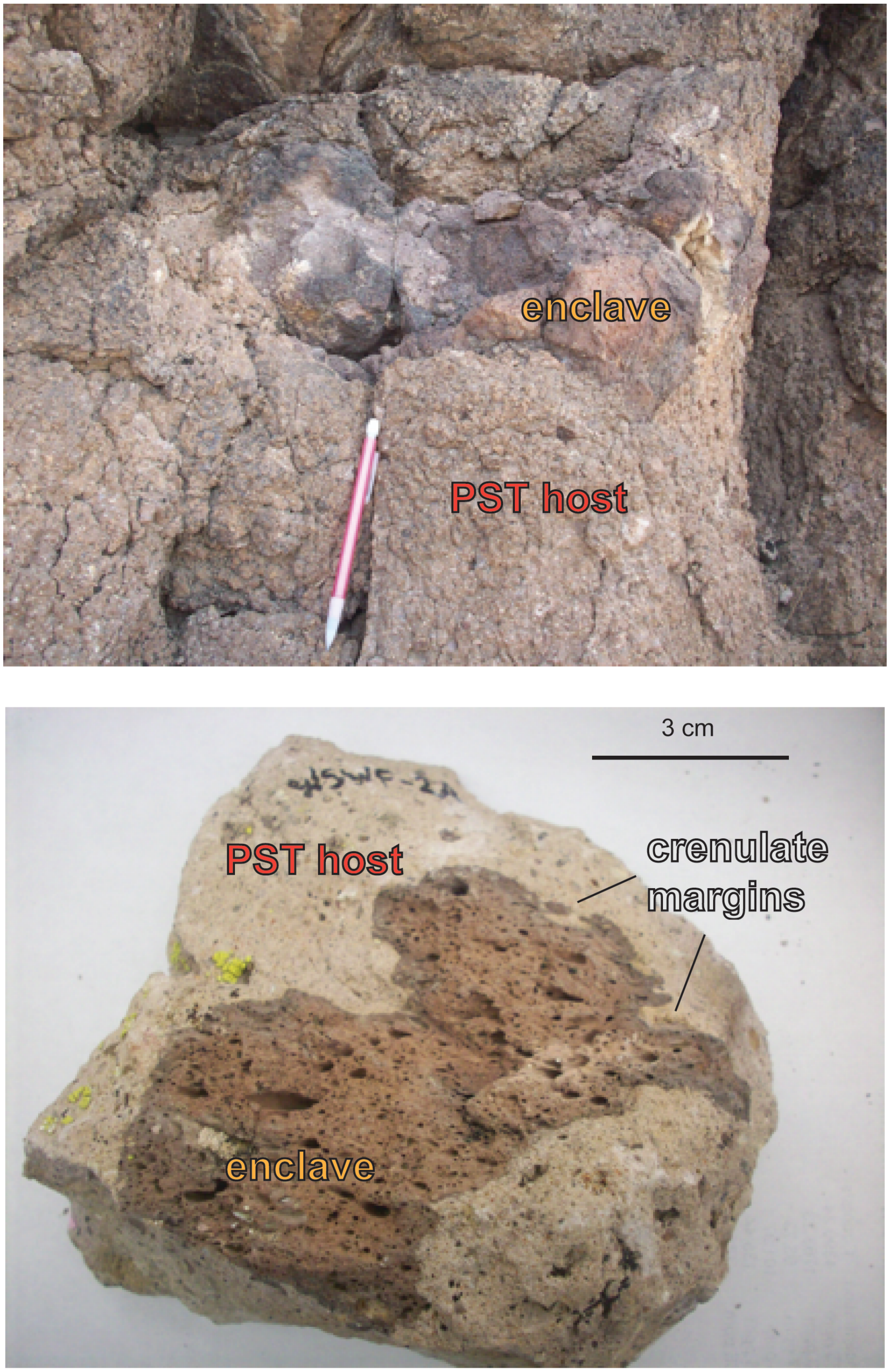

Figure 14a. Two of the enclaves from Warm Springs West (WSWF-3 above, WSWF-2A, below), showing the range in size. Pencil is 15 cm.

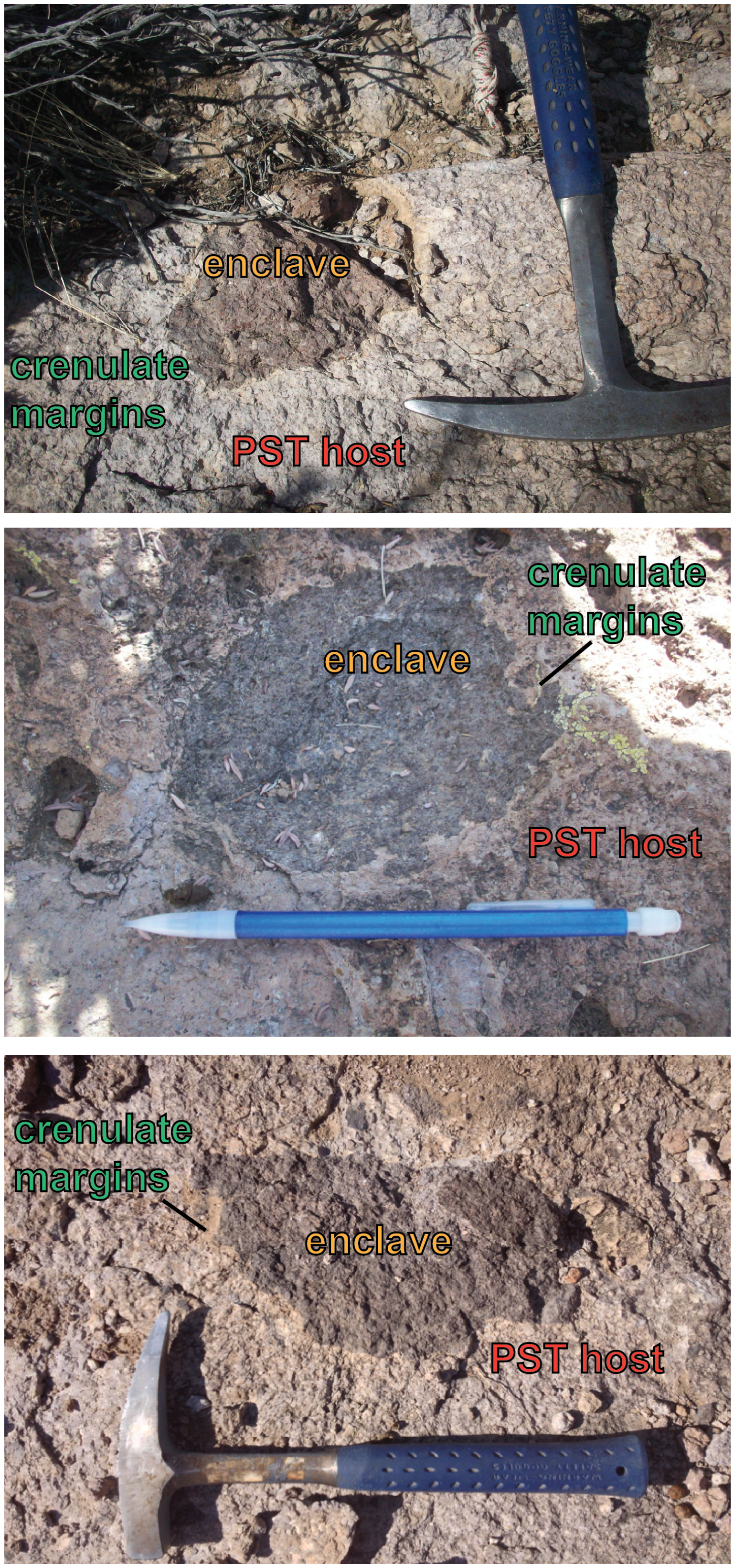

Figure 14b. Enclaves from northwest of Kingman, Arizona. None sampled, but at same location as KPF-1 through KPF-8. Pencil is 15 cm.

Petrography

Thin sections of nine samples revealed distinct types of lavas in the region. Samples MBF-1, MBF-4, WSWF-1, and CS-MF1 looked distinctly mafic and were similar in thin section. Sample MBF-5 is from the Esperanza Trachyte. Samples SPF-1A, SPF-1B, and SPF-2 were similar in appearance and were from the region just below the Peach Spring Tuff unconformity. Sample RWF-1 is from the thick trachyte sequence below the units of interest in this study and will not be discussed in depth.

Thin section MBF-5 is of the Esperanza trachyte at McHeffy Butte. As it was in hand sample, it was nearly aphyric with less than 1% phenocrysts. Phenocrysts that did exist were generally < 2 mm and consisted of elongate plagioclase, rare biotite, and iron-oxides from alteration of either olivine or pyroxene (Figure 15a). The groundmass was fine-grained plagioclase, often with flow orientation around phenocrysts.

Thin sections MBF-1 (Figure 15b) and MBF-4 were both from the mafic lava flows at McHeffy Butte. These samples were fairly similar, with 10% and 5 % phenocrysts respectively. Phenocryst assemblage was dominantly plagioclase (2-4 mm) with clusters of clinopyroxene (clusters 1-5 mm) and alteration products of olivine. Plagioclase crystals commonly had reaction rims (Figure 15c). The groundmass was composed of fine-grained plagioclase, often oriented in one direction, presumably that of flow (Figure 15d). These samples were heavily vesiculated and many vesicles contained secondary minerals such as quartz.

WSWF-1 was from a mafic lava lying directly below the Peach Spring Tuff at Warm Springs West and also contained reaction rims around plagioclase and clustered clinopyroxene (Figure 15e). CS-MF1 from Caliche Springs was strikingly similar to WSWF-1 in thin section. Both thin sections displayed 15-20% phenocrysts of plagioclase (2-5mm), zoned clinopyroxene (0.5-3mm) (Figure 15f), olivine (2 mm), and alteration products of olivine. CS-MF1, while displaying clustered clinopyroxene like WSWF-1, also contained secondary iron-oxide minerals (Figure 15g). The groundmass here was also composed of fine-grained plagioclase.

Thin sections from the Secret Pass wash (SPF-1A, SPF-1B, and SPF-2) were distinct from the previously described mafic units and the Esperanza Trachyte. SPF-1A was from the red "host" body shown in Figure 12b and SPF-1B contained the contact between the gray body and the red body. SPF-2 was from the gray/purple body shown in Figure 12b and was typically more mafic than SPF-1A and SPF-1B. In thin section, SPF-1A had a red, swirled or banded appearance with what appeared to be 2-5 mm blebs of different, more phenocryst-rich, lava within it. These blebs had sharp edges and are likely lithic clasts. The red host contained 5% rounded crystals, dominantly zoned plagioclase (70%) and clinopyroxene (30%) (Figure 15h). Secondary minerals included magnetite, ilmenite, and chlorite.

SPF-1B in thin section displayed identical characteristics in its red host body as SPF-1A. The gray lithic clast in SPF-1B contained approximately 30% phenocrysts, with 70% plagioclase, 25% biotite, and 5% clinopyroxene. This lithic clast had a sharp contact with the red "host" body (Figure 15i). Sample SPF-2 was fairly similar to SPF-1A but lacks the banded appearance in thin-section. The sample contained 5% phenocrysts, with over 95% of those being plagioclase and approximately 5% being clinopyroxene. The larger plagioclase crystals were clumped together in clusters. The fine-grained plagioclase groundmass appeared blocky instead of needle-like as in the samples from McHeffy Butte, Warm Springs West, and Caliche Springs. The red "host" bodies in these Secret Pass wash samples are likely volcanogenic sediments (Lee et al., 2014).

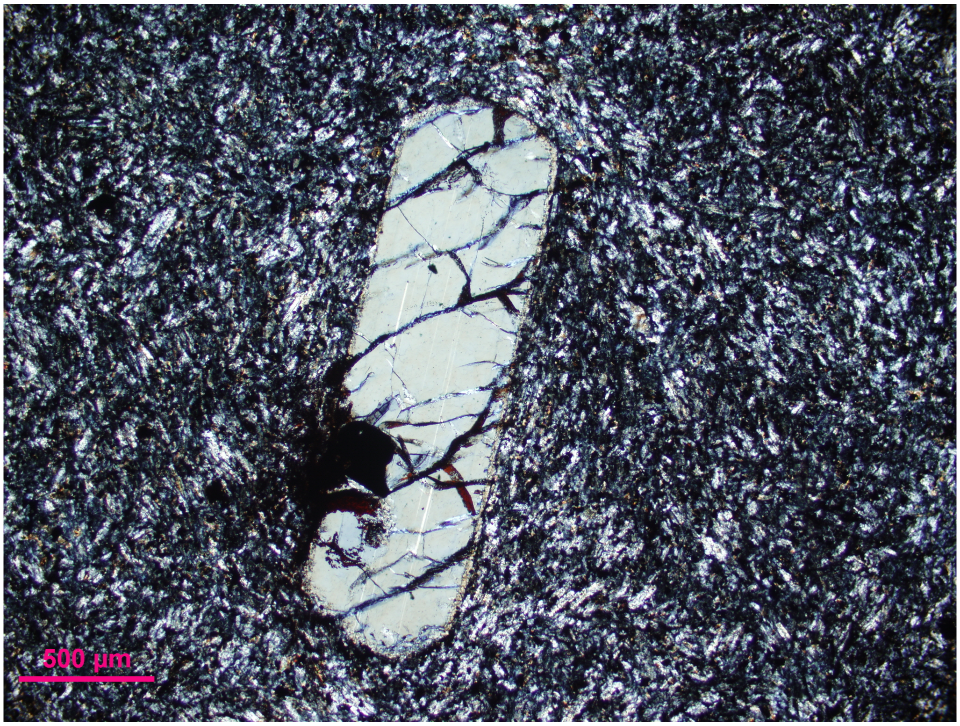

Figure 15a. Micrograph of MBF-5 (Esperanza Trachyte) in XPL. One long (2 mm) plagioclase crystal with a reaction rim in the fine-grained plagioclase groundmass.

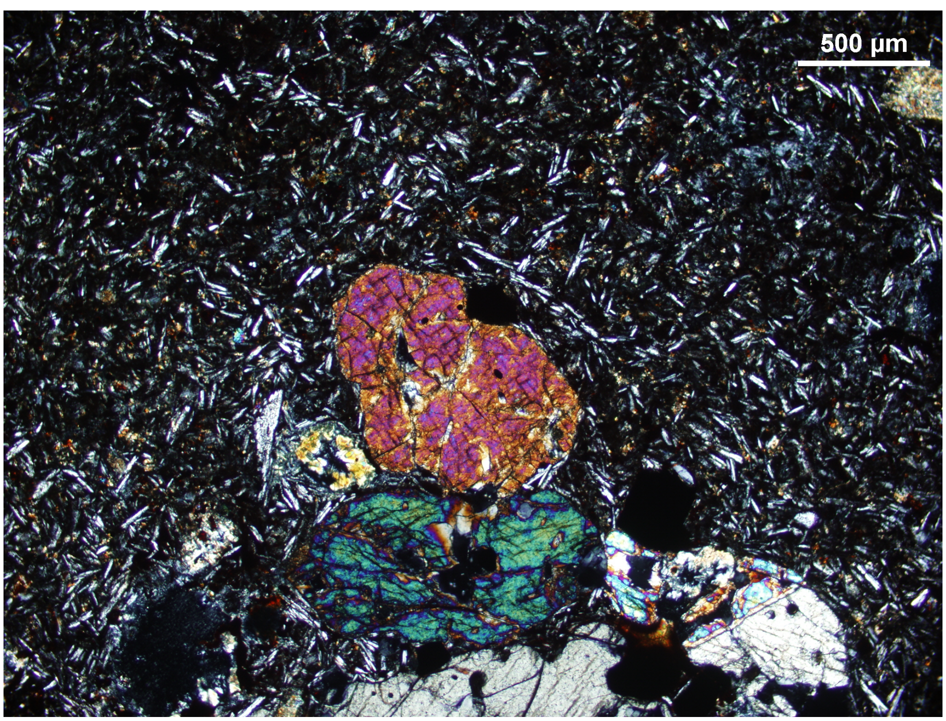

Figure 15b. Micrograph of MBF-1 in XPL, showing clustered clinopyroxene.

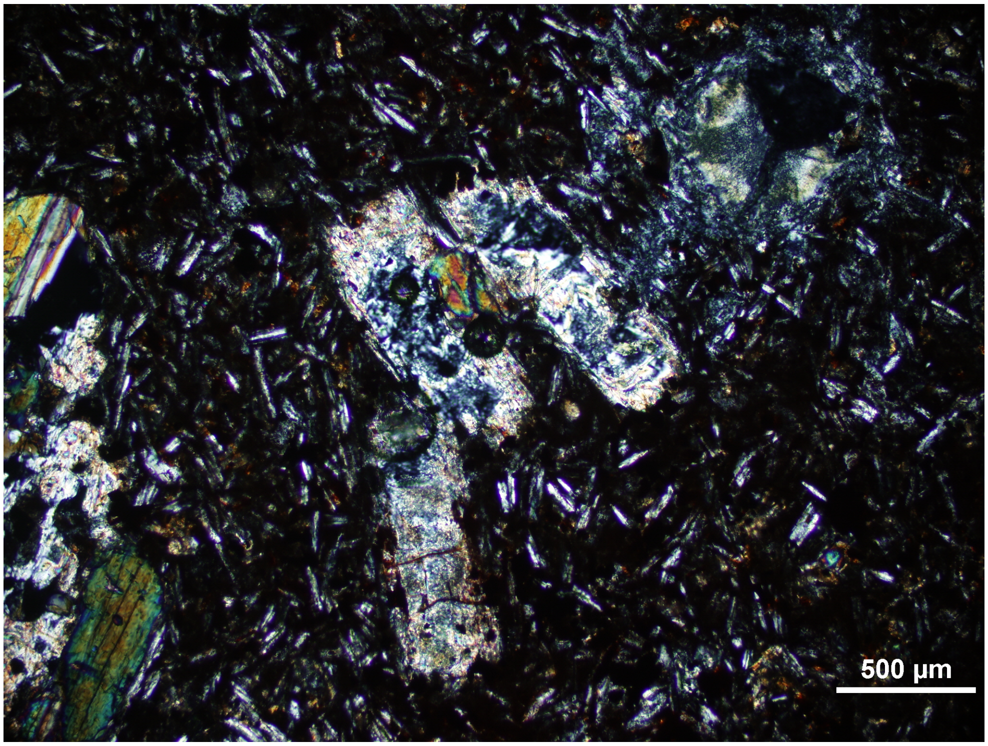

Figure 15c. Micrograph of MBF-1 in XPL, showing reaction rims around plagioclase crystals.

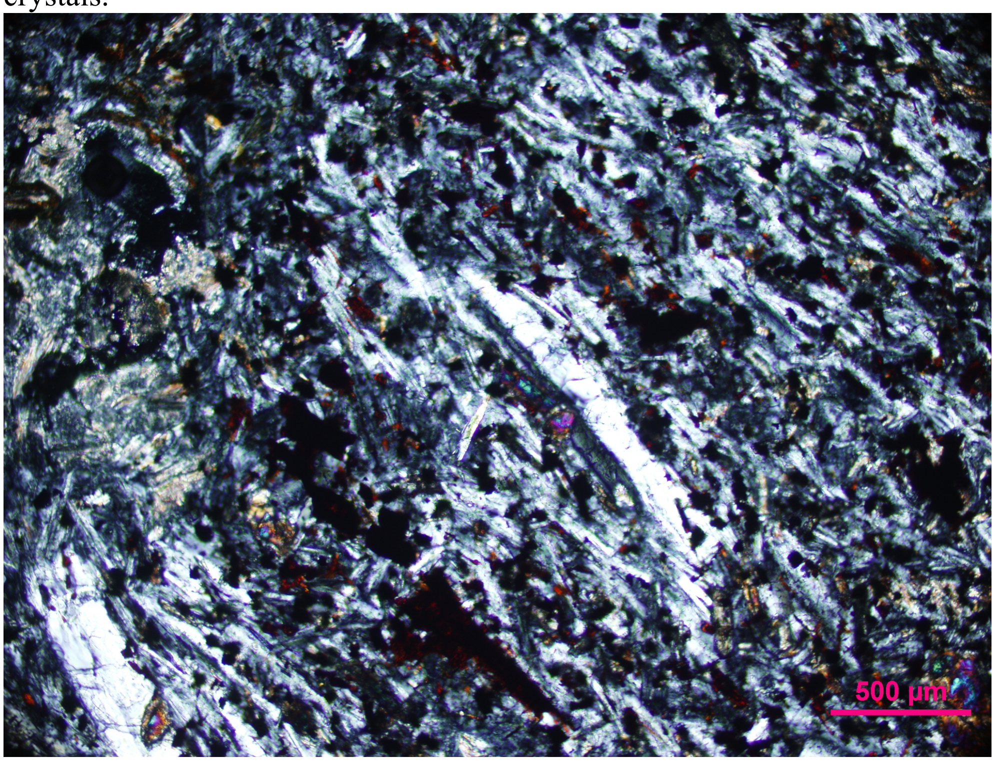

Figure 15d. Micrograph of MBF-4 in XPL, showing flow-oriented plagioclase groundmass with a 1 mm plagiclase crystal in the middle of the image.

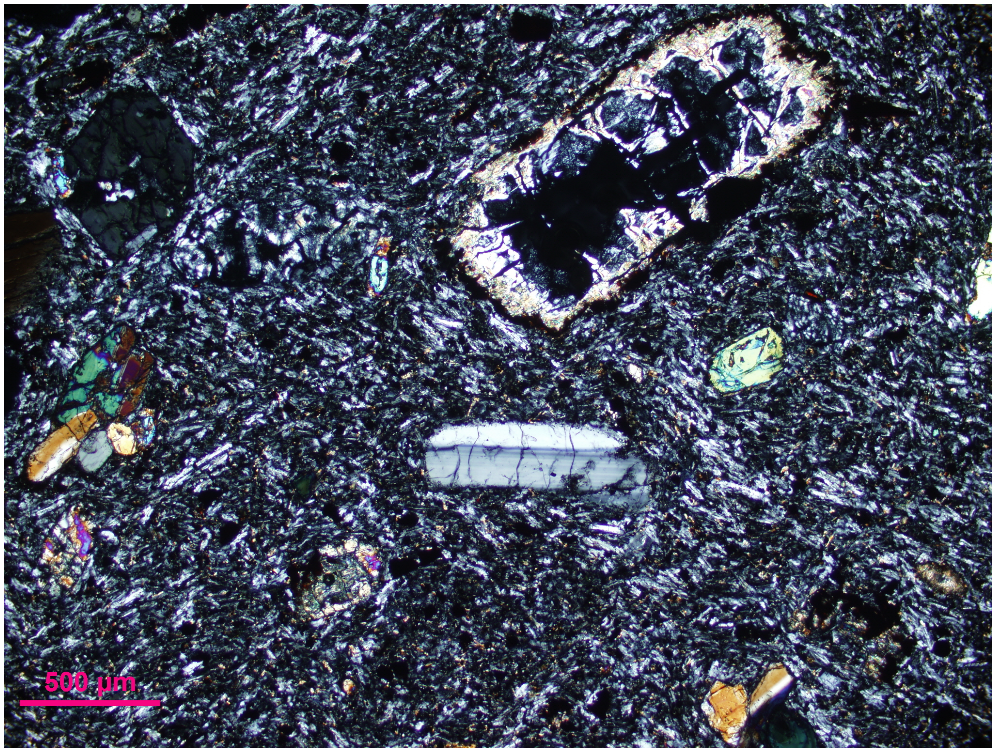

Figure 15e. Micrograph of WSWF-1 in XPL. Clinopyroxene clusters, twinned plagioclase, olivine, and a reaction rim are evident.

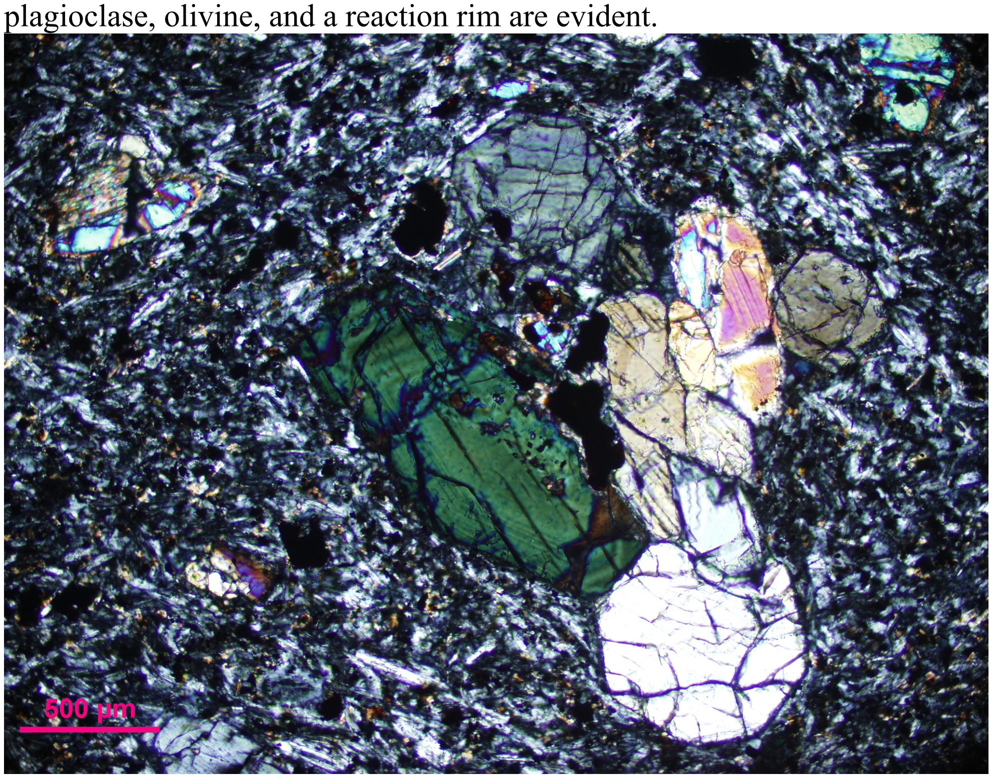

Figure 15f. Micrograph of a zoned clinopyroxene in WSWF-1 in XPL.

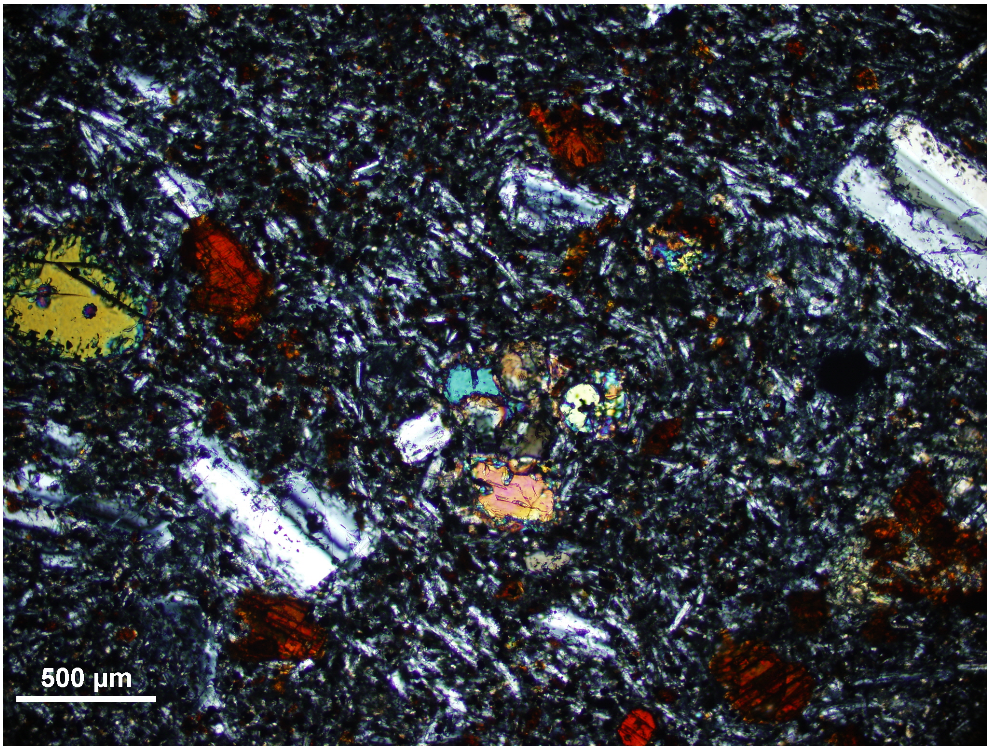

Figure 15g. Micrograph of CS-MF1 in XPL showing a cluster of clinopyroxene and fine plagioclase groundmass. The sample also contains many iron oxides as secondary minerals.

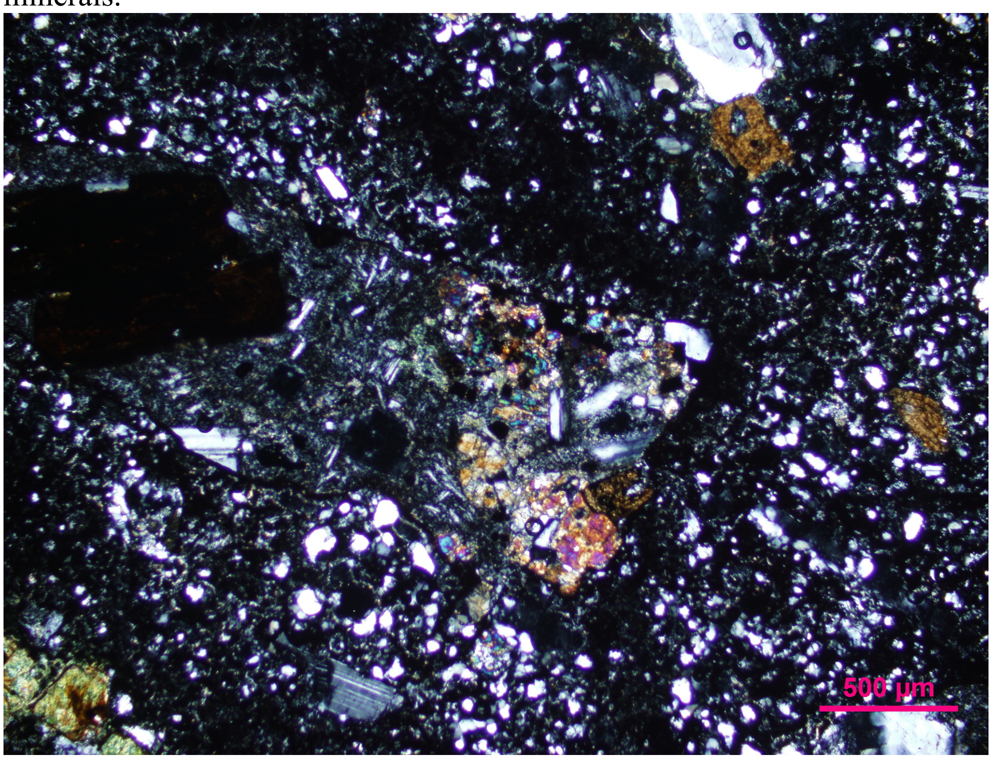

Figure 15h. Micrograph of SPF-1A in XPL. A small clinopyroxene cluster is present in the center.

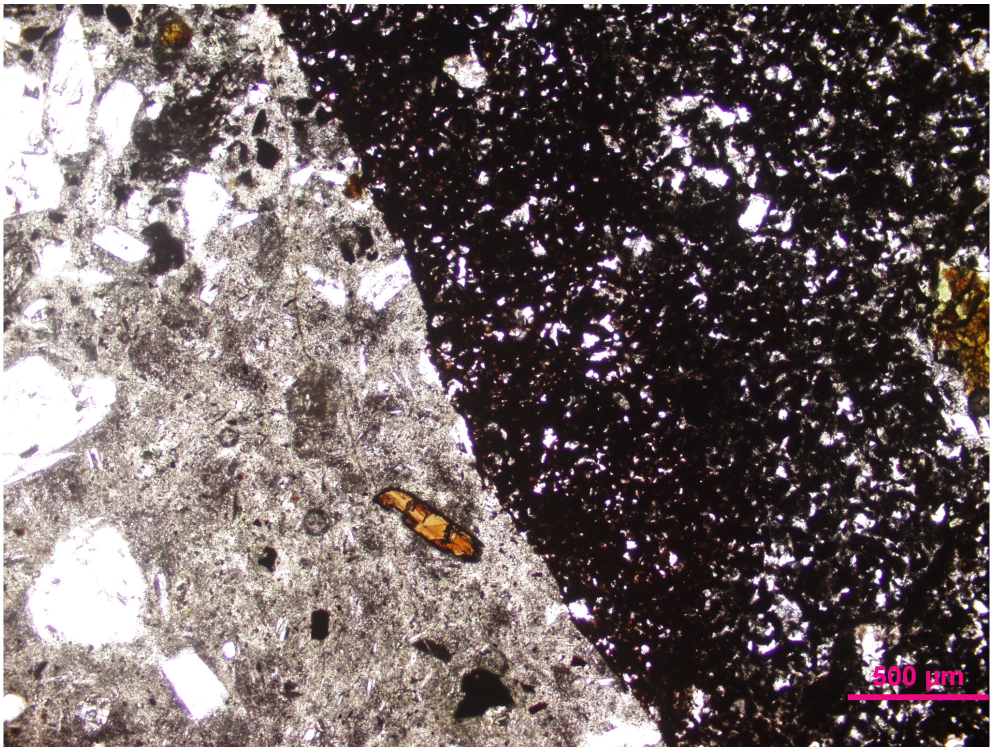

Figure 15i. Micrograph of the contact between the red (right) and gray (left) bodies of SPF-1B in PPL. The gray body shows plagioclase and biotite, the red body shows some plagioclase but is much finer grained and is likely composed of volcanogenic sediments.

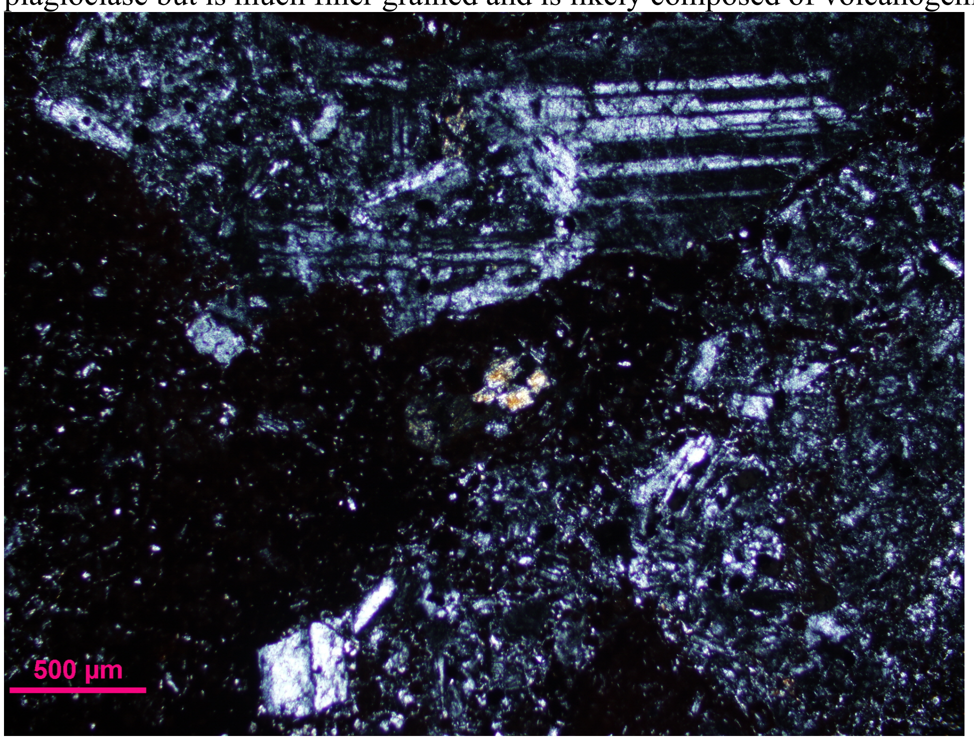

Figure 15j. Micrograph of SPF-2 in XPL. Some larger plagioclase crystals are present within the finer-grained plagioclase groundmass.

Thin sections of magmatic enclaves included samples WSWF-3, WSWF-5, KPF-5, and KPF-6. Samples WSWF-3 and WSWF-5 were similar mineralogically, though their appearance differs: WSWF-3 appeared much more altered than WSWF-5, giving it a brown appearance in plane-polarized light. Phenocrysts (15%) in WSWF-3 were 45% elongate plagioclase (2-4 mm) some of which was zoned, 45% clinopyroxene clusters, and possibly some altered olivine (5%). Opaques and iron oxides were also present in relatively small amounts. Plagioclase phenocrysts within WSWF-3 locally had reaction rims and replacement minerals (micas) surrounding them (Figure 16a). Phenocrysts in WSWF-5 were 15% abundant and were also elongate plagioclase crystals (50%) and clinopyroxene (40%) with alterations of olivine (10%) (Figure 16b). Sample WSWF-5 looked fairly similar to lava sample WSWF-1 (Figure 16e).

Thin section KPF-5 contained 10% phenocrysts, dominantly elongate plagioclase (2-4 mm) (75%) and minor amounts of clinopyroxene (< 5%) in a fine but blocky plagioclase matrix. Plagioclase was typically zoned and twinned (Figure 16c). Crystals also included alteration products such as biotite and weathering products such as iron-oxides (20% of phenocrysts). KPF-6, though from the same location and bearing the same alteration marks such as biotite, differed from KPF-5 and contained 15% phenocrysts. Phenocrysts in KPF-6 were dominantly blocky plagioclase (70%, 2-4 mm) (Figure 16d), minor clinopyroxene (< 1%), and biotite (20%) from weathering. On the whole, the Kingman enclaves contained more plagioclase, less clinopyroxene, and more biotite (as an alteration product) than did the Warm Springs West enclaves.

A comparison of these magmatic enclaves within the Peach Spring Tuff would be incomplete without looking at Pamukcu et al. (2013)'s definitive enclave identified previously from Warm Springs West. The thin section of WSWPST-1 clearly displayed crenulate margins and contained 10% phenocrysts composed of 70% plagioclase and 30% clinopyroxene with minor amounts of apatite. Some of the clinopyroxene phenocrysts were zoned and the sample also had a fine-grained plagioclase groundmass.

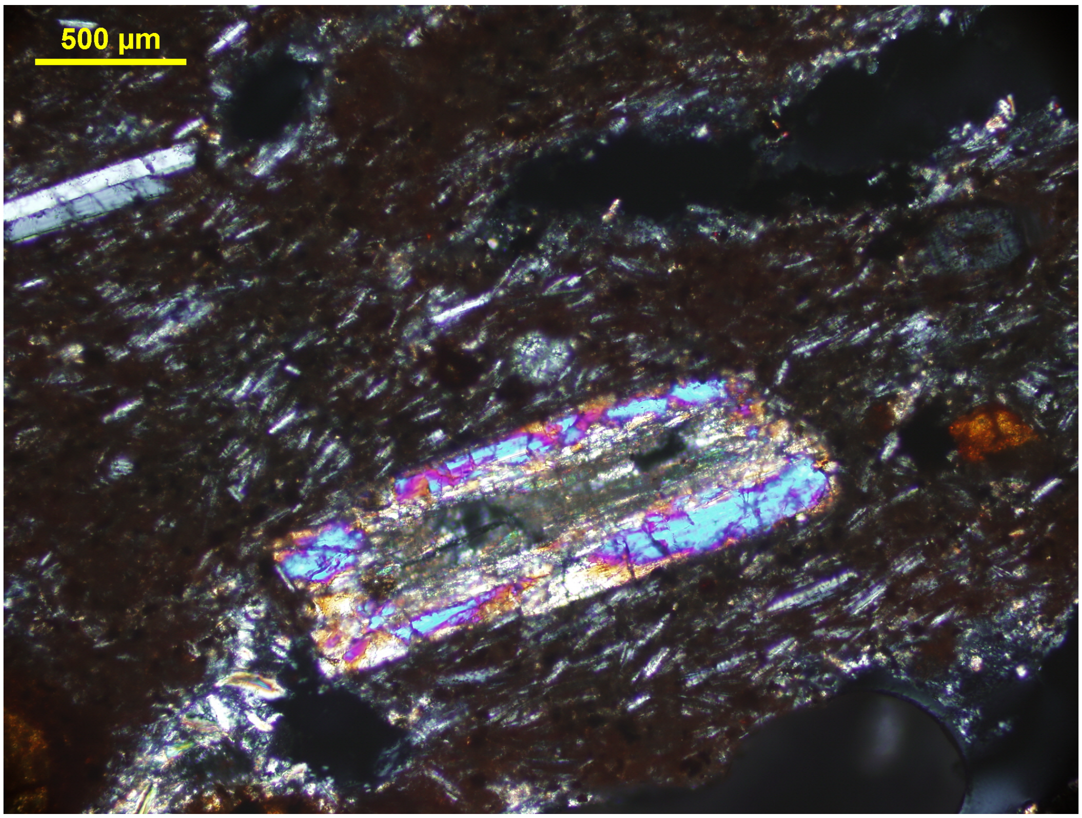

Figure 16a. Micrograph of WSWF-3 in XPL. A reaction rim on plagioclase is in the center of the micrograph.

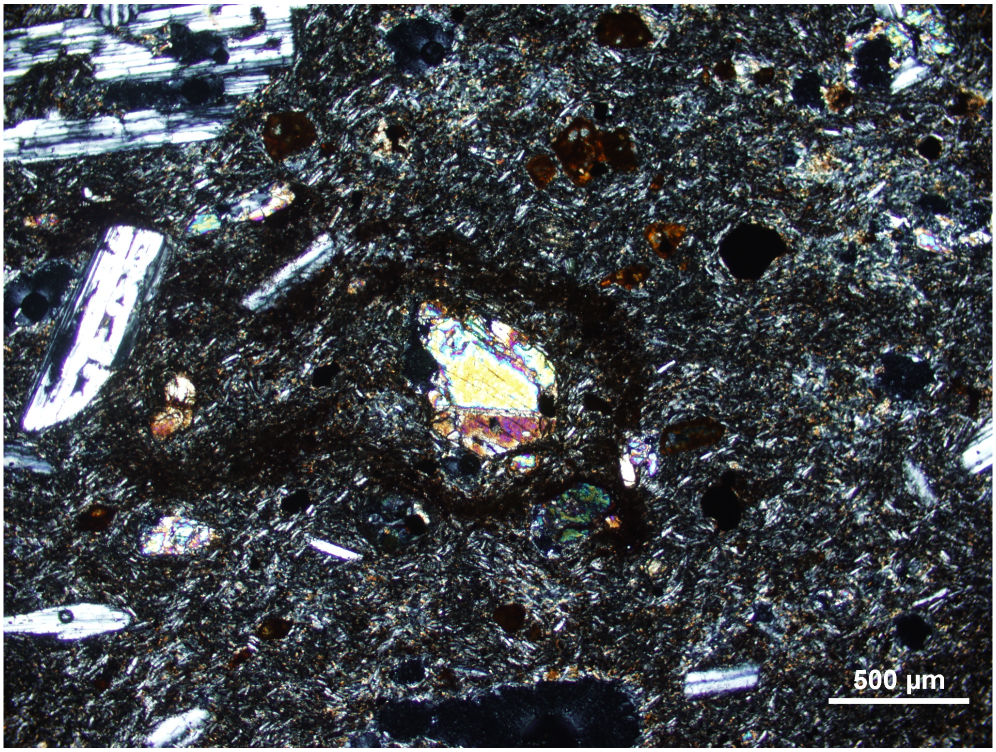

Figure 16b. Micrograph of WSWF-5 in XPL. A reaction rim on a clinopyroxene crystal is in the center of the image and elongate plagioclases can be seen on the left side of the image.

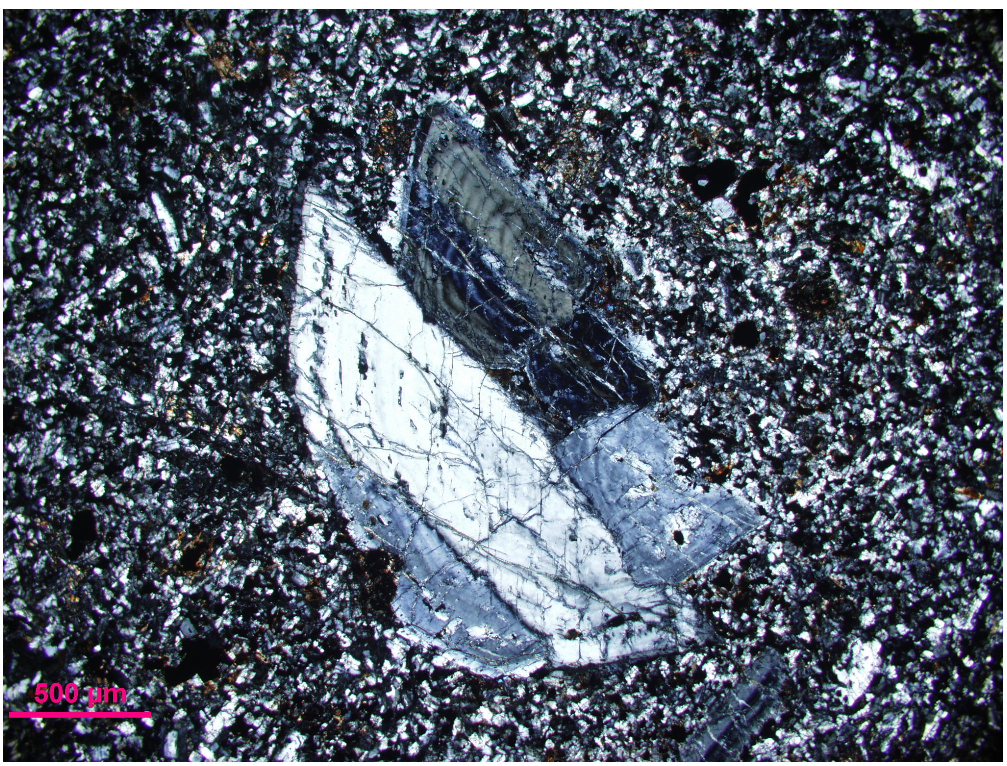

Figure 16c. Micrograph of a zoned, twinned, blocky plagioclase crystal within the fine plagioclase groundmass of KPF-5 in XPL.

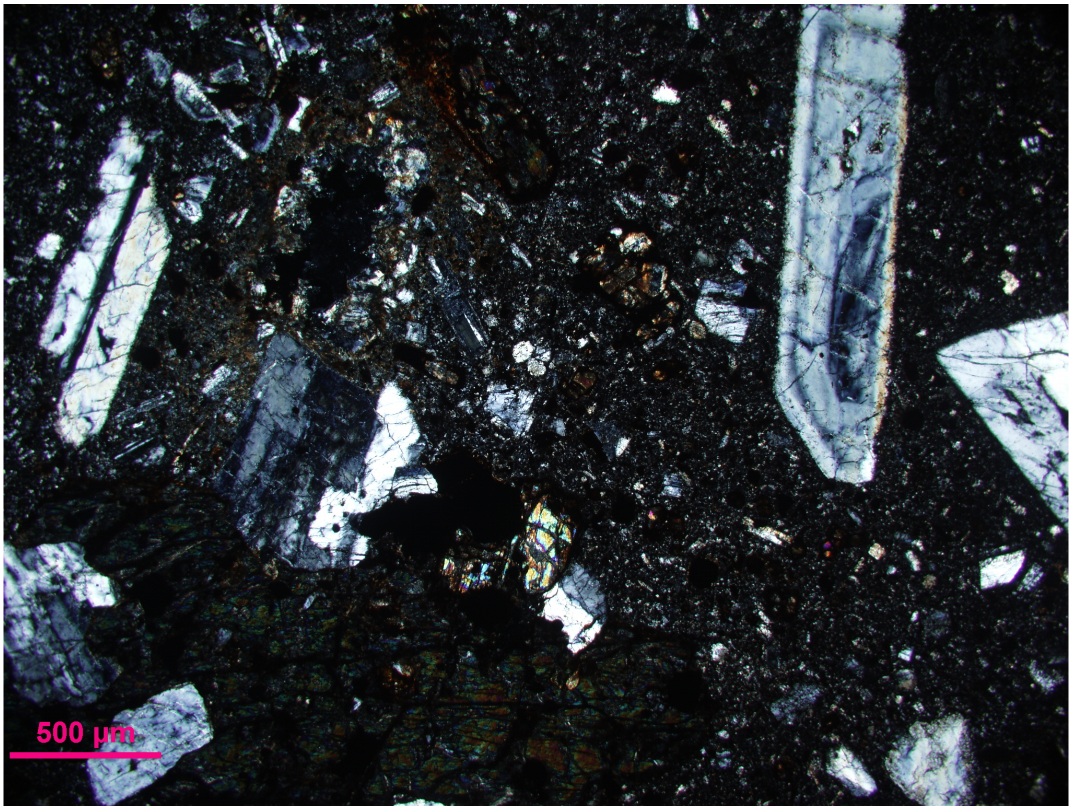

Figure 16d. Micrograph showing an elongate, zoned plagioclase crystal in KPF-6 in XPL.

Whole Rock Geochemistry

X-ray fluorescence analyses done at MTSU gave a range from 49% to 62% SiO_2 for the mafic to intermediate lavas. XRF analysis yielded 62% SiO_2 for the Esperanza trachyte, placing it just within the trachyte range. We classified the lava and the enclave samples based on their weight percent Na_2O and K_2O against their silica content on a Total Alkali Silica diagram (Figure 17). The lavas we analyzed (MBF-1, MBF-4, MBF-5, WSWF-1, CS-MF1, SPF-1A, SPF-1B, and SPF-2) ranged from the most mafic in the trachy-basalt field to the trachytic Esperanza (MBF-5, the high-silica outlier). The high-silica, low alkali outlier (SPF-1A) plotted within the andesite field, though this was due to low %Na_2O. Magmatic enclaves (WSWF-3, WSWF-5, KPF-5, and KPF-6) shared a similar range of SiO_2 content, from 53% to 61%, within the basaltic trachy-andesite and trachy-andesite fields (Figure 17).

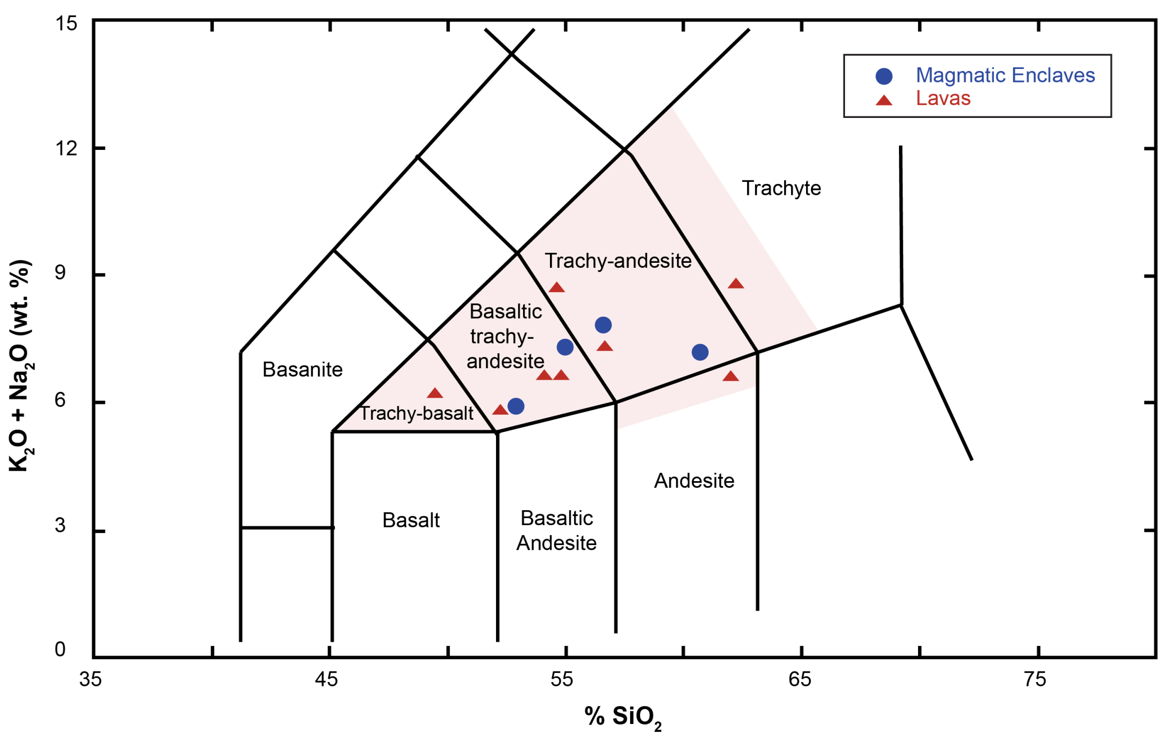

Figure 17. TAS diagram showing the 12 samples (8 lavas and 4 enclaves) based on their alkali and silica content obtained through XRF. The pink shading highlights fields where the samples plot.

The TAS classification showed two outliers: the high silica outlier and the low-alkali outlier. The high-silica outlier plotted in the trachyte field and is the Esperanza Trachyte sample (MBF-5). The low-alkali outlier plotted in the andesite field and is a lava sampled in the wash at Secret Pass (SPF-1A). This plotted within the andesite field because its %Na_2O is extremely low for volcanic rocks in the region and this was possibly due to instrumentation error, but more likely was due to alteration. The major element compositions for the lavas and the enclaves analyzed are shown in Tables 1 and 2, respectively.

SAMPLE	SiO_2	Al_2O_3	Fe_2O_3	Adjusted Fe_2O_3	FeO	MnO	MgO	CaO	Na_2O	K_2O	TiO_2	P_2O_5	Total
MBF-1	54.79	18.17	8.27	2.48	5.79	0.03	3.82	6.47	3.18	3.52	1.27	0.49	**100**
MBF-4	49.44	19.03	10.99	3.30	7.69	0.07	3.48	8.06	3.68	2.60	1.89	0.76	**100**
AVG MBF-5	62.21	17.99	5.15	1.55	3.61	0.09	0.82	3.43	4.67	4.20	0.92	0.52	**100**
WSWF-1	54.04	16.24	8.56	2.57	5.99	0.07	4.61	7.54	3.06	3.66	1.37	0.85	**100**
AVG CS-MF1	52.24	17.58	8.99	2.70	6.29	0.08	4.59	8.69	3.21	2.69	1.29	0.63	**100**
SPF-1A	61.97	15.11	7.85	2.36	5.50	0.04	2.19	4.56	2.07	4.60	1.08	0.52	**100**
SPF-1B	54.60	19.34	7.75	2.33	5.43	0.11	2.41	5.49	3.43	5.36	1.01	0.50	**100**
SPF-2	56.65	20.02	7.37	2.21	5.16	0.14	2.15	4.50	3.58	3.82	1.25	0.52	**100**

Table 1. Normalized whole rock geochemistry data of the major elements for the eight lava samples analyzed by XRF.

SAMPLE	SiO_2	Al_2O_3	Fe_2O_3	Adjusted Fe_2O_3	Fe0	MnO	MgO	CaO	Na_2O	K_2O	TiO_2	P_2O_5	Total
WSWF-3	54.96	17.63	9.06	2.72	6.35	0.05	2.89	5.97	2.97	4.33	1.30	0.83	**100**
WSWF-5	52.83	17.61	8.45	2.54	5.92	0.08	4.61	8.70	3.20	2.69	1.20	0.63	**100**
KPF-5	56.57	17.98	8.04	2.41	5.63	0.17	2.85	4.12	3.71	4.11	1.63	0.82	**100**
KPF-6	60.66	16.96	7.04	2.11	4.93	0.09	2.72	3.99	3.27	3.92	0.99	0.37	**100**

Table 2. Normalized whole rock geochemistry data of the major elements for the four enclave samples analyzed by XRF.

The weight percentage of other oxides was also plotted against weight percentage SiO_2. Lava samples ranged from approximately 4.5-9% CaO and magmatic enclaves ranged from approximately 4-9% CaO. Percent K_2O was also within a similar range for both the lavas and the enclaves: from 2.5-5.5% for the former and 2.5-4.5% for the latter. Phosphorus also showed similarity between the enclaves and the lavas in P_2O_5 weight percent: lavas ranged from approximately 0.5-0.9% and enclaves had a very similar range of approximately 0.3-0.8%. As silica content increased, CaO and P_2O_5 content decreased, while K_2O content increased (Figure 18a).

Iron and magnesium oxides occurred in relatively high amounts across sample types. Lavas ranged from approximately 5-11% Fe_2O_3(tot) while the enclaves had a smaller range of 7-9% Fe_2O_3(tot). Magnesium oxide ranges were very similar between lavas and enclaves: both have a range of approximately 2-5% MgO (the 1% MgO outlier is the Esperanza Trachyte). These oxide weights are shown in Figure 19b, as well as Mg# (see Tables 1 and 2 in Appendix B). Not surprisingly, MgO and Fe_2O_3(tot) content both decreased as silica content increased. A similar trend is shown for Mg# (Figure 18b). Harker diagrams of major elements are on the following few pages. The data appears to plot over a large range because of the narrow range on the y-axis in comparison to the range of the x-axis (silica content).

Other major element Harker diagrams also showed similarity between the the pre-Peach Spring Tuff mafic lavas and the Peach Spring Tuff magmatic enclaves. Aluminum oxide ranged from 16-20% in the lava samples (Esperanza Trachyte excluded) and from 17-18% in the enclave sampels. Weight percentage Na_2O clusters between 3% and 3.5% for both sample types. The low-Na2O outlier is SPF-1A, at around 2% Na2O, and the high-Na2O outlier is MBF-5, the Esperanza Trachyte, and both are excluded from this range. Finally, %TiO2 was in a range of 1-1.9% for the lava samples and ranged from 1-1.6% for the enclaves. These three Harker plots are shown in Figure 18c.

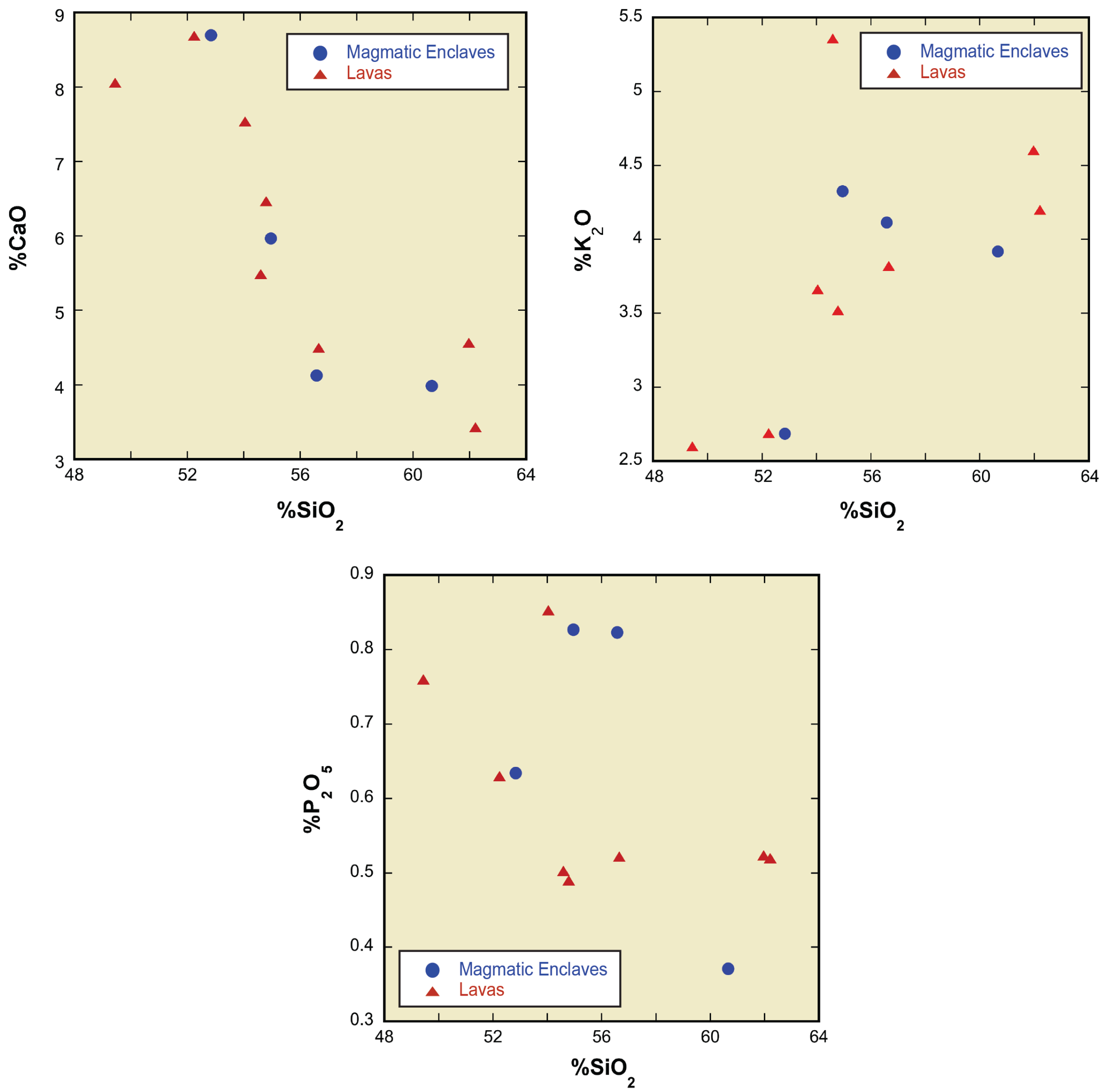

Figure 18a. Harker diagrams: CaO, K_2O, and P_2O_5 weight percentages plotted against weight percent SiO_2. The high-silica outlier is the Esperanza Trachyte (MBF-5).

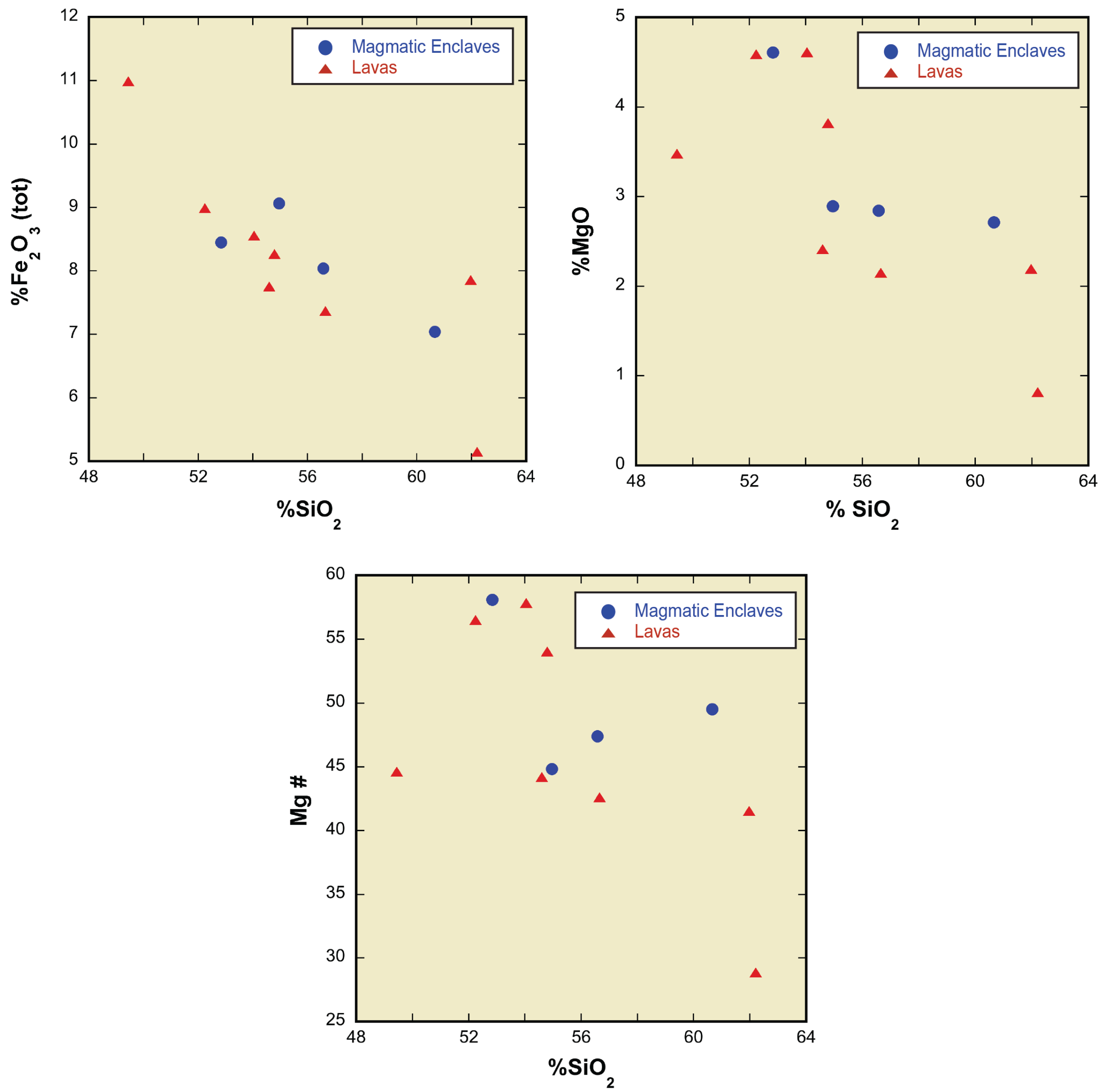

Figure 18b. Harker diagrams: Fe_2O_3(tot) content, MgO content, and Mg# plotted against weight percent SiO_2. The high-silica outlier is the Esperanza Trachyte (MBF-5).

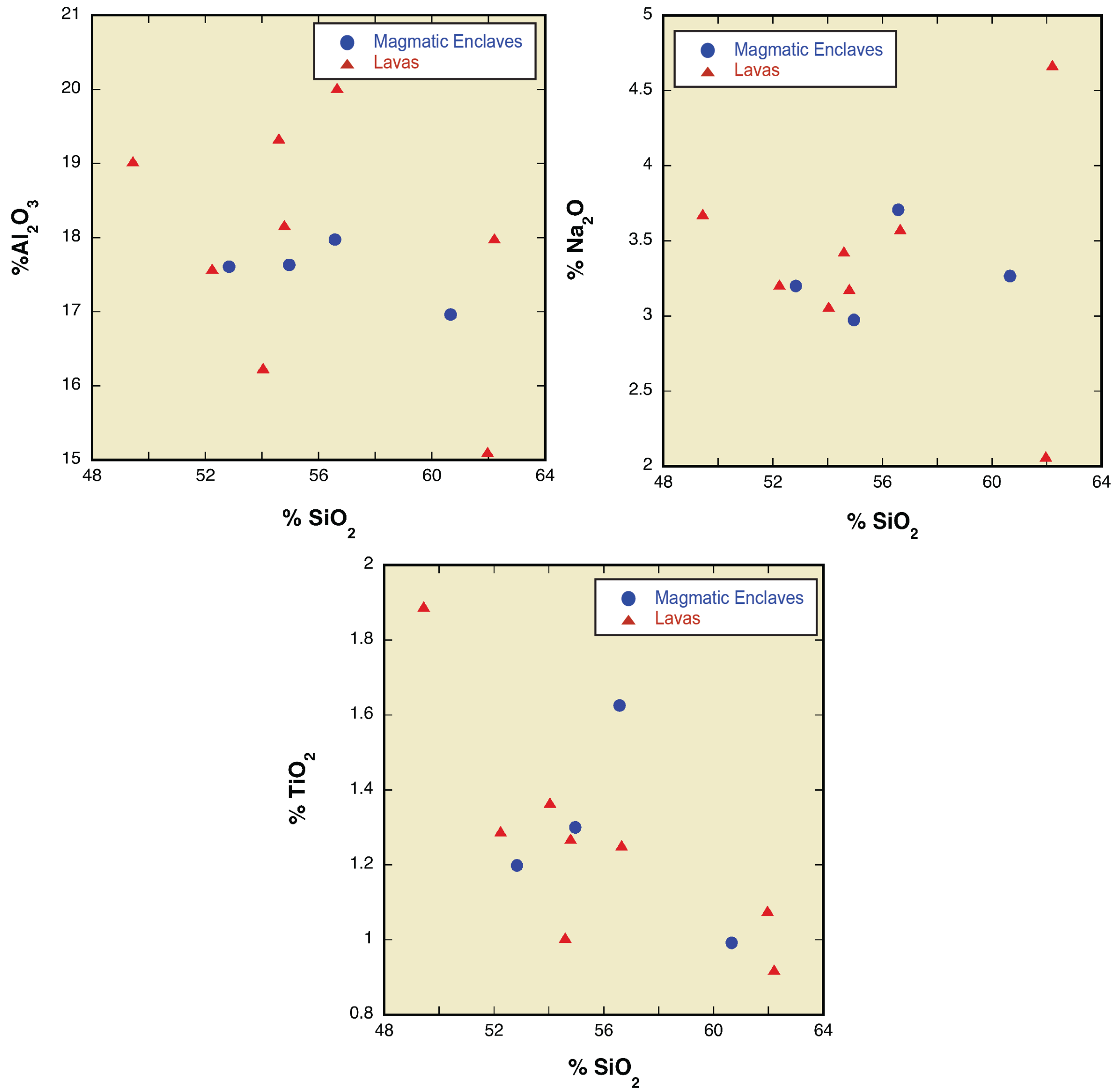

Figure 18c. Harker diagrams: Al_2O_3 content, Na_2O content, and TiO_2 content plotted against weight percent SiO_2. The high-silica outlier is the Esperanza Trachyte (MBF-5). The low-sodium outlier is a lava from Secret Pass Wash (SPF-1A).

Selected minor elements were also analyzed by XRF (Tables 3 and 4 below). Minor elements further the comparison between the pre-Peach Spring Tuff mafic lavas and the Peach Spring Tuff magmatic enclaves by displaying similarities (Figure 19). Of the selected minor elements, the lavas and enclaves ranged as follows:

- ppm Ba: Lavas ~1200-1800, magmatic enclaves ~1150-1800
- ppm Rb: Lavas ~15-85, magmatic enclaves ~10-90
- ppm Sr: Lavas ~700-1350, magmatic enclaves ~750-1400
- ppm Zr: Lavas ~275-425, magmatic enlcaves ~360-450

SAMPLE	Sr (ppm)	Zr (ppm)	Rb (ppm)	Y (ppm)	Nb (ppm)	Ba (ppm)
MBF-1	920	346	67	16	12	1279
MBF-4	1128	335	33	16	11	1105
AVG MBF-5	1050	380	107	13	15	2285
WSWF-1	1342	432	85	17	20	1746
AVG CS-MF1	1098	328	43	17	13	1300
SPF-1A	687	276	16	7	0.1	1149
SPF-1B	816	402	71	9	10	1813
SPF-2	832	277	54	11	7	1477

Table 3. Minor elements detected with XRF of the eight lava samples analyzed.

SAMPLE	Sr (ppm)	Zr (ppm)	Rb (ppm)	Y (ppm)	Nb (ppm)	Ba (ppm)
WSWF-3	1327	405	12	6	2	1500
WSWF-5	1398	444	87	15	17	1809
KPF-5	850	398	58	14	12	1210
KPF-6	720	363	40	10	2	1081

Table 4. Minor elements detected with XRF of the four enclaves analyzed.

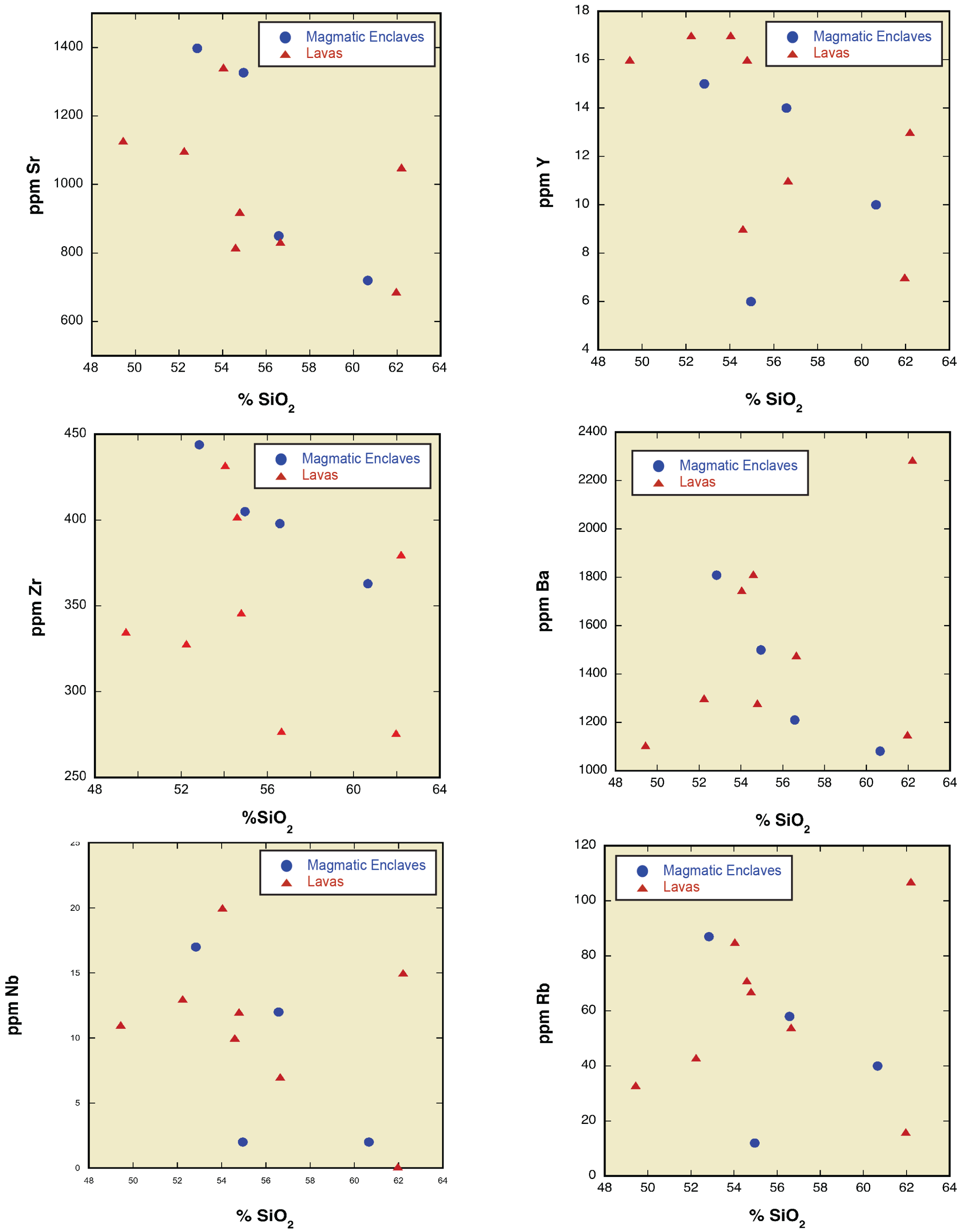

Figure 19. Harker diagrams: selected minor elements detected with XRF. Lavas and enclaves plot within similar ranges. The high-silica outlier is the Esperanza Trachyte (MBF-5).

Full Elemental Analyses with Induced Coupled Plasma Mass Spectroscopy

Rare earth elements provided another comparison between the two sample types. The similarity between the two sample types and among all of the samples was significant, particularly in REE composition (Figure 20). The full analyses are given in Tables 1, 2, 3, and 4 of Appendix D along with analyses of the enclave identified by Pamukcu et al. (2013), WSW-PST1. All of the samples were enriched in what are considered incompatible elements for mantle minerals—elements such as K, Rb, Ba, Sr, and rare earth elements (REE).

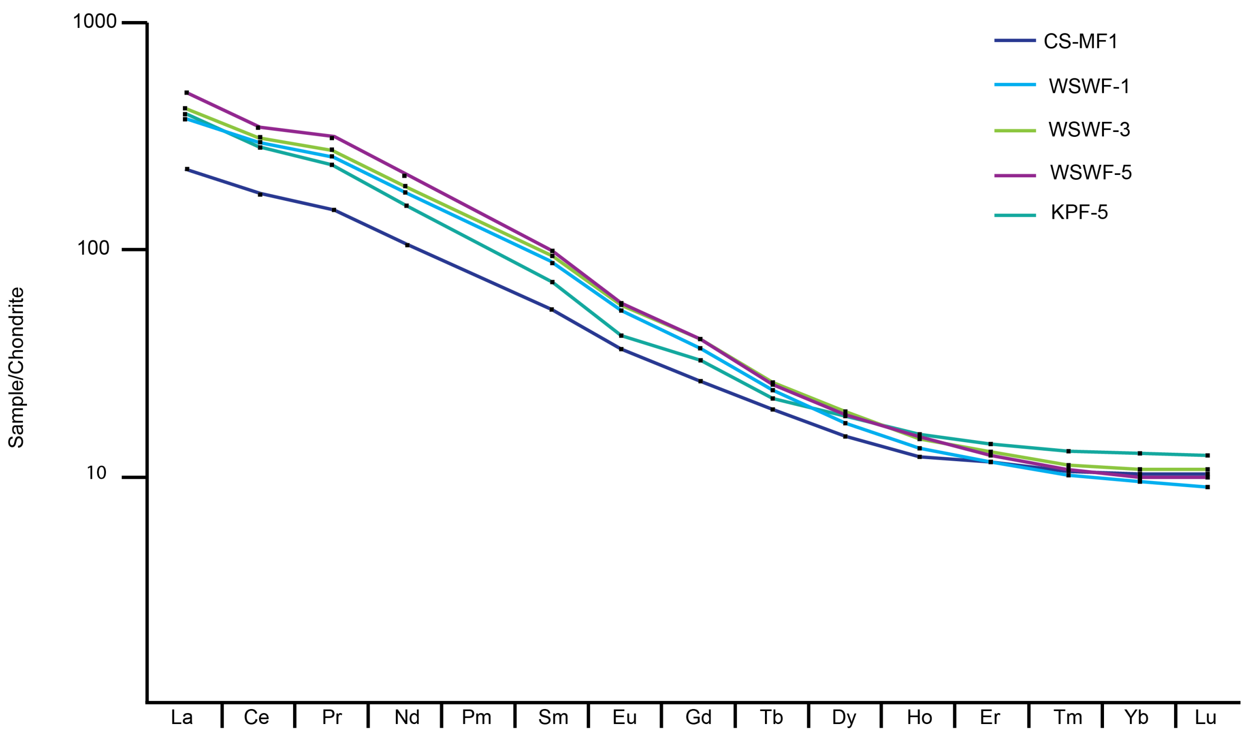

Figure 20. Chondrite-normalized, rare earth element plot of two lavas (WSWF-1 and CS-MF1) and three enclaves (WSWF-3, WSWF-5, and KPF-5) analyzed with ICP-MS. Chondrite from ActLabs.

Scanning Electron Microscope Analyses

The scanning electron microscope (SEM) was used primarily to determine elemental compositions of zoned phenocrysts and of the groundmass, as well as to identify any accessory minerals such as microphenocrysts of apatite or zircon. We analyzed lavas MBF-1, MBF-4, MBF-5, WSWF-1, SPF-1A, and SPF-1B and enclaves WSWF-5 and KPF-5. Zoned phenocrysts included clinopyroxene and plagioclase feldspar. In general, zoned clinopyroxenes were normally zoned with iron-rich rims and magnesium-rich cores (Table 1 in Appendix E). Zoned clinopyroxene crystals were typically elongate, rather than blocky (Figure 21a).

Zoned plagioclase feldspars in the lava samples generally contained more calcium in their cores and more sodium in their rims (Figure 21b). This is evidence of normal zoning, as is expected for hot mafic magmas injected into cooler felsic ones. Interestingly, though phenocrysts commonly appeared zoned in enclave samples in thin section, the calcium and sodium content of the zones is relatively constant in SEM analysis (Table 2 in Appendix E). The groundmass composition, in both lava and enclave samples, was very close to that of the rims of zoned plagioclase feldspars, suggesting a mostly sodium plagioclase melt body at the time of cooling (Table 3 in Appendix E).

Microphenocrysts consisted of apatite and zircon crystals. Apatite was much more abundant than zircon and was found in all samples analyzed with the SEM, except for lava SPF-2 (samples with apatite: MBF-1, MBF-4, MBF-5, WSWF-1, WSWF-3, WSWF-5, SPF-1A, SPF-1B, KPF-5). Enclave KPF-6 and lava CS-MF1 were not analyzed with the SEM. Figure 21c is of an apatite microphenocryst in the Esperanza

Trachyte (MBF-5) approximately 60 micrometers long. Zircon was discovered in only one sample, enclave KPF-5 (Figure 21d). Scanning electron microscope analyses also revealed hornblende phenocrysts within samples SPF-1A and SPF-1B.

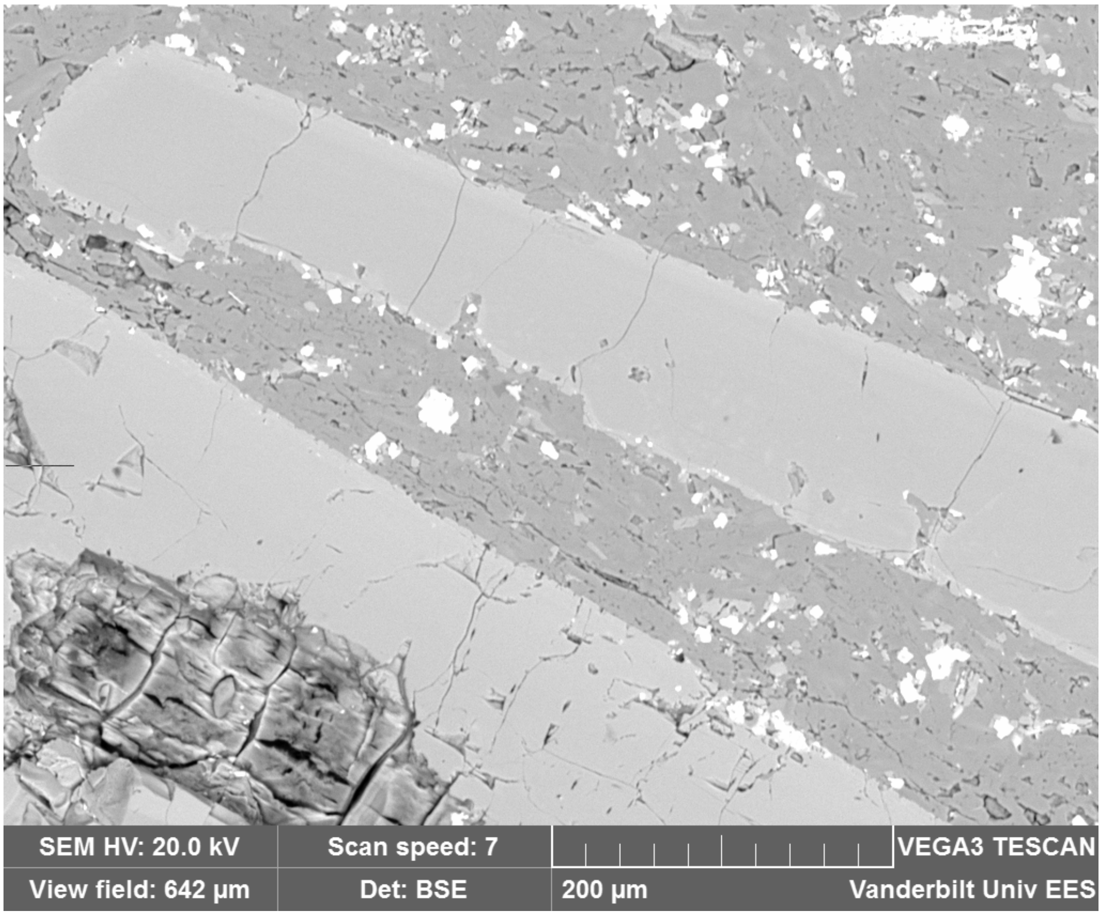

Figure 21a. Scanning electron image of an elongate, zoned clinopyroxene crystal from lava WSWF-1. The zoning is evident in this image as a lighter gray rim around the crystal, which is Fe-rich (denser).

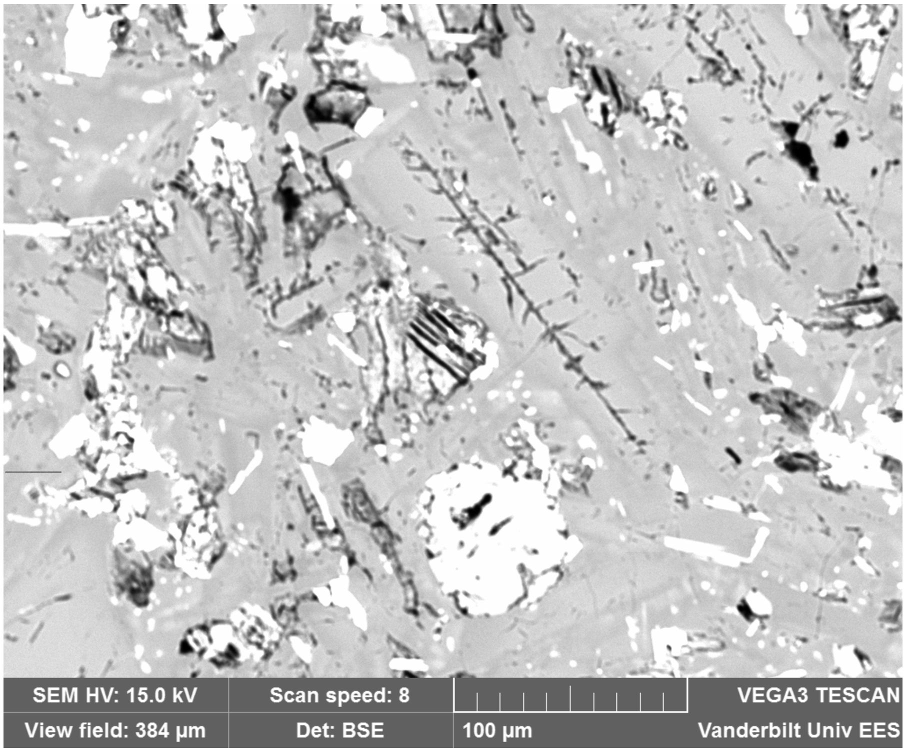

Figure 21b. Scanning electron image of an elongate, zoned plagioclase phenocryst from lava MBF-4. The zoning is the darker gray rim around the crystal, which is Na-rich (less-dense), in the middle of the image.

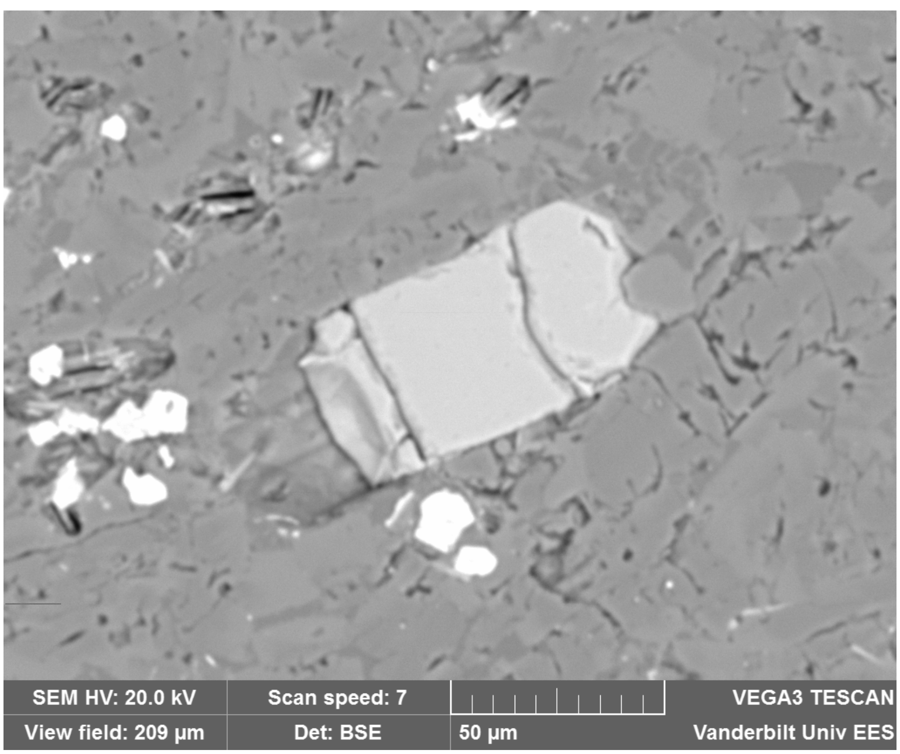

Figure 21c. Scanning electron image of an apatite microphenocryst in MBF-5, the Esperanza Trachyte.

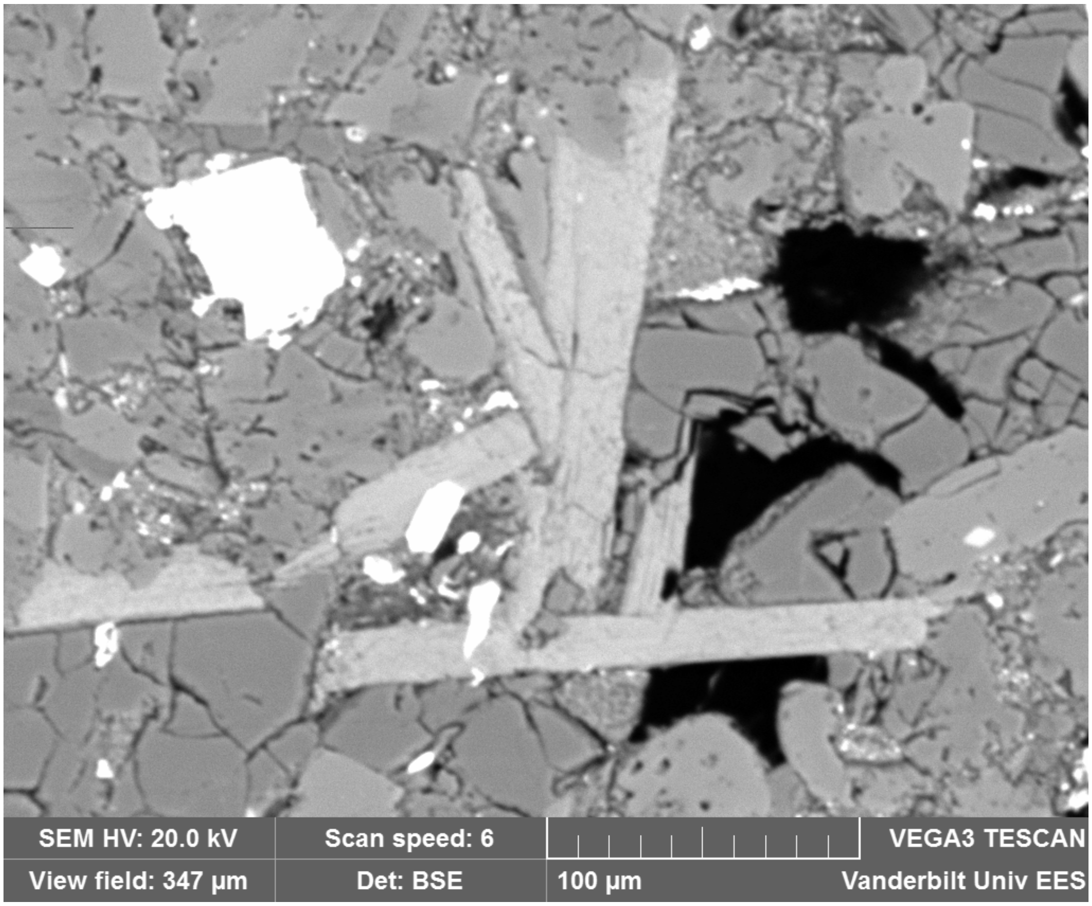

Figure 21d. Scanning electron image of a zircon microphenocryst, the bright object in the top left corner of the image, and needle-like plagioclase crystals in enclave KPF-5.

Temperature Modeling

Whole rock geochemical data was used to model the temperatures of the magmas. Of particular interest was comparing the mafic lavas with the magmatic enclaves discovered within the Peach Spring Tuff and comparing the Esperanza Trachyte with the main trachyte sequence below it. These comparisons helped illuminate the temperature dynamics of the Black Mountains volcanic system preceding supereruption.

Through the use of the Excel-MELTS program, we were able to dynamically model our samples through cooling (as temperature decreased). Samples were run three times: with varying H_2O at 1%, 2%, and 3% in order to get a better idea of what reasonable liquidi temperatures would be. Tables 5 and 6 below show the melt temperatures obtained through different runs of the Excel-MELTS program. This temperature was assumed to be the temperature of the melt the moment before eruption. Liquidi temperatures, the temperature above which the melt is entirely liquid with no solid crystals, at different water weight percentages is shown in Tables 1 and 2 of Appendix C. The lavas deemed most similar to the enclaves were determined based on the closest SiO_2 weight percentage and tie-lines are drawn between these lavas and the enclaves in Figure 22. Figure 23a-c shows the program outputs at 1% H_2O, Figure 24a-c shows the program outputs at 2% H_2O, and Figure 25a-c shows the program outputs for 3% H_2O. Temperatures were determined from these outputs based on the percentage of phenocrysts existant within each sample (the percent total solids existing in the melt/total liquids, or groundmass).

Sample	Temp at 1% H_2O	Temp at 2% H_2O	Temp at 3% H_2O	SiO_2%
MBF-1	1087	1045	1015	54.79
MBF-4	1125	1095	1075	49.44
MBF-5	1070	1025	1015	62.21
WSWF-1	1100	1080	1055	54.04
CS-MF1	1100	1050	1030	52.24
SPF-1A	1075	1040	1020	61.97
SPF-1B	1035	980	935	54.60
SPF-2	1085	1040	1000	56.65

Table 5. Excel-MELTS temperatures from observed phenocryst percentage of lava samples (see arrows on Figures 23-25).

Sample	Temp at 1% H_2O	Temp at 2% H_2O	Temp at 3% H_2O	SiO_2%
WSWF-3	1070	1020	985	54.96
WSWF-5	1105	1070	1050	52.83
KPF-5	1062	1015	985	56.57
KPF-6	1040	1000	955	60.66

Table 6. Excel-MELTS temperatures from observed phenocryst percentage of lava samples (see arrows on Figures 23-25).

As expected, melt temperatures decreased as silica content increased in all MELTS outputs. However, a few outliers in the middle of the silica range made it hard to fit the trends with an ideal function that had a high R^2 value (Figure 26). Additionally, as water content increased, temperatures produced in the outputs decreased (Figure 22).

For melts with 1 wt. % H_2O, lavas ranged from 1035°C to 1125°C and enclaves ranged from 1040°C to 1105°C. At 2 wt. % H_2O, the lava samples ranged from 980°C to 1095°C. Enclaves ranged from 1000°C to 1070°C at 2 wt. % H2O. Melts containing 3 wt. % H_2O yielded lava temperatures from 935°C to 1075°C and enclave temperatures from 955°C to 1050°C. All lava ranges excluded the Esperanza Trachyte, since it is not mafic and therefore not comprable to the mafic magmatic enclaves.

The Esperanza Trachyte was also of note, since it is atypically hot when compared to the trachyte sequence below it. The melt temperatures for the Esperanza (MBF-5) were 1070°C, 1025°C, and 1015°C at 1%, 2%, and 3% H_2O respectively. This contrasted with the rest of the thick trachyte sequence at temperatures near 850°C when modeled with 2% H_2O (Rice et al., 2014).

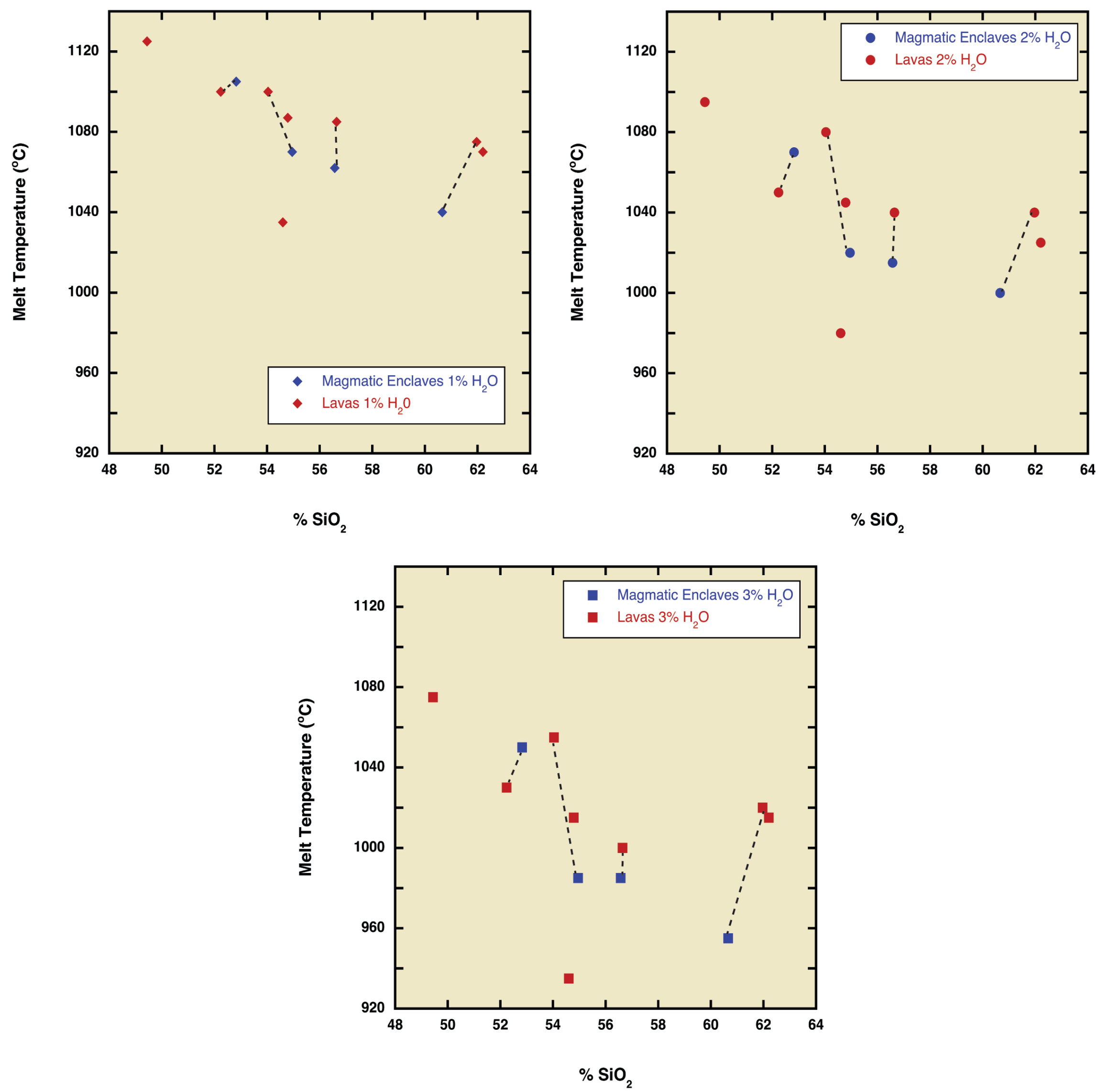

Figure 22. Temperatures obtained through Excel-MELTS at the three different water weight percentages. Tie-lines are between those lavas closest in SiO_2% to an enclave.

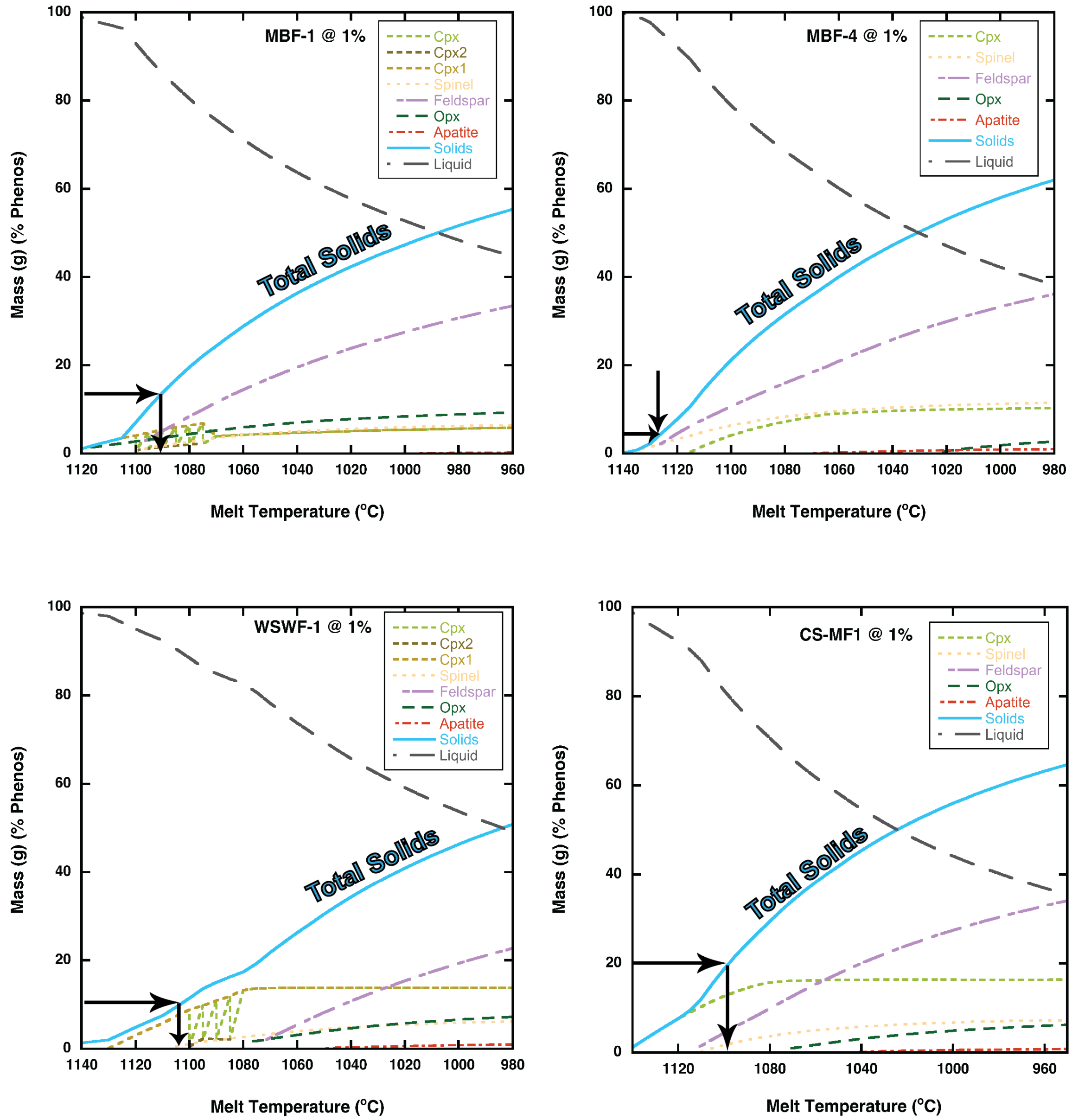

Figure 23a. Lavas MBF-1, MBF-4, WSWF-1, and CS-MF1 Excel-MELTS program outputs at 1% H_2O. Arrows are drawn out from the percent phenocrysts in the sample on the y-axis. Once the arrow intercepts the total solids line, the second arrow drops down to the corresponding temperature of the melt before eruption.

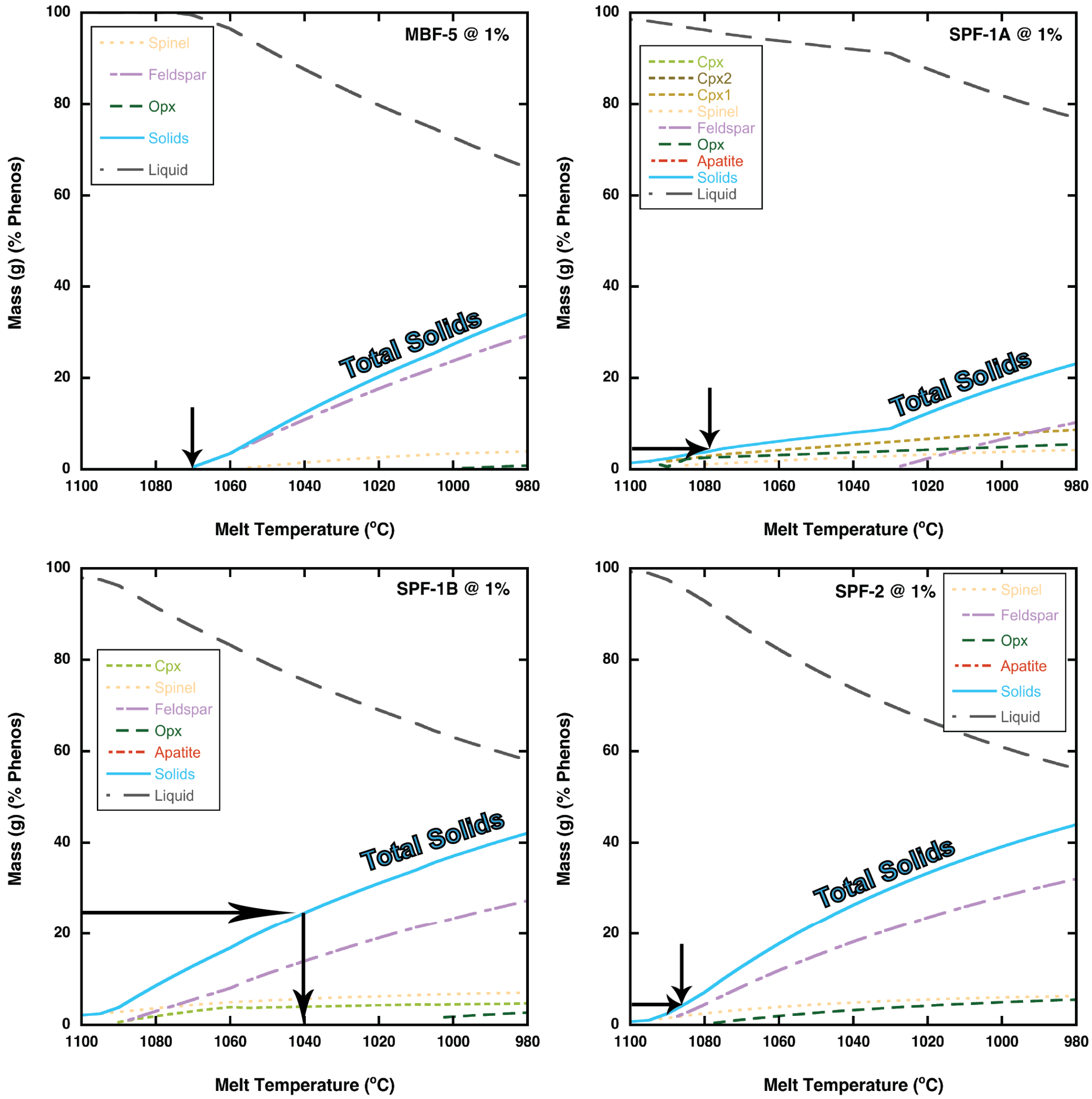

Figure 23b. Lavas MBF-5, SPF-1A, SPF-1B, and SPF-2 Excel-MELTS program outputs at 1% H_2O. Arrows are drawn out from the percent phenocrysts in the sample on the y-axis. Once the arrow intercepts the total solids line, the second arrow drops down to the corresponding temperature of the melt before eruption.

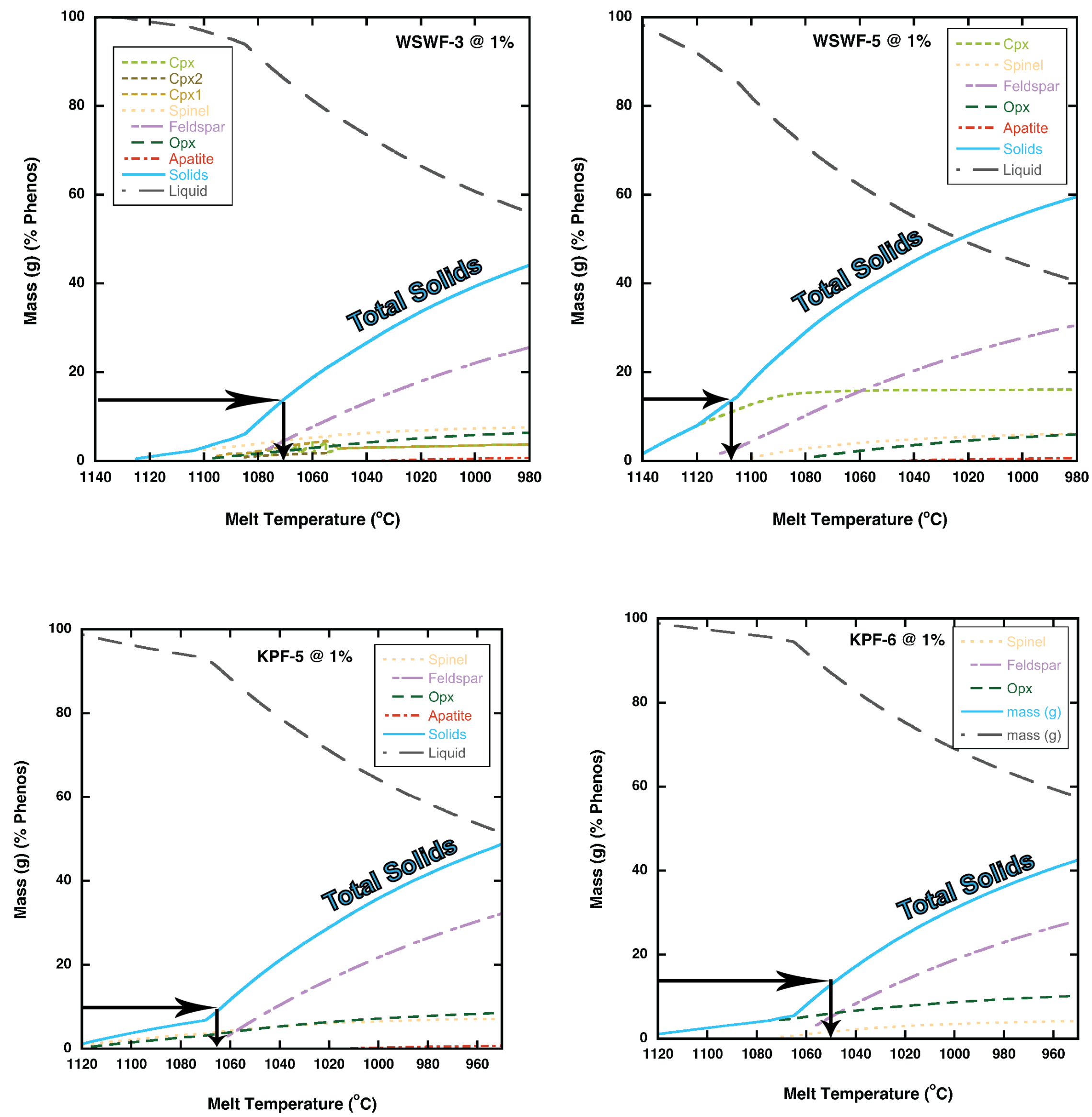

Figure 23c. Enclaves WSWF-3, WSWF-5, KPF-5, and KPF-6 Excel-MELTS program outputs at 1% H_2O. Arrows are drawn out from the percent phenocrysts in the sample on the y-axis. Once the arrow intercepts the total solids line, the second arrow drops down to the corresponding temperature of the melt before eruption.

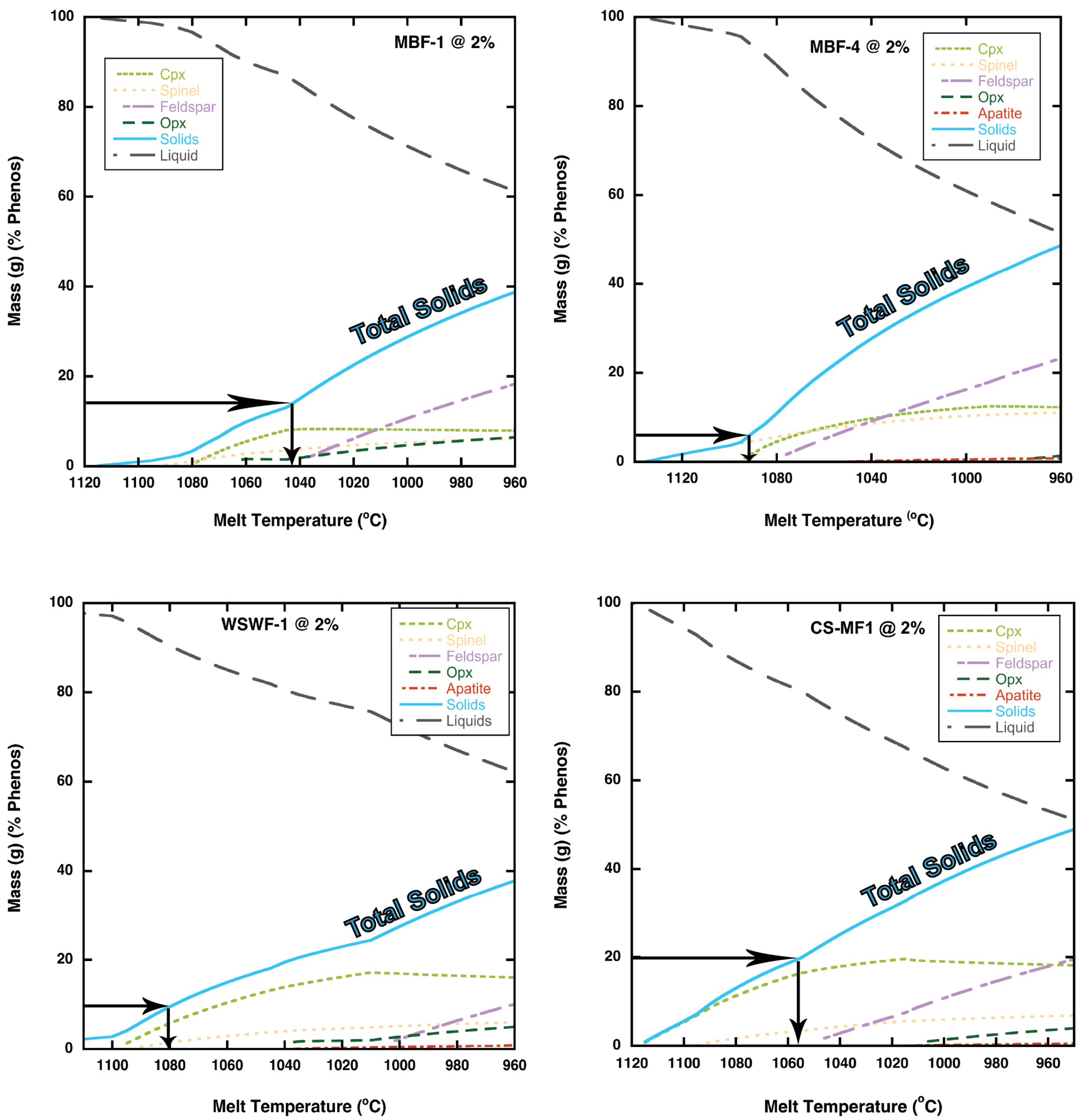

Figure 24a. Lavas MBF-1, MBF-4, WSWF-1, and CS-MF1 Excel-MELTS program outputs at 2% H_2O. Arrows are drawn out from the percent phenocrysts in the sample on the y-axis. Once the arrow intercepts the total solids line, the second arrow drops down to the corresponding temperature of the melt before eruption.

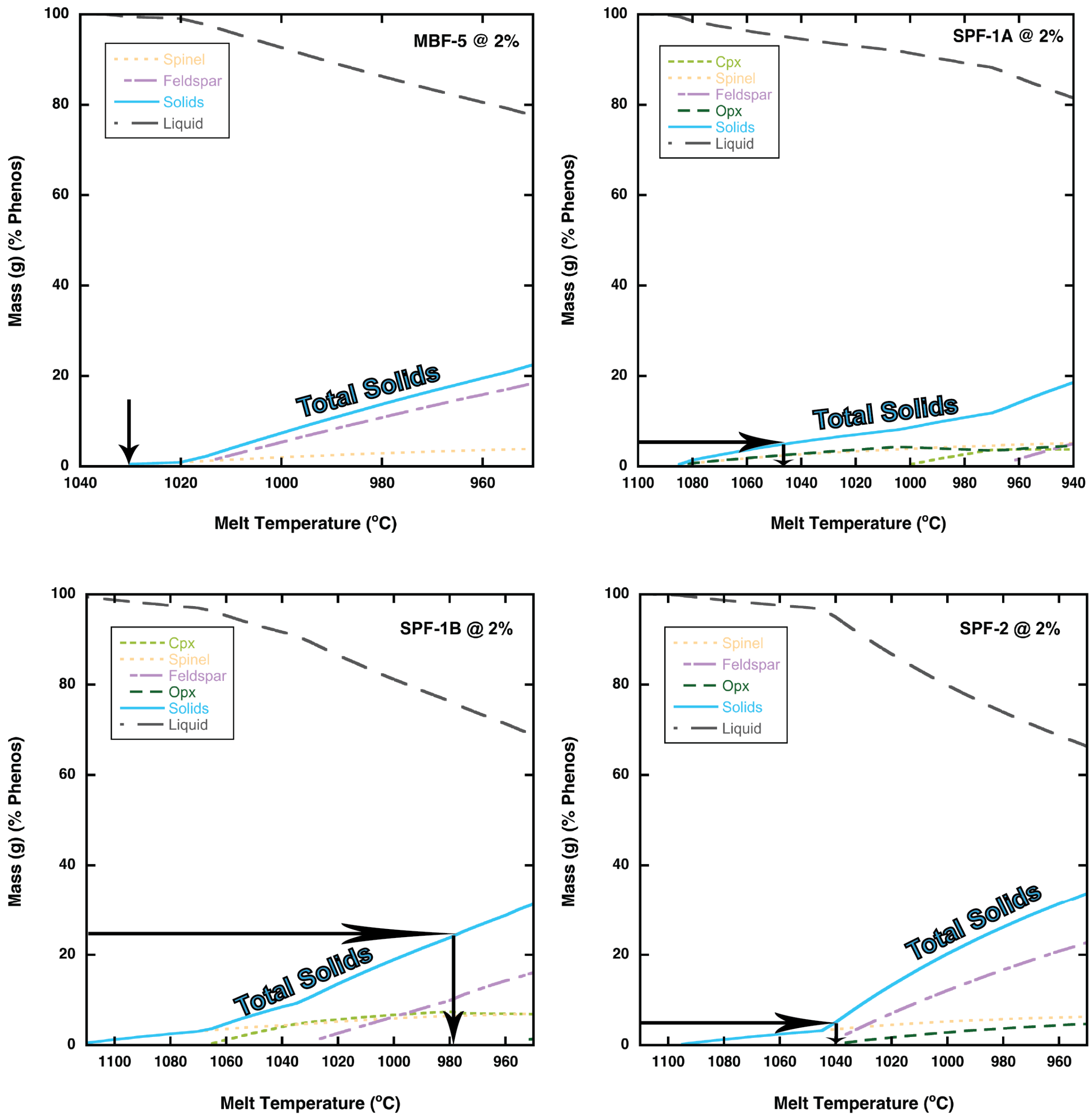

Figure 24b. Lavas MBF-5, SPF-1A, SPF-1B, and SPF-2 Excel-MELTS program outputs at 2% H_2O. Arrows are drawn out from the percent phenocrysts in the sample on the y-axis. Once the arrow intercepts the total solids line, the second arrow drops down to the corresponding temperature of the melt before eruption.

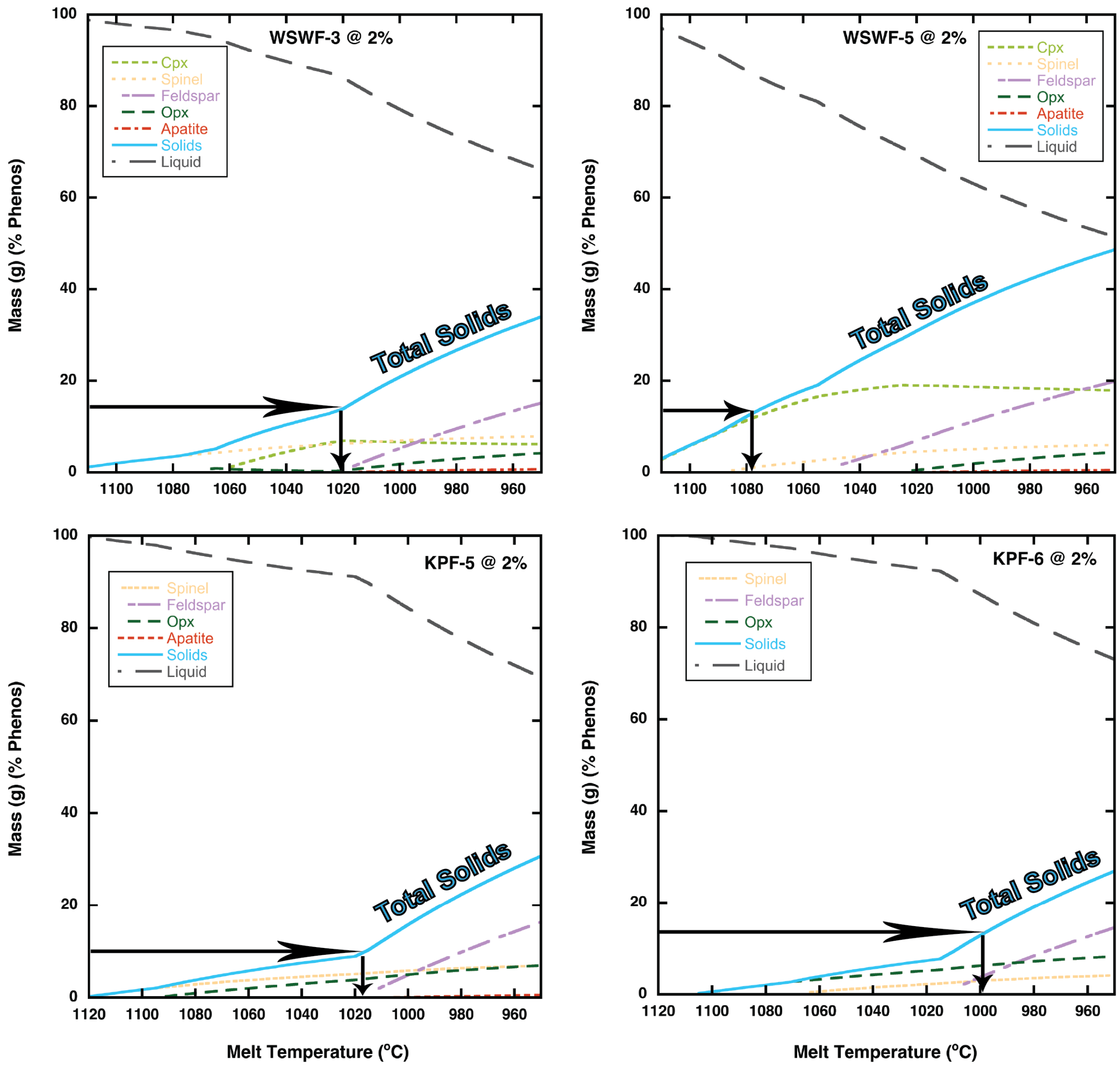

Figure 24c. Enclaves WSWF-3, WSWF-5, KPF-5, and KPF-6 Excel-MELTS program outputs at 2% H_2O. Arrows are drawn out from the percent phenocrysts in the sample on the y-axis. Once the arrow intercepts the total solids line, the second arrow drops down to the corresponding temperature of the melt before eruption.

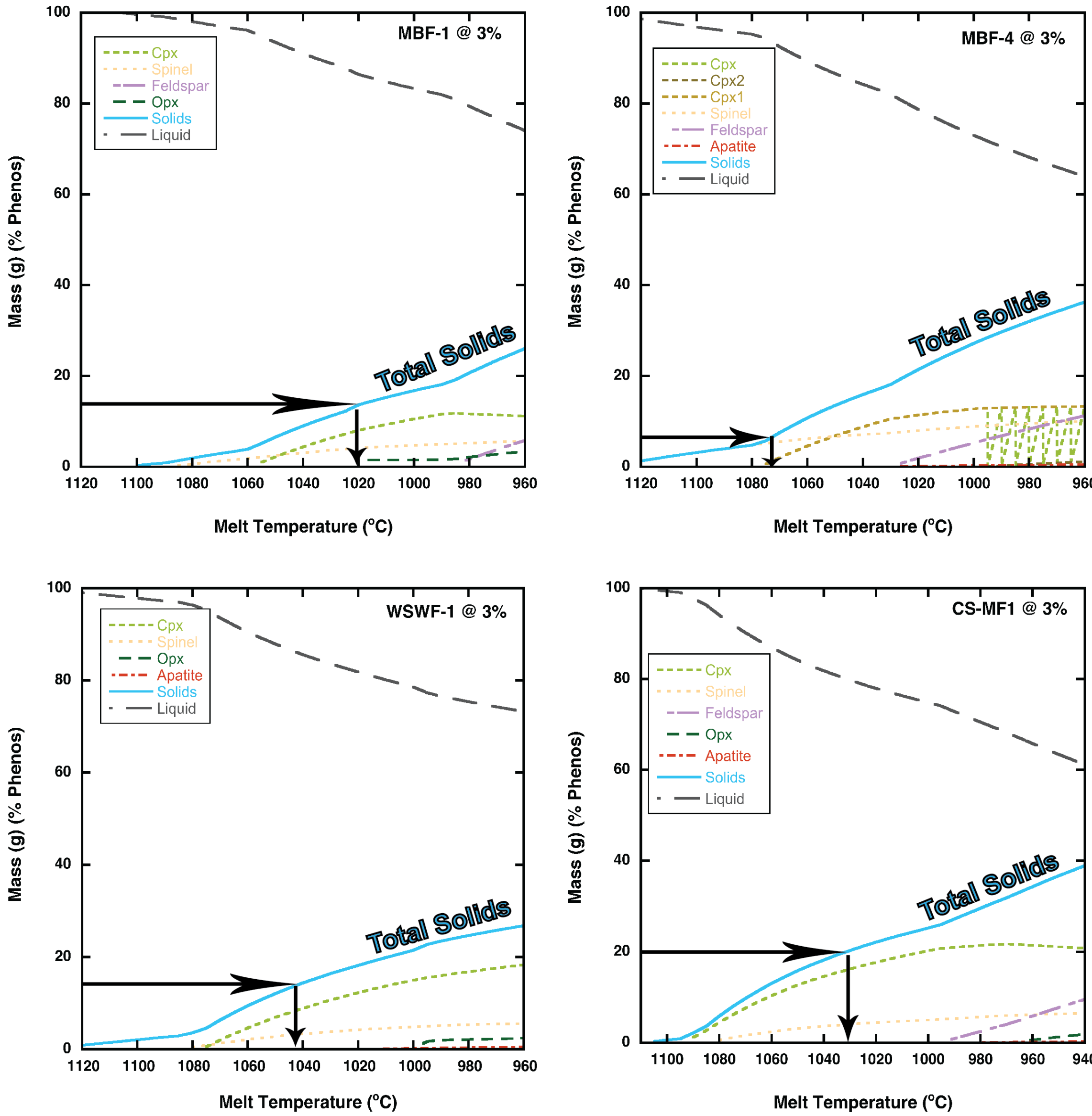

Figure 25a. Lavas MBF-1, MBF-4, WSWF-1, and CS-MF1 Excel-MELTS program outputs at 3% H_2O. Arrows are drawn out from the percent phenocrysts in the sample on the y-axis. Once the arrow intercepts the total solids line, the second arrow drops down to the corresponding temperature of the melt before eruption.

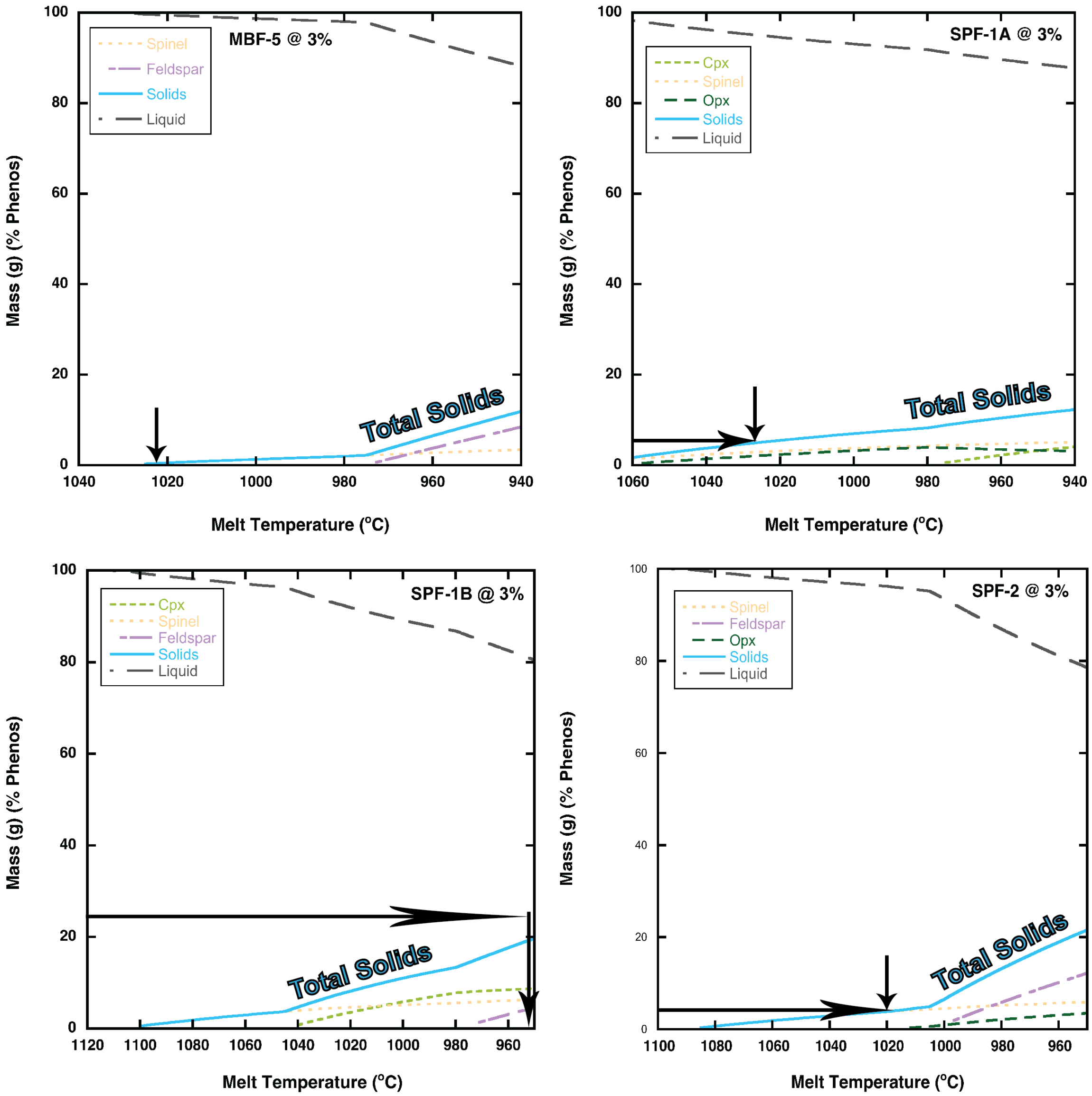

Figure 25b. Lavas MBF-5, SPF-1A, SPF-1B, and SPF-2 Excel-MELTS program outputs at 3% H_2O. Arrows are drawn out from the percent phenocrysts in the sample on the y-axis. Once the arrow intercepts the total solids line, the second arrow drops down to the corresponding temperature of the melt before eruption.

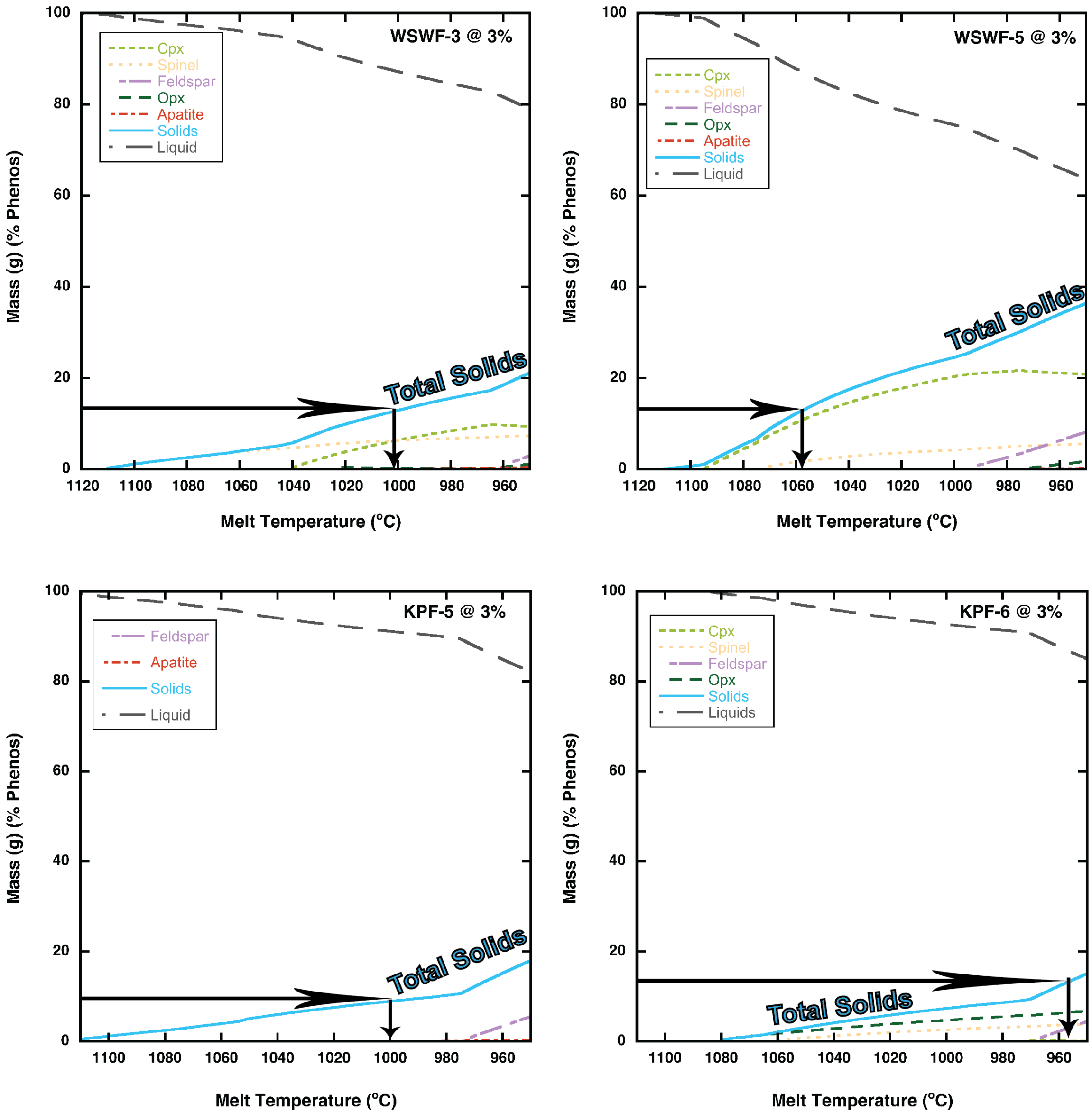

Figure 25c. Enclaves WSWF-3, WSWF-5, KPF-5, and KPF-6 Excel-MELTS program outputs at 3% H_2O. Arrows are drawn out from the percent phenocrysts in the sample on the y-axis. Once the arrow intercepts the total solids line, the second arrow drops down to the corresponding temperature of the melt before eruption.

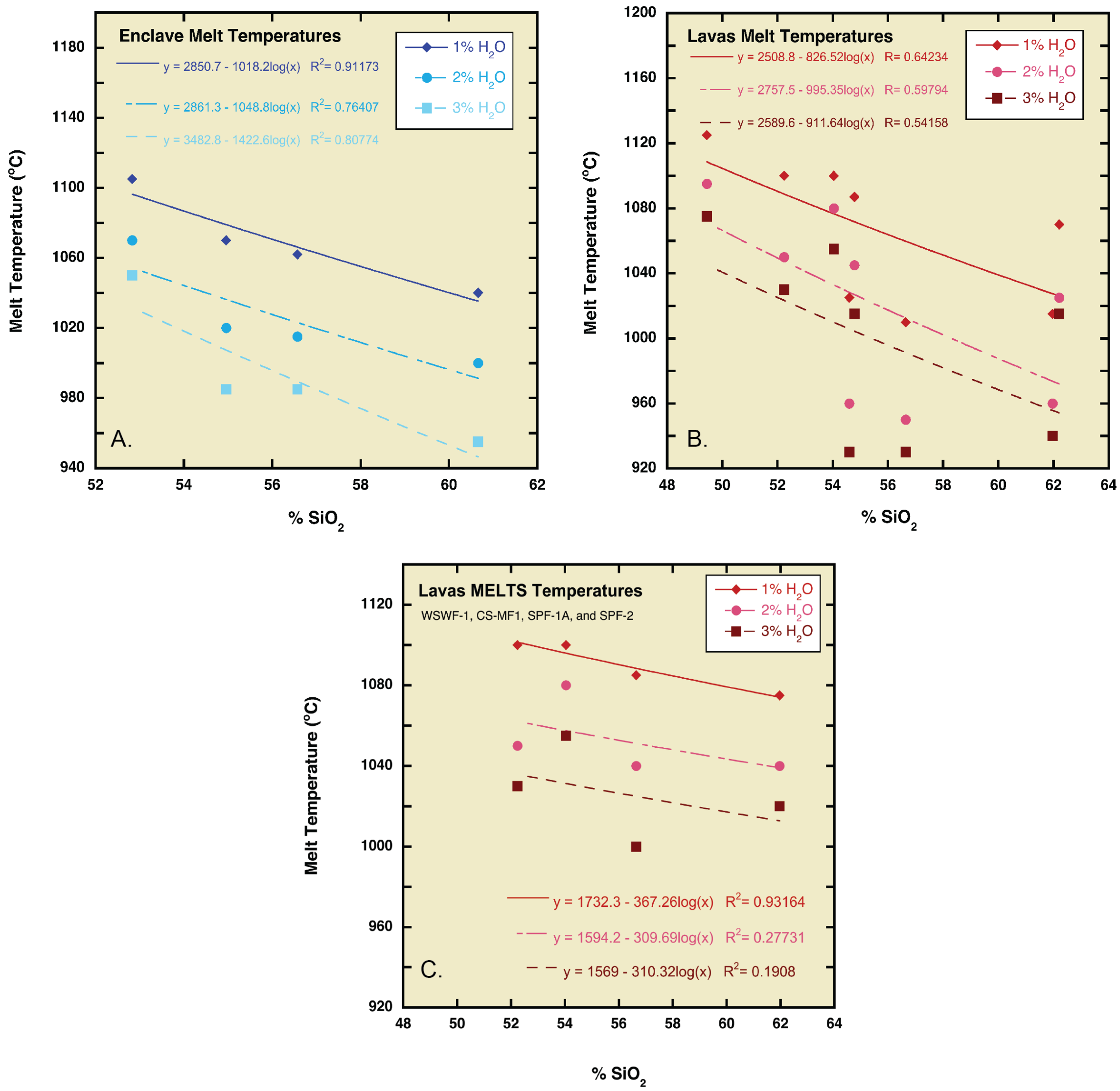

Figure 26. Excel-MELTS temperatures of enclaves are displayed on the top left, temperatures of all lavas are on the top right, and the most similar lavas are on the bottom. The data are fit with logarithmic functions.

Apatite- and zircon-saturation thermometry models were employed to provide another source of melt temperatures and thereby cross-check the Excel-MELTS program. Apatite phenocyrsts were discovered in all samples examined with the SEM (MBF-1, MBF-4, MBF-5, WSWF-1, WSWF-3, WSWF-5, SPF-1A, SPF-2, KPF-5). However, because they were only detectable in SEM, these crystals can be considered as either quench crystals or microphenocrysts. Quench crystals form during the freezing (or quenching) of the melt while microphenocrysts existed within the melt itself before solidifying. Because it was hard to tell between the two crystal forms, we assumed that where apatite did exist in samples, they are microphenocrysts and as such existed before the melt cooled. The temperatures obtained through apatite-saturation thermometry (Figure 27) were taken as minima in samples where apatite did not exist, but were reliable in samples where apatite existed because the melt must have been at that temperature for apatite crystals to form. Apatite-saturation temperatures and calculations are in Tables 3 and 4 of Appendix C.

Only one zircon microphenocryst was discovered through use of the scanning electron microscope. This zircon was found in a magmatic enclave from the Peach Spring Tuff northwest of Kingman, Arizona (KPF-5). Except for KPF-5, the zircon-saturation temperatures are considered minima because zircon was not found in the samples. Zircon-saturation temperatures (Figure 27) and calculations are in Tables 5 and 6 of Appendix C. Temperatures obtained through apatite- and zircon-saturation thermometry were plotted with the temperatures obtained with the Excel-MELTS program at 2% H_2O (Figure 28). Zircon and apatite data obtained through use of the SEM are shown in Table 4 of Appendix E.

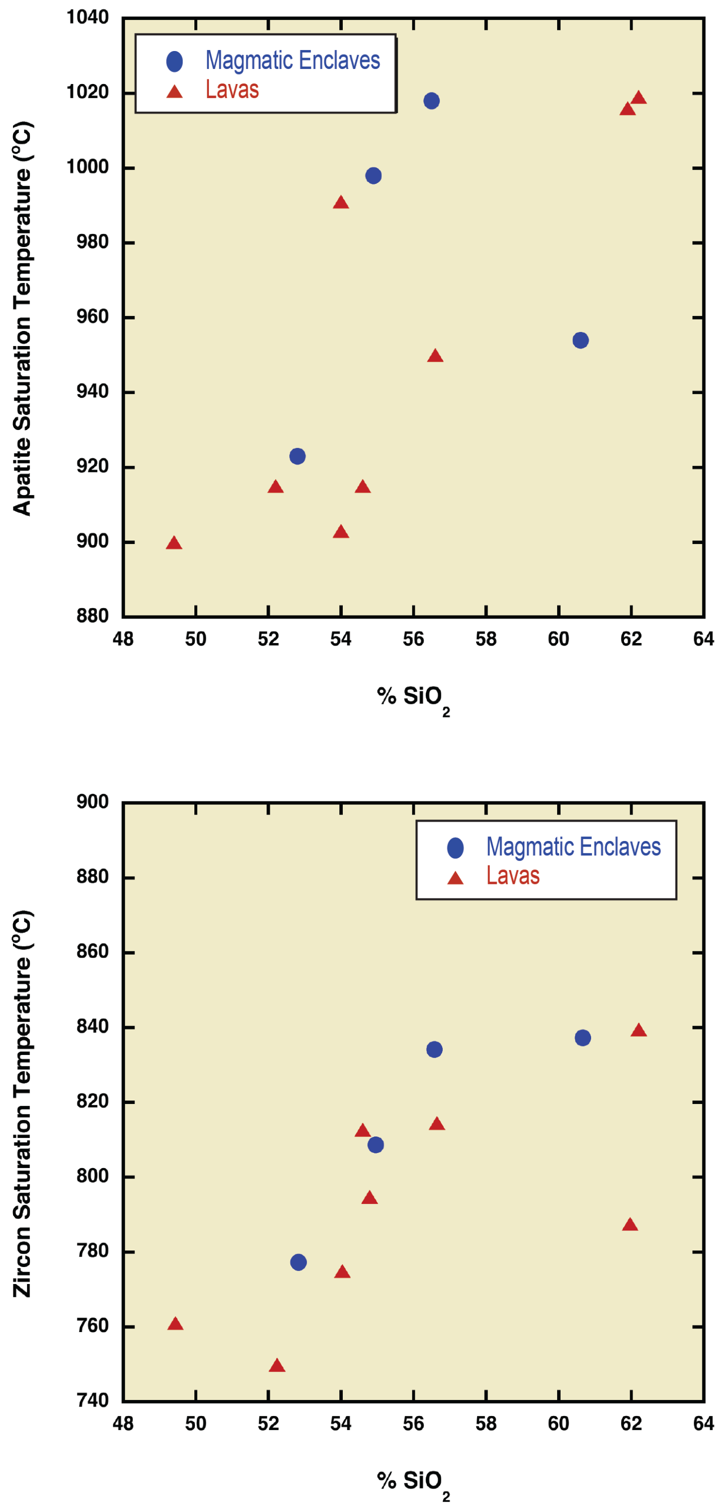

Figure 27. Temperatures obtained through apatite-saturation temperatures can be interpreted as the temperature of the melt itself and zircon-saturation thermometry temperatures can be interpreted as minima.

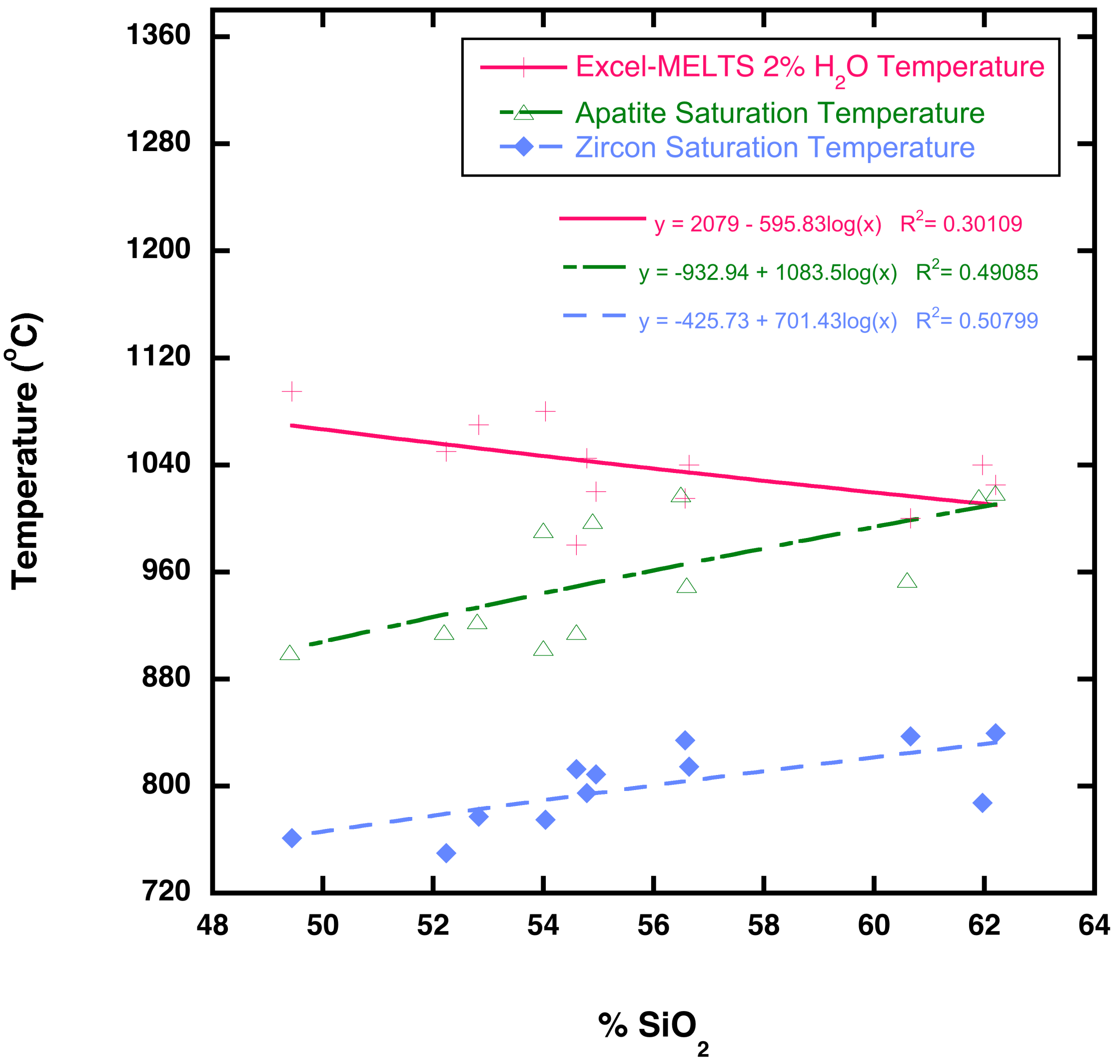

Figure 28. Temperatures obtained through Excel-MELTS and apatite-saturation temperatures can be interpreted as the temperature of the melt itself and zircon-saturation thermometry temperatures can be interpreted as minima.

Discussion

The volcanic stratigraphy of the southern Black Mountains (Figure 14a) was key to understanding the relationship and importance of the mafic lavas sampled in this study. Laying between the 19.0 Ma trachyte sequence below (McDowell et al. 2014) and the 18.8 Ma Peach Spring Tuff above (Ferguson et al. 2013), these lavas flowed onto the surface within a geologically short time span prior to the Peach Spring supereruption. The volcanic stratigraphy at the Peach Spring Tuff unconformity (Figure 13b) in Secret Pass Wash (Figure12) was different than the stratigraphy elsewhere. Here, the mafic lavas were interbedded with sandstones sourced from the basement and the trachyte sequence below the mafic lavas (Lee et al., 2014). These mafic lavas looked different from those found elsewhere in the study area (i.e. the existence of flow banding), but geochemically they were within the range of other mafic lavas sampled. Additionally, the presence of sedimentary units within these lavas and above them suggests that the area was a topographic low capable of receiving sediment.

Hand sample and thin section petrography revealed that the pre-Peach Spring Tuff mafic lavas and the Peach Spring Tuff magmatic enclaves shared a similar phenocryst assemblage. Pre-PST mafic lavas contained 5-15% phenocrysts, with elongate plagioclase and zoned clinopyroxene most common, and small amounts of iron oxides and altered olivine crystals. The enclaves contained 5-18% phenocrysts, again with plagioclase and clinopyroxene dominant and minor biotite in some samples within a fine-grained plagioclase groundmass. Reaction rims were evident in both the mafic lava thin sections and within the magmatic enclave samples.

Major and minor element analyses revealed more similarities between the two sample types. Mafic lavas sampled from Warm Springs West and Caliche Springs, in particular, were alike to the magmatic enclaves from Warm Springs West. Although the Kingman enclaves were slightly more silicic than the Warm Springs West enclaves, they plotted into the range of major element concentrations of the lavas from both the southern and northern extent of the study area, seen on previous plots (Figures 18a, 18b, and 18c). The lavas ranged from trachy-basalt to trachy-andesite in composition (with SPF-1A plotting just within the andesite field) and were comparable to the enclaves that ranged from basaltic trachy-andesite to trachy-andesite.

A high-silica outlier (sample SPF-1A) plotted just within the andesite field on the TAS diagram (Figure 18). This sample was part of the mafic lava discovered just below the Peach Spring Tuff unconformity at Secret Pass Wash and is close to trachytic in composition, making it different from the other mafic lavas examined in this study. One possibility for this difference is that this lava was a melt geochemically "in between" that which produced the trachyte sequence below and the more mafic lavas sampled just below the Peach Spring Tuff at Warm Springs West and McHeffy Butte. More likely, however, is that it plotted within the andesite field because its Na_2O weight percentage is extremely low (~ 2 wt. %, Table 1) for a realistic magma. This low Na_2O% may be due to alteration, dissolution at the surface after eruption, or from instrumentation error.

Full elemental analyses from ICP-MS revealed another interesting characteristic of the samples (lavas WSWF-1 and CS-MF1 and enclaves WSWF-5, WSWF-3, and KPF-5). Rare earth elements showed similar patterns among the three enclaves and the two lavas. This provided further strength to the possibility of a relation between the melts that produced the enclaves and the lavas. All of the samples were enriched in what are considered incompatible elements for mantle minerals—elements such as K, Rb, Ba, Sr, and rare earth elements (REE). The fact that they were enriched in these incompatible elements would preclude them as being direct parental magmas of the more silicic bodies in the region such as the Cook Canyon Tuff and the Peach Spring Tuff. This enrichment was also suggestive of a lack of crustal contamination in these samples, since crust-contaminated magmas would not be enriched in REEs. Therefore, the melts that produced these magmatic enclaves and mafic lava flows were presumable juvenile melts from the mantle. Though these magmas were likely uncontaminated by the crust, they definitely could have provided heat into the Black Mountains volcanic system and possibly supplied a mixing component to the more silicic hybrids in the region.

Aside from providing information on microcphenocrysts (summarized below), the scanning electron microscope (SEM) yielded information on phenocryst zoning. Zoning is quite common among clinopyroxene crystals in both enclave samples and in lava samples, with the same general trend of iron-enriched cores and magnesium-enriched rims. Plagioclase is commonly normally zoned in both the lava samples and the enclaves: the crystals have calcic cores and sodic rims. Additionally, our SEM analysis did discover some hornblende within the trachy-andesite and andesite lavas at the Peach Spring Tuff unconformity (at Secret Pass Wash, samples SPF-1A, SPF-1B), but this could be due to their slightly higher silica content. Finally, we analyzed the groundmass compositions with SEM of lava samples SPF-1A, SPF-2, and the Esperanza Trachyte MBF-5. The only enclave with reliable groundmass analysis was KPF-5. These groundmass analyses were dramatically different, but were certainly more mafic than any other lavas before the Peach Spring Tuff.

The Excel-MELTS program proved a useful way to model the temperature of varying magmas before their eruption. All water weight percentages (1%, 2%, and 3%) showed decreasing temperatures as silica content of the melt increased, as expected (Figures 22 and 28). Temperature ranges were also similar between the trachy-basalt to trachy-andesite lavas and the magmatic enclaves (Tables 3 and 4). The Esperanza Trachyte modeled at much higher temperatures (~1030°C) than the rest of the sequence below it modeled by Rice et al. (2014) at approximately 850°C.

Temperatures determined with apatite-saturation thermometry ranged from 910°C to 1060°C. Because apatite was discovered in all samples analyzed with the SEM, these temperatures are reliable. However, it is unclear whether or not apatite existed in samples SPF-2 or KPF-6 because no SEM analyses were done on them. Zircon-saturation thermometry placed minimum temperatures on the melts that we examined. Because these were minima temperatures, the actual temperature of the melt(s) was understood to be considerably higher. These minima were all below the Excel-MELTS temperatures (at 2% H_2O) and showed that all of the melts were likely much hotter; typically well above 1000°C (Figure 28). However, it appeared that the 3% H2O Excel-MELTS temperatures would have plotted closer to the apatite-saturation thermometry temperatures.

Interpretations

Our data suggest an interesting and dynamic story preceding the supereruption of the Peach Spring Tuff 18.8 Mya in the southern Black Mountains. Evidence of significant heat input into the Black Mountains volcanic system was first indicated by the aphyric (<1% phenocrysts) and atypically hot (~1030°C) Esperanza Trachyte at the top of the ~1 km thick pre-Peach Spring Tuff trachyte sequence. The preceding trachyte lavas contrasted with this last trachyte lava at temperatures around 850°C (Rice et al. 2014). The high temperature and the presence of mafic lavas directly above this last trachyte flow in the volcanic stratigraphy were strong indicators of heat input into the local volcanic system even before the eruption of mafic lavas onto the surface.

Heat input into the Black Mountains volcanic system continued after the eruption of the Esperanza Trachyte with the eruption of the mafic lava flows. Pre-Peach Spring Tuff trachy-basalt to trachy-andesite lavas closely preceded the eruption of the Peach Spring Tuff itself. These lavas had an estimated temperature range of 1000°C to 1095°C using the Excel-MELTS program at 2% H_2O and thus represented a magma body much hotter than the calculated temperatures of the Peach Spring Tuff (see Gualda et al., 2012 and Pamukcu et al., 2013). The existence of post-Peach Spring Tuff volcanic units indicates volcanism continued after supereruption, as the system cooled over hundreds of thousands of years.

The presence of magmatic enclaves ranging from basaltic trachy-andesite to trachy-andesite within the Peach Spring Tuff was an indicator that a more mafic magma was in the Peach Spring Tuff magma body at the time of supereruption. These enclaves had similar geochemical and petrographic characteristics as the pre-Peach Spring Tuff mafic lavas, as well as a similar range of calculated MELTS temperatures (1010°C to 1085°C), and likely represented the same magma input or at the very least similar melt sources.

Future Work

Due to the limited time we had to analyze our samples at Vanderbilt University and at Middle Tennessee State University (MTSU), we were unable to get geochemical data on many of the samples collected in the field. For example, we collected over ten magmatic enclaves but were only able to analyze four of them with the XRF-detector at MTSU. Having more samples, both magmatic enclaves and lavas, with major and minor elemental compositions would greatly add to the data set and the temperature models presented in this thesis and produce more reliable conclusions. Time constraints also limited the number of mounts I was able to analyze with the SEM. Perhaps there were zircon or apatite microcphenocrysts in these samples as well. Additionally, more thorough SEM analyses would help reveal whether or not microcphenocrysts are true phenocrysts or quench crystals.

On the microscopic level, it would be interesting to look for reversely-zoned phenocrysts within the Peach Spring Tuff itself. Nakagawa et al. (2002) cites reverse zoning as arising as a result of magma mixing in clinopyroxene crystals and this could possibly be applied to the Peach Spring Tuff itself as further evidence of magma mixing or mingling. The "host" tuff around the magmatic enclaves we sampled would be ideal to examine for this evidence of magma mingling.

Finally, more pre-Peach Spring Tuff mafic lavas exist within the southern Black Mountains (Beckens et al., 2014). In addition to adding more detail to the generalized geologic map of the study area, these mafic lavas would also shed light on the process of heat input into this dynamic volcanic system that preceded supereruption.

Conclusions

Our data suggests that there was on-going heat input into the southern Black Mountains preceding the 18.8 Ma supereruption of the Peach Spring Tuff. This is evidenced in the aphyric, atypically hot Esperanza Trachyte which is followed in the volcanic stratigraphy by relatively mafic lavas that are much hotter and lay just below the Peach Spring Tuff itself. These mafic lavas were erupted in the stratigraphy within a 200 ka time range and thus are significant to understanding the history of the southern Black Mountains preceding supereruption. Furthermore, there was mafic magma in the Peach Spring Tuff magma body at the time of supereruption, evidenced by the existence of conclusive magmatic enclaves, indications of magma mingling, within the Peach Spring Tuff. Geochemical, petrographical, and temperature modeling results are similar between the trachy-basalt to trachy-andesite lavas and the basaltic trachy-andesite to trachy-andesite magmatic enclaves. This leads us to conclude that the two sample types likely came from very similar juvenile melts from the mantle. This leads to the overall conclusion that mafic magma injection was a possible eruption trigger mechanism for the Peach Spring Tuff supereruption 18.8 Mya in the southern Black Mountains, Arizona.

Acknowledgements

Many people played a part in this project. First and foremost, I would like to thank my advisors, Dr. Calvin F. Miller (Vanderbilt University) and Dr. Christopher "Chuck" Bailey (College of William & Mary), for their expert advice throughout the project. This project was part of an NSF-REU program (Grant EAR-120523) and the other REU leaders deserve to be recognized: Dr. Susanne M. McDowell (Hanover College), Dr. Nick Lang (Mercyhurst University), Dr. Lily. L. Claiborne (Vanderbilt University), and Charles A. Ferguson (Arizona State Geological Survey). Dr. J. Warner Cribb (Middle Tennessee State University) is thanked for his help with the XRF-detector and Aaron Covey (Vanderbilt University) is thanked for his help with the SEM. Two of the other Supereruptions REU undergraduates mapped the Peach Spring Tuff unconformity and helped me examine the mafic lavas below it within Secret Pass Wash: Jake Lee (University of Kentucky) and Scott Williams (Occidental College). For all the teamwork and the great times, I wish to thank the rest of the Supereruptions REU undergraduates: Michelle Foley (Western Kentucky University), Brandt Gibson (University of Tennessee-Martin), Stacey Rice (Stonybrook University), Shannon Porter-Rentz (Middle Tennessee State University), Daniel Pratt (Austin-Peay State University), Holland Beckens (University of Vermont), and Sarah McGuinness (Slippery Rock University).

References Cited

Annen, C., 2011, Implications of incremental emplacement of magma bodies for magma differentiation, thermal aureole dimensions and plutonism-volcanism relationships: Tectonophysics, v. 500, no. 1-4, p. 3-10.

Bachmann, O., and Bergantz, G., 2003, Rejuvenation of the Fish Canyon magma body: A window into the evolution of large-volume silicic magma systems: Geology, v. 31, no. 9, p. 789-792, doi:10.1130/G19764.1.

Bachmann, O., and Bergantz, G., 2008, Deciphering magma chamber dynamics from styles of compositional zoning in large silicic ash flow sheets: Reviews in Mineralogy and Geochemistry, v. 6, no. 1, p. 651-674, doi:10.2138/rmg.2008.69.17.

Bachmann, O., and Bergantz, G., 2008, The magma reservoirs that feed supereruptions: Elements, v. 4, no. 1, p. 17-21, doi:10.2113/GSELEMENTS.4.1.17.

Bachmann, O., Dungan, M. A., and Bussy, F., 2005, Insights into shallow magmatic processes in large silicic magma bodies: the trace element record in the Fish Canyon magma body, Colorado: Contributions to Mineralogy and Petrology, v. 149, no. 3, p. 338-349, doi:10.1007/s00410-005-0653-z.

Beckens, H., Lang, N.P., and Miller, C.F., 2014, Exploring the extent of Miocene-aged mafic rock units in the Black Mountains, AZ, using satellite imagery: Geological Society of America Abstracts with Programs, v. 46, no. 6, p. 550.

Billingsley, G.H., Weinrich, K.J., Huntoon, P.W., and Young, R.A., 1999, Breccia-pipe and geologic map of the southwestern part of the Hualapai Indian Reservation and vicinity, Arizona: USGS Miscellaneous Investigations Series Map, I-2554.

Buesch, D. C., 1992, Incorporation and redistribution of locally derived lithic fragments within a pyroclastic flow: Geological Society of America Bulletin, v. 104, p. 1193-1207.

Charlier, B. L. A., Morgan, D. J., Wilson, C. J. N., Wooden, J. L., Allan, A. S. R., and Baker, J. A.. 2012, Lithium concentration gradients in feldspar and quartz record the final minute of magma ascent in an explosive supereruption: Earth and Planetary Science Letters, v. 319-320, p. 218-227.

Eichelberger, J. C., and Izbekov, P. E., 2000, Eruption of andesite triggered by dyke injection: contrasting cases at Karymsky Volcano, Kamchatka and Mt Katmai, Alaska: Philosophical Transactions of the Royal Society of London. Series A: Mathematical, Physical and Engineering Sciences, v.358, no.1770, p.1465-1485.

Faulds, J. E., Feuerbach, D. L., Miller, C. F., and Smith, E. I., 2001, Cenozoic evolution of the northern Colorado River extensional corridor, southern Nevada and northwest Arizona: Utah Geological Association Publication, v. 30, p. 239-263.

Ferguson, C. A., McIntosh, W. C., and Miller, C. F., 2013, Silver Creek caldera--the tectonically dismembered source of the Peach Spring Tuff: Geology, v. 41, no. 1, p. 3-6, doi:10.1130/G33551.1.

Fowler, S. J., and Spera, F. J., 2010, A metamodel for crustal magmatism: phase equilibria of giant ignimbrites: Journal of Petrology, v. 51, no. 9, p.1783-1830.

Glazner, A. F., Nielson, J. E., Howard, K. A., and Miller, D. M., 1986, Correlation of the Peach Springs Tuff, a large-volume Miocene ignimbrite sheet in California and Arizona: Geology, v. 14, p. 840-843.

Gregg, P. M., de Silva, S. L., Grosfils, E. B., and Permigiani, J. P., 2012, Catastrophic caldera-forming eruptions: Thermomechanics and implications for eruption triggering and maximum caldera dimensions on Earth: Journal of Volcanology and Geothermal Research, v. 241-242, p. 1-12.

Gualda, G. A. R., Ghiorso, M. S., Lemons, R. V., and Carley, T. L., 2012, Rhyolite-MELTS: a modified calibration of MELTS optimized for silica-rich, fluid-bearing magmatic systems: Journal of Petrology, v. 53, no. 5, p. 875-890, doi:10.1093/petrology/egr080.

Gusa, S., Nielson, J.E., and Howard, K.A., 1987, Heavy-mineral suites confirm the wide extent of the Peach Springs Tuff in California and Arizona, U.S.A.: Journal of Volcanology and Geothermal Research, v. 33, p. 343-347.

Henry, C. D., Hinz, N. H., Faulds, J. E., Colgan, J. P., John, D. A., Brooks, E. R., Cassel, E.J., Davis, D.A., and Castor, S. B. (2012). Eocene-early Miocene paleotopography of the Sierra Nevada-Great Basin-Nevadaplano based on widespread ash-flow tuffs and paleovalleys: Geosphere, v. 8, no.1, p. 1-227, doi:10.1130/GES00727.1.

Lang, N. P., Walker, B. J., Claiborne, L. E., Miller, C. F., Hazlett, R. W., and Heizler, M. T., 2008, The Spirit Mountain batholith and Secret Pass Canyon volcanic center: A cross-sectional view of the magmatic architecture of the uppermost crust of an extensional terrain, Colorado River, Nevada-Arizona: The Geological Society of America Field Guide, v. 11, p. 1-28.

Le Bas, M.J., Le Maitre, R.W., Streckeisen, A., and Zanettin, B., 1986, A chemical classification of volcanic rocks based on the total alkali-silica diagram: Journal of Petrology, v. 27, no. 3, p. 745-750.

Lee, J. W., Williams, S.H., Flansburg, M.E., Miller, C.F., and Cribb, J.W., 2014, Implications of eruptive, erosive, and depositionsal processes prior to a super eruption in the southern Black Mountains: Geological Society of America Abstracts with Programs, v. 46, no. 6, p.512.

McDowell, S.M., Miller, C.F., Mundil, R., Ferguson, C.A., and Wooden, J.L., 2014, Zircon evidence for a ~200 k.y. supereruption-related thermal flare-up in the Miocene southern Black Mountains, western Arizona, USA: Contributions to Mineralogy and Petrology (in review).

Miller, C. F., Furbish, D. J., Walker, B. A., Claiborne, L. L., Koteas, G. C., Bleick, H. A., and Miller, J. S., 2011, Growth of plutons by incremental emplacement of sheets in crystal-rich host: Evidence from Miocene intrusions of the Colorado River region, Nevada, USA: Tectonophysics, v. 500, no.1-4, p. 65-77.

Miller, J.S., Heizler, M.T., and Miller, C.F., 1998, Timing of magmatism, basin formation, and tilting of the west edge of the Colorado River extensional corridor: Results from single-crystal 40Ar/39Ar geochronology of tertiary rocks in the Old Woman Mountains area, southeastern California: Journal of Geology, v. 106, no. 2, p. 195-210.

Nakagawa, M., Wada, K., and Wood, C.P., 2002, Mixed magmas, mush chambers and eruption triggers: Evidence from zoned clinopyroxene phenocrysts in andesitic scoria from the 1995 eruptions of Ruapehu Volcano, New Zealand: Journal of Petrology, v. 43, no. 12, p. 2279-2303.

Nelson, S. A., 2012, Magmatic Differentiation: www.tulane.edu/`sanelson/eens212/magmadiff.htm (accessed March 2014).

Nielson, J.E., Lux, D.R., Dalrymple, G.B., and Glazner, A.F., 1990, Age of the Peach Springs Tuff, southeastern California and western Arizona: Journal of Geophysical Research, v. 95, p. 571-580.

Pallister, J.S., Hoblitt, R.P., and Reyes, A.G., 1992, A basalt trigger for the 1991 eruptions of Pinatubo volcano?: Nature, v. 356, p. 426-428.

Pamukcu, A. S., Carley, T. L., Gualda, G. A. R., Miller, C. F., and Ferguson, C. A., 2013, The evolution of the Peach Spring giant magma body: evidence from accessory mineral textures and compositions, bulk pumice and glass geochemistry, and rhyolite-MELTS modeling: Journal of Petrology, v. 54, no.6, p. 1109-1148.

Pearthree, P.A., Ferguson, C.A., Johnson, B.J., and Guynn, J., 2009, Geologic map and report for the proposed State Route 95 realignment corridor, Mohave County, Arizona: Arizona Geological Survey (DGM-65), v. 1, 1:24000 scale, 5 sheets, 44 pp.

Ransome, F. L., 1923, Geology of the Oatman gold district, Arizona: A preliminary report: United States Geological Survey Bulletin, v. 743, no. i-iv, p. 1-58.

Rice, S. A., Claiborne, L.L., Rentz, S.P., and Cribb, J.W., 2014, Voluminous intermediate, effusive magmatism in the Black Mountains, AZ, preceding the Peach Spring supereruption, and evaluation of its potential relationship to the supervolcano magma chamber: Geological Society of America Abstracts with Programs, v. 46, no. 6, p. 510.

Sparks, R. S. J., and Wilson, L., 1976, A model for the formation of ignimbrite by gravitational column collapse: Journal of Geological Society of London, v. 132, p. 441-451.

Sparks, R.S.J., Sigurdsson, H., and Wilson, L., 1977, Magma mixing-mechanism for triggering acid explosive eruptions: Nature, v. 5909, p. 315-318.

Spencer, J.E., Ferguson, C.A., Pearthree P.A., and Richard, S.M., 2007, Geologic map of the Boundary Cone 7 ½' Quadrangle, Mohave County, Arizona: Arizona Geological Survey Digital Map 54 (DGM-54), v. 1.0, scale 1:24 000, 1 sheet, with text.

Thorson, J.P., 1971, Igneous petrology of the Oatman district, Mohave County, Arizona [Ph.D. thesis]: University of California—Santa Barbara, 189 p.

United States Geological Survey, 2012, Volcano Hazards Program: Yellowstone Volcano Observatory: Questions about Supervolcanoes: http://volcanoes.usgs.gov/volcanoes/yellowstone/yellowstone_sub_page_49.html (February 2014).

Walker, B. A., Miller, C. F., Claiborne, L. L., Wooden, J. L., and Miller, J. S., 2007, Geology and geochronology of the Spirit Mountain batholith, southern Nevada: Implications for timescales and physical processes of batholith construction: Journal of Volcanology and Geothermal Research, v. 167, no.1-4, p. 239-262.

Wark, D.A., and Miller, C.F., 2008, Supervolcanoes and their explosive supereruptions: Elements, v. 4, p. 11-15.

Wells, R.E., and Hillhouse, J.W., 1989, Paleomagnetism and tectonic rotation of the lower Miocene Peach Springs Tuff: Colorado Plateau, Arizona, to Barstow, California: Geological Society of America Bulletin, v. 101, p. 846-863.

Williams, S.H., Lee, J.W., Miller, C.F., and Flansburg, M. E., 2014, Magmatic insights from a sedimentary sequence in a dynamic volcanic center, Black Mountains, AZ: Geological Society of America Abstracts with Programs, v. 46, no. 6, p. 550.

Young, R.A., and Brennan, W.J., 1974, Peach Springs Tuff: Its bearing on structural evolution of the Colorado Plateau and development of Cenozoic drainage in Mohave County, Arizona: Geological Society of America Bulletin, v. 85, p. 83-90.

Appendices

Appendix A. Sample Location and Hand Sample Petrography

Table 1. Locations, unit names, brief descriptions of all samples.

Sample #	Northing (UTM)	Easting (UTM)	Unit	Hand Sample Petrography (Field)	Location Name and Notes
MBF-1	3867963	737075	Mafic Lava	mafic lava, gray/purple, plagioclase, pyroxenes (2?), amygdules	McHeffy Butte
MBF-2	3867922	737127	Mafic Lava	mafic, pheno poor, one large pyx?	McHeffy Butte
MBF-3	3867894	737190	Esperanza Trachyte	trachytic lava, pheno poor, plagioclase	McHeffy Butte
MBF-4	3868074	737143	Mafic Lava	mafic, small pyx?	McHeffy Butte
MBF-5	3868154	737321	Esperanza Trachyte	trachytic lava, pheno poor, elongate plag	McHeffy Butte
WSWF-1	3864623	739728	Mafic Lava	mafic lava, elongate plag, black and green pyx, euhedral crystals, 10-15% phenos	Warm Springs West, mapped between CCT and PST?,
WSWF-2 (A-F)	3864331	740168	PST Mafic Enclaves	plagioclase and pyx, range 10-15% phenos, size range 2-20cm across, crenulated margins	Warm Springs West, SAMPLES a, c, and d look best
WSWF-3	3864293	740220	PST Mafic Enclave	HUGE enclave (~40 cm across), weathered--hard to tell composition	Warm Springs West
WSWF-4	3864291	740242	PST Mafic Enclave	another large enclave, in many pieces when extracted, very weathered	Warm Springs West
WSWF-5	3864290	740227	PST Mafic Enclave	elongate plag, green and black pyx?, looks very similar to WSWF-1 :)	Warm Springs West
RWF-1	3893411	736137	Part of trachyte sequence	<5% phenos, plag, one dark mineral? mafic?	Walk to Rosetta Stone, a more mafic trachyte? possibly Esperanza?
RWF-2	3892022	736671	Andesite	<5% phenos, plag, biotite, hornblende?	Walk to Rosetta Stone, Nick has it mapped above a 18.1 Ma tuff, so likely too young
CS-MF1	3867669	753966	Mafic Lava	5% phenos, plag, mafics, vesicles and	Caliche Springs, I was not there--

				amygdules	Calvin took the sample, at base of section?
SPF-1	3892029	736616	Grumpy (mafic within)	host sand or basalt? weathered, bands, 5% phenos?, plag and some mafics	Near Secret Pass, intermingled with red ss? some trachyte enclaves?
SPF-2	3892135	737618	Grumpy (mafic within)	host sand or basalt? weathered, bands, 5% phenos?, plag and some mafics	Near Secret Pass, intermingled with red ss?
SPF-3	3891274	737412	Grumpy (mafic within)	host sand or basalt? weathered, bands, 5% phenos?, plag and some mafics	Near Secret Pass, intermingled with red ss?
CPF-1	3899419	762960	CCT lithics (possible enclaves?)	very small, probably can't do much with them	Coyote Pass, near Kingman
KPF-1	3899396	767850	PST Mafic Enclaves	plag, coppery weathered biotite, maybe pyx?, 15-20% phenos	Kingman park, some vesicular, beautiful crenulated margins
KPF-2	3899396	767850	PST Mafic Enclave	See KPF-1	See KPF-1
KPF-3	3899396	767850	PST Mafic Enclave	See KPF-1	See KPF-1
KPF-4	3899403	767810	PST Mafic Enclave	See KPF-1	See KPF-1
KPF-5	3899403	767810	PST Mafic Enclave	See KPF-1	See KPF-1
KPF-6	3899403	767810	PST Mafic Enclave	See KPF-1	See KPF-1
KPF-7	3899403	767810	PST Mafic Enclave	See KPF-1	See KPF-1
KPF-8	3899403	767810	PST Mafic Enclave	See KPF-1	See KPF-1
KPPF-1	3892817	773148	PST Mafic Enclave	5% phenos, plag, coppry weathered biotite, maybe a dark mafic (pyx?)	Northwest Homestead, in float
KPPF-2	3892817	773148	PST Mafic Enclave	5% phenos, plag, coppry weathered biotite, maybe a dark mafic (pyx?)	Northwest Homestead, on top of ridge
KPPF-3	3892357	773283	Mafic Lava	very weathered and vesicular, lots of amygdules	Northwest Homestead, BAD sample
KPPF-4	3892777	773203	Mafic Lava	fresh, porhyritic, plag <5%	Northwest Homestead, compare to mafic enclaves here

Appendix B. Whole Rock Geochemistry

Table 1. Mg # and K_2O and Na_2O calculations for the eight XRF-analyzed lava samples.

SAMPLE	MOL % MgO	MOL % FeO	Mg #	$K_2O + Na_2O$
MBF-1	0.0948	0.0806	54.0367912	6.70
MBF-4	0.0864	0.1071	44.6271861	6.28
AVG MBF-5	0.0203	0.0502	28.8385193	8.87
WSWF-1	0.1145	0.0834	57.8422418	6.72
AVG CS-MF1	0.1139	0.0876	56.512176	5.90
SPF-1A	0.0544	0.0766	41.5455651	6.67
SPF-1B	0.0599	0.0756	44.2051198	8.79
SPF-2	0.0534	0.0718	42.6161133	7.40

Table 2. Mg # and K_2O and Na_2O calculations for the four XRF-analyzed enclave samples.

SAMPLE	MOL % MgO	MOL % FeO	Mg #	$K_2O + Na_2O$
WSWF-3	0.07180468	0.08837088	44.8287362	7.30
WSWF-5	0.11433275	0.08240345	58.114751	5.89
KPF-5	0.07060865	0.07839268	47.387933	7.82
KPF-6	0.06737367	0.06866807	49.5242614	7.18

Appendix C. Temperature Modeling

Table 1. Excel-MELTS liquidi in degrees Celsius of lava samples.

Sample	Liquidus at 1% H2O	Liquidus at 2% H2O	Liquidus at 3% H2O	SiO2 %
MBF-1	1131.3	1117	1105.1	54.79
MBF-4	1147.1	1141.4	1137.7	49.44
MBF-5	1071.7	1034.2	1025.4	62.21
WSWF-1	1160	1145.9	1134.2	54.04
CS-MF1	1142.8	1119.7	1109.7	52.24
SPF-1A	1116.6	1088.6	1075.9	61.97
SPF-1B	1123	1111.1	1101.6	54.60
SPF-2	1107	1096.5	1088.1	56.65

Table 2. Excel-MELTS liquidi in degrees Celsius of enclave samples.

Sample	Liquidus at 1% H2O	Liquidus at 2% H2O	Liquidus at 3% H2O	SiO2 %
WSWF-3	1128.5	1121.7	1111.7	54.96
WSWF-5	1144.1	1120.7	1110.7	52.83
KPF-5	1131.8	1123.4	1116.8	56.57
KPF-6	1133	1106.4	1084	60.66

Table 3. Apatite-saturation thermometry of lava samples.

SiO2	% SiO2	Temp (deg C)	ln (D)	D	Conc. P2O5 (in melt)	ln(P2O5 in melt)		ln (D)		Sample
0.622	62.2	1019	4.3816272	79.968055	0.0052	-3.504557245	0.0300601	5.0204431	2.6274872	**MBF-5**
0.619	61.9	1016	4.3783178	79.70384	0.0052	-3.501247766	0.0301597	5.0171336	2.6241777	**SPF-1A**
0.54	54	991	3.8850127	48.667559	0.0085	-3.007942658	0.0493932	4.5238285	2.1308726	**WSWF-1**
0.566	56.6	950	4.3746499	79.412031	0.0052	-3.497579877	0.0302706	5.0134657	2.6205099	**SPF-2**
0.522	52.2	915	4.186796	65.81159	0.0063	-3.30972596	0.0365262	4.8256118	2.4326559	**CS-MF1**
0.546	54.6	915	4.4225293	83.306726	0.0050	-3.545459293	0.0288554		2.6683893	**SPF-1B**
0.54	54	903	4.4448163	85.18423	0.0049	-3.567746327	0.0282194		2.6906763	**MBF-1**
0.494	49.4	900	4.000487	54.624743	0.0076	-3.123416957	0.0440065		2.2463469	**MBF-4**

Table 4. Apatite-saturation thermometry of enclave samples.

SiO2	% SiO2	Temp (deg C)	ln (D)	D	Conc. P2O5 (in melt)	ln(P2O5 in melt)		ln (D)		Sample
0.606	60.6	954	4.7122504	111.30235	0.0037	-3.83518	0.0215974	5.3510662	2.9581103	**KPF-6**
0.565	56.5	1018	3.9297862	50.896096	0.0082	-3.052716	0.0472305	4.5686021	2.1756462	**KPF-5**
0.549	54.9	998	3.9191506	50.357652	0.0083	-3.042081	0.0477355	4.5579665	2.1650106	**WSWF-3**
0.528	52.8	923	4.1942716	66.305415	0.0063	-3.317202	0.0362541	4.8330874	2.4401316	**WSWF-5**

Apatite-saturation thermometry calculations:

Define: $D = \frac{conc.\ P\ in\ apatite}{conc.\ P\ in\ melt}$

Assume: The concentration of phosphorous in the melt can be substituted with the concentration of phosphorous (P_2O_5) in the groundmass analyzed with XRF. The groundmass is assumed to be a close representation of the melt in this case.

Define: Concentration of P in apatite = 0.416 wt. %; T is temperature

Define: $\ln D = \frac{8400 + (SiO_2 - 0.5)(2.64 \times 10^4)}{T} - [3.1 + 12.4(SiO_2 - 0.5)]$

Solve for T:

$$T = \frac{8400 + (SiO_2 - 0.5)(2.64 \times 10^4)}{\ln(conc.\ P_2O_5 in\ melt) - \ln 0.416 + 3.1 + 12.4(SiO_2 - 0.5)}$$

Table 5. Zircon-saturation thermometry of lava samples.

Sample	Zr, ppm	SiO_2	TiO_2	Al_2O_3	Fe_2O_3	MnO	MgO	CaO	Na_2O	K_2O	P_2O_5	total mol	M	T, K	T, C
MBF-5	380	62.21	0.92	17.99	5.15	0.09	0.82	3.43	4.67	4.20	0.52	1.79580184	1.78	1112	839
MBF-1	346	54.79	1.27	18.17	8.27	0.03	3.82	6.47	3.18	3.52	0.49	1.7845251	2.24	1068	795
MBF-4	335	49.44	1.89	19.03	10.99	0.07	3.48	8.06	3.68	2.6	0.76	1.77478479	2.67	1034	761
WSWF-1	432	54.04	1.37	16.24	8.56	0.07	4.61	7.54	3.06	3.66	0.85	1.78265566	2.77	1048	775
CS-MF1	328	52.24	1.29	17.58	8.99	0.08	4.59	8.69	3.21	2.69	0.63	1.78458355	2.80	1023	750
SPF-1A	276	61.97	1.08	15.11	7.85	0.04	2.19	4.56	2.97	4.6	0.52	1.77847753	2.07	1060	787
SPF-1B	402	54.6	1.02	19.34	7.75	0.11	2.41	5.49	3.43	5.36	0.5	1.79040566	2.18	1086	813
SPF-2	277	56.65	1.25	20.02	7.37	0.14	2.15	4.5	3.58	3.82	0.52	1.78462907	1.72	1087	814

Table 6. Zircon-saturation thermometry of enclave samples.

Sample	Zr, ppm	SiO_2	TiO_2	Al_2O_3	Fe_2O_3	MnO	MgO	CaO	Na_2O	K_2O	P_2O_5	total mol	M	T, K	T, C
WSWF-3	405	54.96	1.3	17.63	9.06	0.05	2.89	5.97	2.97	4.33	0.83	1.77037189	2.24	1082	809
WSWF-5	444	52.83	1.2	17.61	8.45	0.08	4.61	8.7	3.2	2.69	0.63	1.78748611	2.77	1050	777
KPF-5	398	56.57	1.63	17.98	8.04	0.17	2.85	4.12	3.71	4.11	0.82	1.78214667	1.90	1107	834
KPF-6	363	60.66	0.99	16.96	7.04	0.09	2.72	3.99	3.27	3.92	0.37	1.77854102	1.75	1110	837

Zircon-saturation thermometry calculations:

Total mol = total mols of all cations

$$M = \frac{\frac{(mols\ K + Na + 2Ca)}{total\ cation\ mols}}{\left(\frac{mols\ Al}{total\ cation\ mols}\right) \times \frac{mols\ Si}{total\ cation\ mols}}$$

$$T, in\ K = \frac{12900}{2.95 + 0.85(M) + \ln\frac{476000}{Zr\ in\ melt}}$$

Appendix D. Full Elemental Analyses

Table 1. Major elemental analyses from ICP-MS. Enclave WSW-PST1 is from Pamukcu et al. (2013).

Sample	SiO_2	Al_2O_3	Fe_2O_3(Tot)	MnO	MgO	CaO	Na_2O	K_2O	TiO_2	P_2O_5	LOI	Total
KPF-5	57.39	17.02	7.15	0.195	2.29	4.31	3.75	4.11	1.562	0.76	2.03	100.6
CS-MF1	52.23	15.94	8.43	0.119	4.06	8.07	3.25	2.66	1.396	0.57	2.25	98.98
WSWF-1	53.41	14.75	7.22	0.1	4.01	6.95	3.3	3.83	1.32	0.8	2.63	98.32
WSWF-3	52.64	14.63	7.4	0.089	3.15	7.32	3.08	4.28	1.318	0.84	4.02	98.78
WSWF-5	54.97	15.5	7.33	0.079	2.43	5.3	3.35	4.49	1.267	0.8	3.74	99.26
WSW-PST1	55.29	16.28	7.18	0.064	2.4	5.19	3.36	4.41	1.271	0.53	1.82	97.79

Table 2. Full elemental analyses from ICP-MS. Enclave WSW-PST1 is from Pamukcu et al. (2013).

Sample	Au	Ag	As	Ba	Be	Bi	Br	Cd	Co	Cr	Cs	Cu	Ga	Ge	Hf	Hg	In	Ir
KPF-5	2	< 0.5	4	1652	5	< 0.1	< 0.5	< 0.5	18.8	15.4	5	20	23	1.2	9	< 1	0.2	< 1
CS-MF1	< 1	< 0.5	5	1361	2	< 0.1	< 0.5	< 0.5	30.6	102	0.6	30	20	1.4	4.9	< 1	< 0.1	< 1
WSWF-1	3	0.8	24	1933	4	< 0.1	< 0.5	< 0.5	25.8	263	5.2	30	21	1.6	7	< 1	< 0.1	< 1
WSWF-3	1	< 0.5	46	2101	4	< 0.1	< 0.5	< 0.5	24.4	247	5.7	31	22	1.8	6.7	< 1	0.2	< 1
WSWF-5	3	< 0.5	58	2062	3	< 0.1	4.3	< 0.5	24.1	134	4.1	32	23	1.5	7.5	< 1	0.2	< 1
WSW-PST1	<1	<0.5	70	--	--	<0.1	<0.5	0.8	14.4	123	6.3	33	22	1.9	9	<1	<0.1	<1

Table 3. Full elemental analyses from ICP-MS, continued. Enclave WSW-PST1 is from Pamukcu et al. (2013).

Sample	Mo	Nb	Ni	Pb	Rb	S	Sb	Sc	Se	Sn	Sr	Ta	Th	U	V	W	Y
KPF-5	5	27.5	18	30	160	0.027	0.7	9.85	< 0.5	3	961	1.65	17.4	3.23	145	< 1	32
CS-MF1	< 2	16.9	69	11	45	0.04	0.3	20.8	< 0.5	2	1106	1.07	9.76	2.02	201	< 1	24
WSWF-1	< 2	19.5	140	16	96	0.028	17.2	15.1	< 0.5	2	1412	1.15	16.8	3.13	146	< 1	27
WSWF-3	2	20.2	88	18	112	0.159	60.2	15	< 0.5	3	1427	1.2	17.7	3.87	142	< 1	31
WSWF-5	< 2	19	83	27	109	0.082	50.5	14.5	< 0.5	3	1496	1.1	19.6	4.26	145	< 1	29
WSW-PST1	<2	21.5	51	46	96	0.035	83.6	12.2	<0.5	3	--	1.27	20.3	4.15	--	7	--

Table 4. Full elemental analyses from ICP-MS, continued. Enclave WSW-PST1 is from Pamukcu et al. (2013).

Sample	Zn	Zr	La	Ce	Pr	Nd	Sm	Eu	Gd	Tb	Dy	Ho	Er	Tl	Tm	Yb	Lu
KPF-5	165	438	127	233	26.7	94.5	14	3.05	8.47	1.13	6.01	1.08	2.97	0.51	0.408	2.63	0.401
CS-MF1	81	247	72.1	144	16.8	63.5	10.6	2.64	6.85	0.96	4.91	0.87	2.47	0.14	0.34	2.13	0.33
WSWF-1	82	356	120	243	28.7	107	16.9	3.87	9.46	1.17	5.75	0.93	2.48	0.29	0.333	1.98	0.292
WSWF-3	89	368	133	256	31.1	114	18	4.14	10.5	1.29	6.33	1.03	2.74	0.63	0.36	2.24	0.344
WSWF-5	118	375	150	273	33.5	123	18.7	4.15	10	1.2	5.96	1.02	2.62	0.63	0.34	2.05	0.32
WSW-PST1	87	400	135	235	30.8	113	15	3.01	11	<0.1	5.64	1.01	2.74	0.54	0.365	2.56	0.32

Appendix E. Scanning Electron Microscope Analyses

Table 1. Clinopyroxene analyses of lavas MBF-1, MBF-4, MBF-5, WSWF-1, and SPF-1B and enclave WSWF-5.

Mount	*Site*	*Spectra*	Na_2O	MgO	Al_2O_3	SiO_2	P_2O_5	K_2O	CaO	TiO_2	MnO	FeO	Cr_2O_3	Notes
MBF-1	*6*	*35*	0.32	16.3	1.99	51.98	0	0	19.07	0.69	0	9.64		
MBF-1	*6*	*42*	0.37	15.65	2.66	51.22	0	0.15	19.05	1.26	0	9.65		
MBF-1	*7*	*45*	0.26	16.74	1.97	52.43	0	0	18.52	1.02	0	9.06		
MBF-1	*7*	*46*	0.42	15.73	2.68	50.83	0	0	19.06	1.2	0.45	9.64		
MBF-1	*7*	*47*	0.59	15.2	2.55	51.67	0	0	18.26	0.91	0	10.82		
MBF-1	*7*	*48*	0.47	15.74	2.89	51	0	0	19.32	1.04	0.46	9.08		
MBF-1	*8*	*51*	0.42	15.88	2.65	51.01	0	0	19.07	1.19	0	9.79		
MBF-1	*9*	*56*	0.44	14.37	3.32	50.4	0	0.14	19.19	1.63	0	10.51		
MBF-1	*10*	*61*	0.39	15.62	2.83	51.4	0	0.2	18.58	1.13	0	9.84		
MBF-1	*10*	*62*	0.33	17.54	2.1	51.89	0	0	17.74	0.92	0	9.48		
MBF-1	*11*	*64*	0.4	14.91	2.49	51.92	0	0	19.44	1.04	0	9.8		
MBF-1	*20*	*122*	0.33	15.62	2.46	51.63	0	0	19.2	1.07	0	9.69		
MBF-4	*13*	*67*	0.26	15.87	3.72	50.69	0	0	20.44	0.94	0	8.07		
MBF-4	*13*	*71*	0.44	14.46	4.22	48.97	0	0	20.53	1.79	0	9.59		
MBF-4	*13*	*73*	0.35	15.09	3.22	50.84	0	0	20.06	1.18	0	9.26		
MBF-4	*14*	*77*	0.45	14.05	3.9	49.42	0	0	20.95	1.74	0	9.49		
MBF-4	*14*	*81*	0.41	13.62	6.62	47.92	0	0	21.01	1.56	0	8.86		
MBF-4	*14*	*83*	0.63	14.24	4.3	49.33	0	0.16	20.24	1.94	0	9.16		
MBF-4	*14*	*84*	0.46	15.05	3.21	50.99	0	0	20.5	1.24	0	8.54		
MBF-4	*15*	*87*	0.41	14.92	3.14	51.42	0	0	20.22	0.91	0	8.99		
MBF-4	*15*	*89*	0.52	14.1	3.76	50.24	0	0	20.71	1.9	0	8.76		
MBF-4	*15*	*92*	0.3	13.72	4.63	49.38	0	0	20.61	1.95	0	9.4		
MBF-4	*16*	*96*	0.44	14.29	7.11	47.52	0	0	20.62	1.97	0	8.05		
MBF-4	*16*	*98*	0.44	16.01	4.28	49.72	0	0	19.55	1.37	0	8.63		
MBF-4	*16*	*103*	0.48	15.39	2.1	51.69	0	0	19.93	1.22	0	9.19		
MBF-5	*28*	*184*	0.51	18.45	11.93	42.44	0	9.41	0	2.87	0	10.37		Not Normalized
WSWF-1	*23*	*152*	0.54	16.28	3.25	51.81	0	0	21.29	0.97	0	5.86		core/middle
WSWF-1	*23*	*153*	0.49	14.93	2.03	52.02	0	0	19.71	0.75	0	10.07		core/middle
WSWF-1	*23*	*154*	0.51	14.27	4.87	49.64	0	0	21.4	1.41	0	7.91		rim
WSWF-1	*23*	*155*	0.43	15.79	3.63	51.49	0	0	21.45	0.89	0	6.32		mostly rim
WSWF-1	*23*	*156*	0.35	14.21	2.36	49.13	0	0	24.76	1	0	8.19		core/inclusion
WSWF-1	*23*	*157*	0.42	16.11	2.75	52.35	0	0.13	21.01	0.79	0	6.44		middle
WSWF-1	*23*	*158*	0.67	13.8	5.51	46.81	0.51	0	21.43	2.47	0	8.79		
WSWF-1	*24*	*164*	0.47	16.64	2.33	52.29	0	0	22.14	0.66	0	4.61	0.87	middle
WSWF-1	*24*	*165*	0.51	14.45	4.56	48.9	0	0	21.78	1.54		8.27		rim
WSWF-1	*24*	*166*	0.23	17.55	1.73	53.01	0	0	21.5	0.63		4.79	0.56	core
WSWF-1	*24*	*167*	0.53	15.77	3.91	50.76	0	0	20.96	0.99		6.73	0.35	middle close to rim
WSWF-1	*24*	*168*	0.5	14.02	4.88	48.53	0.49	0	21.25	1.77		8.58		rim

Table 1, con't.

SPF-1B	***33***	***219***	**0**	**15.72**	**3.77**	**51.31**	**0**	**0**	**21.11**	**1.09**		**6.99**	
SPF-1B	*36*	*243*	0	14.88	1.6	52.43	0	0.74	20.13	0	0	10.23	
WSWF-5	*9*	*69*	0.43	15.41	2.55	50.86	0	0	21.36	1.18		8.2	CPX
WSWF-5	*9*	*70*	0.44	15.39	1.99	51.55	0	0	20.83	0.95		8.85	
WSWF-5	*9*	*71*	0.32	15	2.81	50.84	0	0	21.7	1.2		8.14	
WSWF-5	*10*	*74*	0.47	15.83	2.44	51.88	0	0	22.43	0.56		6.38	CORE
WSWF-5	*10*	*75*	0.39	15.71	2.33	52.08	0	0	23.38	0.5		5.61	RIM
WSWF-5	*10*	*76*	0	15.35	2.32	51.31	0	0	21.3	1.15		8.58	
WSWF-5	*14*	*102*	0	15.23	2.97	50.43	0	0	21.69	1.25		8.42	
WSWF-5	*14*	*103*	0.51	14.55	3.26	50.09	0	0	21.43	1.4		8.76	

Table 2. Plagioclase analyses of lavas MBF-1, MBF-4, MBF-5, WSWF-1, SPF-1A, SPF-1B, and SPF-2 and enclaves WSWF-5 and KPF-5. Some groundmass analyses included.

Sample	***Site***	***Spectra***	**Na_2O**	**MgO**	**Al_2O_3**	**SiO_2**	**P_2O_5**	**K_2O**	**CaO**	**TiO_2**	**FeO**	**BaO**	**Notes**
MBF-1	*10*	*60*	5.12	0.22	26.84	55.66	0	0.94	10.05	0	1.17		grdms
MBF-1	*12*	*114*	4.96	0	27.56	55.56	0	0.94	9.91	0.25	0.81		rim
MBF-1	*12*	*115*	6.02	0	25.62	58.72	0	1.61	7.52	0	0.52		core
MBF-1	*12*	*116*	4.96	0	27.8	55.7	0	1.01	9.92	0	0.61		rim
MBF-1	*12*	*117*	5.74	0	24.22	59.26	0	2.62	6.72	0.39	1.05		small, needle-like
MBF-1	*12*	*118*	5.15	0	26.86	56.33	0	1.06	9.81	0	0.78		small, needle-like
MBF-1	*20*	*119*	5.52	0	26.99	56.4	0	0.94	9.23	0	0.92		
MBF-1	*20*	*120*	5.63	0	26.62	56.43	0	0.98	9.17	0	1.17		
MBF-1	*20*	*121*	5.22	0	26.37	56.98	0	1.72	8.59	0.24	0.88		
MBF-1	*20*	*123*	5.1	0	27.47	55.45	0	0.79	10.19	0	0.99		
MBF-4	*13*	*68*	4.85	0.39	26.07	56.45	0	2.28	8.63	0	1.34		grdms
MBF-4	*17*	*104*	4.72	0	28.78	53.38	0	0.51	11.43	0	1.18		core
MBF-4	*17*	*105*	5.63	0.34	26.92	56.95	0	0.66	8.67	0	0.83		rim
MBF-4	*17*	*106*	4.14	0	29.59	52.69	0	0.37	12.22	0	0.99		core
MBF-4	*17*	*107*	4.02	0.21	29.56	52.4	0	0.31	12.34	0	1.16		core?
MBF-4	*17*	*108*	6.71	0	25.28	58.88	0	1.1	6.97	0.43	0.62		rim
MBF-4	*18*	*109*	3.81	0.21	29.94	52.23	0	0.34	12.7	0	0.77		core
MBF-4	*18*	*110*	3.86	0	29.38	52.96	0	0.36	12.16	0	1.28		middle
MBF-4	*18*	*111*	5.3	0	27.48	55.66	0	0.58	9.99	0	0.99		rim
MBF-4	*18*	*112*	6.02	0	24.31	59.57	0	2.8	6.51	0	0.78		rim
MBF-5	*28*	*183*	5.24	0.21	19.16	66.39	0	5.42	2.38	0.5	0.71		grdms
MBF-5	*28*	*186*	4.39	0	19.27	65.04	0	9.59	1.01	0.4	0.3		grdms (k-rich)
MBF-5	*31*	*200*	7.32	0	23.73	61.73	0	1.3	5.4	0	0.52		rim
MBF-5	*31*	*202*	7	0	24.1	61.04	0	1	6.19	0	0.65		rim or whole
MBF-5	*31*	*207*	7.34	0	22.38	63.17	0	2.32	3.97	0	0.36	0.46	
MBF-5	*32*	*208*	6.78	0	24.41	61.13	0	1.14	6.1	0	0.44		rim/middle
MBF-5	*32*	*209*	5.94	0	26.53	57.86	0	0.66	8.17	0	0.85		core
MBF-5	*32*	*212*	5.62	0	26.79	56.93	0	0.58	9.38	0	0.71		core
MBF-5	*32*	*213*	7.49	0	23.45	62.04	0	1.11	5.41	0	0.5		rim

Table 2, con't.

WSWF-1	***22***	***144***	**1.96**	**0**	**7.2**	**22.56**	**0**	**2.16**	**0.79**	**0.17**	**0.23**		**core**
WSWF-1	*22*	*145*	5.23	2.73	18.34	63.97	0	5.38	1.96	0.22	2.18		rim
WSWF-1	*22*	*148*	1.22	0.49	17.35	60.38	0	3.59	13.25	0.88	2.84		core
WSWF-1	*22*	*149*	3.36	2.87	17.01	64.81	0	6.01	2.74	0	3.2		rim
WSWF-1	*22*	*151*	4.12	0.48	15.58	51.46	9.94	5.76	11.65	0.3	0.72		mostly core
WSWF-1	*23*	*160*	5.24	0.25	20.48	63.89	0	6.37	2.24	0	0.63	0.89	one side of twin?
WSWF-1	*24*	*169*	4.69	0.3	19.52	65.28	0	8.04	1.21	0.24	0.71		grdms
WSWF-1	*24*	*170*	4.89	0	22.44	61.26	0	4.9	4.97	0.4	1.13		grdms
WSWF-1	*24*	*171*	4.54	0	19.48	64.97	0	8.83	0.86	0	0.54	0.78	grdms
WSWF-1	*24*	*172*	5.51	0.42	21.09	62.82	0	5.12	3.55	0.41	1.08		grdms
WSWF-1	*24*	*173*	5.33	0	24.28	59.15	0	3.35	6.33	0	0.9	0.66	grdms
WSWF-1	*24*	*174*	4.44	0.22	21.07	63.04	0	7.32	2.77	0.53	0.6		grdms
WSWF-1	*25*	*175*	1.25	0	21.38	56.91	0	1.84	18.63	0	0		core
WSWF-1	*25*	*176*	0.74	0	18.67	56.29	0	1.59	21.27	0	1.44		rim
WSWF-1	*25*	*177*	1.9	0	21.73	57.93	0	1.34	16.08	0	1.02		rim
WSWF-1	*25*	*178*	1.2	0	17.2	61.91	0	5.17	11.47	0	3.04		core
WSWF-1	*25*	*180*	4.75	0	28.1	55.21	0	1.12	10.27	0	0.56		grdms
WSWF-1	*25*	*181*	4.77	0	28.44	54.43	0	0.85	10.93	0	0.58		grdms
SPF-1B	*34*	*229*	5.04	0	26.45	58.03	0	1.13	9.36	0	0		
SPF-1B	*35*	*230*	4.7	0	26.63	57.29	0	0	11.38	0	0		core
SPF-1B	*35*	*231*	5.92	0	27.08	54.84	0	1.39	10.76	0	0		rim
SPF-1B	*35*	*233*	6.17	0	25.3	60.18	0	1.38	6.97	0	0		
SPF-1B	*36*	*239*	6.87	0	24.72	58.41	0	1.12	8.88	0	0		
SPF-1B	*37*	*245*	4.84	0	27.49	56.52	0	0.73	10.41	0	0		core
SPF-1B	*37*	*246*	6.46	0	25.32	59.33	0	1.07	7.83	0	0		rim
SPF-1B	*37*	*247*	5.14	0	28.91	55.52	0	0	10.43	0	0		middle/rim
SPF-2	*38*	*248*	5.06	0	27.4	55.76	0	1	10.16	0	0.62		
SPF-2	*38*	*249*	5.19	0	26.87	56.58	0	1.13	9.63	0	0.6		same crystal as 248
SPF-2	*38*	*250*	5.58	0	26.19	57.61	0	1.11	8.68	0	0.82		
SPF-2	*39*	*256*	5.64	0	26.29	56.31	0	0.7	9.5	0	1.56		
SPF-2	*39*	*257*	4.8	0	28.19	54.41	0	0.62	10.68	0	1.3		
SPF-2	*39*	*258*	5.08	0.2	27.31	55.07	0	0.54	10.2	0	1.6		
SPF-2	*40*	*259*	5.48	0	26.47	57.36	0	1.15	8.9	0	0.66		
SPF-2	*40*	*261*	5.76	0	26.13	57.77	0	1.3	8.48	0	0.56		
SPF-2	*40*	*263*	5.78	0	26.35	57.63	0	1.2	8.36	0	0.66		
SPF-2	*41*	*265*	5.02	0	26.63	56.52	0	1.25	9.83	0	0.75		
SPF-2	*41*	*266*	5.58	0	26.3	57.16	0	1.06	9.05	0	0.85		large crystal, 1.5mm
SPF-2	*41*	*268*	4.75	0	27.38	55.81	0	1.27	9.81	0.25	0.72		
SPF-2	*41*	*270*	5.08	0	27.15	56.65	0	0.93	9.52	0	0.68		
SPF-1A	*2*	*11*	6.45	0	25.93	58.68	0	1.04	7.47	0	0.43		Middle/core
SPF-1A	*2*	*12*	6.32	0	25.8	58.85	0	0.94	7.68	0	0.42		Middle/core
SPF-1A	*2*	*13*	6.54	0	25.21	59.36	0	1.02	7.08	0	0.41	0.38	rim

Table 2, con't.

SPF-1A	**2**	**15**	**5.98**	**0**	**24.57**	**58.47**	**0**	**1.47**	**8.95**	**0**	**0.56**	**core, near apatite**
SPF-1A	4	37	6.02	0	26.71	57.6	0	0.75	8.55	0	0.38	
SPF-1A	6	51	6.01	0	26.01	57.77	0	1.05	8.01	0.16	0.98	W/in hbl
WSWF-5	8	67	4.88	0	21.32	63.26	0	4.89	4.06	0.32	1.27	
WSWF-5	11	80	3.17	0	14.75	55.5	7.13	8.75	8.97	0.46	1.28	k-rich?, rim
WSWF-5	11	81	3.72	1.09	17.41	62.12	1.41	3.13	5.58	1.06	4.49	core
WSWF-5	11	82	5.47	0	26.29	57.23	0	0.77	8.87	0.4	0.98	middle
WSWF-5	11	83	4.07	0.41	18.41	60.35	0.9	7.75	2.63	0.99	2.49	k-rich?, rim
WSWF-5	11	84	3.25	0	17.77	65.38	0	10.23	1.17	0.85	1.35	k-rich?
WSWF-5	12	86	4.92	0.39	20.92	60.94	0	3.71	5.3	0	2.38	Middle
WSWF-5	12	87	3.75	0.55	18.68	58.65	3.22	4.39	7.44	0.8	2.52	core
KPF-5	13	106	5.46	0	27.37	56.37	0	0.58	9.53	0	0.69	possible grdms
KPF-5	13	107	6.38	0	25.58	58.86	0	0.44	8.11	0	0.64	possible grdms
KPF-5	16	119	4.82	0	28.29	54.79	0	0.59	10.82	0	0.68	core
KPF-5	16	120	4.7	0	28.32	54.88	0	0.68	10.87	0	0.55	middle
KPF-5	16	121	5.71	0	27.01	56.73	0	0.45	9.39	0.14	0.57	rim
KPF-5	17	124	4.74	0.12	28.54	54.66	0	0.58	10.77	0	0.59	core
KPF-5	17	125	4.83	0	28.14	54.85	0	0.62	10.76	0.15	0.64	rim
KPF-5	17	126	5.14	0	27.7	55.64	0	0.72	10.08	0	0.72	core
KPF-5	17	127	4.74	0	27.77	53.41	0.17	0.5	10.52	0.15	0.61	rim
KPF-5	17	128	4.85	0	28.44	54.86	0	0.72	10.51	0	0.62	rim/middle
KPF-5	18	131	5.19	0.14	27.76	55.72	0	0.54	10.02	0	0.63	core
KPF-5	18	132	5.3	0.2	27.88	55.28	0	0.43	10.17	0	0.73	rim
KPF-5	18	133	5.29	0	26.79	54.83	0	0.83	9.33	0	0.67	rim
KPF-5	18	134	5.09	0.14	27.23	54.35	0	0.71	9.62	0	0.63	core

Table 3. Groundmass analyses of lavas MBF-5, SPF-1A, and SPF-2 and enclave KPF-5.

Sample	Site	Spectrum	Na_2O	MgO	Al_2O_3	SiO_2	P_2O_5	K_2O	CaO	TiO_2	MnO	FeO	BaO
MBF-5	29	194	5.53	0.22	19.25	65.92	0	4.91	2.76	0	0	0.74	0.67
SPF-2	38	251	5.47	0.85	20.51	57.08	0.39	2.86	4.99	1.18	0	6.67	
SPF-1A	4	39	3.25	0	16.91	66.59	0.8	5.25	4.18	0.57	0	2.44	
KPF-5	16	123	5.94	0.18	20.68	64.42	0	5.37	2.5	0.16		0.75	
KPF-5	18	133	5.05	0.41	18.89	65.97	0.51	5.29	2.72	0.31		0.85	

Table 4. Apatite, Zircon, Biotite, Hornblende analyses.

Sample	*Site*	*Spectra*	Na_2O	MgO	Al_2O_3	SiO_2	P_2O_5	K_2O	CaO	TiO_2	FeO	Ce_2O_3	MoO_3	IrO_2	SO_3	BaO	MnO	In_2O_3	Notes
MBF-1	*8*	*50*	0	0.54	0	0.54	41.19	0	53.56	0	0.5	0							Apatite
MBF-4	*14*	*76*	0.47	0.36	1.16	6.13	37.23	0.48	48.05	0	0.98	1.41							Apatite
MBF-4	*14*	*79*	0.83	18.82	11.02	42.04	0	8.75	0.48	3.99	9.17	0							Biotite
MBF-4	*14*	*82*	0.92	20.17	11.3	39.66	0	8.63	0	4.62	8.48	0							Biotite
MBF-4	*15*	*86*	3.65	0.55	18.02	64.82	0	9.24	0.85	0.39	2.48	0							Ghost eyes, Feldspar/melt inclusion?
MBF-4	*15*	*90*	0.26	0.23	0.82	3.8	38.75	0.45	51.05	0	0.51	0							Apatite
MBF-4	*15*	*94*	0.27	0.54	0.51	3.21	39.37	0.24	50.86	0	0.72	0							Apatite
MBF-4	*16*	*101*	0.75	0.54	2.44	7.8	36.86	0.34	47.49	0	0.85	0							Apatite
MBF-4	*16*	*102*	5.5	0.24	22.8	61.98	0	4.39	4.27	0	0.82	0							Feldspar/melt inclusion?
MBF-5	*30*	*195*	0.47	0	0	0.65	37.68	0	53.54	0	0	0	1.4	3.21					Apatite?, not normalized, sum 96
MBF-5	*30*	*197*	0.38	0	0.23	0.96	41.56	0.22	54.38	0	1.3	0	0.97	0					Apatite, edge
MBF-5	*30*	*198*	0.51	0	0.5	1.69	37.57	0	51.64	0	0.44	0	0	3.98					Apatitite, edge
WSWF-1	*23*	*162*	0.69	0.58	0.4	3.72	35.93	0.34	50.11	0	0.95	1.28			2.72				Apatite, not normalized, sum 96
SPF-1B	*33*	*216*	0	0	0	0	41.28	0	56.38	0	2.34								Apatite, 0% Ta2O5
SPF-1B	*33*	*217*	0	0	0	0	38.98	0.81	57.97	0	2.23								Apatite
SPF-1B	*35*	*232*	0	0	0	0	42.44	0	57.56	0	0								Apatite, hexagonal

Table 4, con't.

SPF-1B	***36***	***237***	**0**	**0**	**0**	**0**	**43.06**	**0**	**56.94**	**0**	**0**					**Apatite**
SPF-1B	*36*	*242*	0	0	0	1.86	40.09	0	58.05	0	0					Apatite
SPF-1A	*2*	*14*	0.43	0.19	0	0.8	40.61	0	53.99	0	0.24		1.03			Apatite, within plag
SPF-1A	*3*	*18*	0.34	0.29	0.15	0.88	40.83	0.13	53.7	0	0.42		0.5			core
SPF-1A	*3*	*19*	0.32	0.19	0	0.92	38.86	0.17	52.91	0	0.51	2.8	0.48			rim
SPF-1A	*3*	*20*	0.45	0.3	0.39	10.15	35.39	0.29	44.6	0	0.58	3.2	0.46			rim
SPF-1A	*3*	*21*	0.23	0.22	0	0.9	38.62	0.21	53.19	0	0.44	2.43	0.52			rim
SPF-1A	*3*	*28*	0.25	0.23	0.22	6.14	36.81	0.24	51.33	0	0.87					rim
SPF-1A	*3*	*29*	0.3	0.16	0.18	1.5	39.4	0.26	54.7	0	0.53		0.53			Apatite
SPF-1A	*4*	*30*	0	0	0	0	46.82	0	53.18	0	0					Apatite
SPF-1A	*4*	*32*	0.76	16.36	14.41	38.37	0	8.88	0	6.5	13.23			1.5		Biotite
SPF-1A	*4*	*33*	0.7	16.26	14.35	38.02	0	8.98	0.17	6.35	13.28			1.66	0.23	Biotite
SPF-1A	*4*	*34*	0.75	16.91	14.33	39.41	0	8.6	0	6.36	12.55			1.09		Biotite
SPF-1A	*4*	*35*	0	6.45	5.51	73.26	0	3.2	1.43	2.05	8.1					Hbl? Biotite?
SPF-1A	*4*	*36*	0.4	10.12	8.21	60.81	0	6.02	0.28	3.9	9.13			1.13		Hbl? Biotite?
SPF-1A	*5*	*40*	0.44	14.74	14.86	38.75	0	9.47	0	6.58	13.44			1.72		Hbl, core
SPF-1A	*5*	*41*	0.54	14.79	15.28	37.78	0	9.01	0	6.58	13.98			2.04		Hbl, rim
SPF-1A	*5*	*42*	0.43	14.8	15.17	39.47	0	9.37	0.17	6.85	12.43			1.31		Hbl, rim
SPF-1A	*5*	*43*	0.26	12.55	13.86	39.4	0	9.29	0.19	7.03	15.56			1.85		Hbl, core
SPF-1A	*5*	*47*	0.59	16.65	15.25	38.89	0	8.94	0	6.1	11.9			1.45	0.22	Hbl
SPF-1A	*6*	*48*	0	0	0	56.1	43.5	0	0	0	0.4					APATITE??? Clay???

Table 4, con't.

SPF-1A	**6**	**49**	**0.67**	**14.53**	**14.5**	**36.93**	**0**	**8.85**	**0**	**6.72**	**15.08**			**2.71**			**Hbl, core**
SPF-1A	*6*	*50*	0.63	14.72	14.41	37.5	0	9.02	0	6.54	15.13			2.05			Hbl, rim
SPF-1A	*6*	*52*	0.65	14.84	14.59	36.99	0	8.61	0	6.53	14.86			2.93			Hbl, core
SPF-1A	*6*	*53*	0.48	0.24	0.17	0.94	38.13	0.32	52.64	0	0.54	2.59	0.91				Apatite, reabsorbed texture
WSWF-5	*7*	*55*	0.34	0.4	0	1.05	38.56	0.18	52.67	0	0			2.22			Apatite
WSWF-5	*7*	*56*	0	0.34	0	0.96	37.96	0	53.83	0	0.7		1.32				Apatite
WSWF-5	*10*	*77*	0	0.43	0	0.76	39.89	0	53.26	0	0						Apatite
WSWF-5	*12*	*88*	1.33	0	6.77	25.21	23.24	3.59	31.99	0.5	2.62						Apatite, inside plag
WSWF-5	*12*	*90*	0.31	0.56	1.78	7.35	35.11	0.63	45.84	0	2.16						Apatite, inside plag
KPF-5	*11*	*88*	0.45	16.32	11.12	38.53	0	9.23	0	4.19	12.44				0.52		Biotite
KPF-5	*11*	*90*	0.48	16.72	11.75	38.84	0	8.96	0	3.99	11.55				0.6		Biotite
KPF-5	*11*	*91*	0.52	17.93	10.94	39.29	0	9.52	0	2.58	10.84				0.59		Biotite
KPF-5	*11*	*92*	0.4	0	1.14	4.32	35.84	0.76	49.23	0	0.26	2.46			0.6		Apatite
KPF-5	*12*	*96*	0.43	17.02	11.02	38.85	0	8.89	0	3.91	11.87				0.57		Biotite
KPF-5	*12*	*97*	0.43	18.51	10.47	39.76	0	8.86	0	2.53	10.64				0.42	0.75	Biotite
KPF-5	*12*	*100*	1.67	0.13	11.79	41.02	15.82	7.98	18.07	0	0.34						Apatite
KPF-5	*12*	*103*	0.5	16.74	11.41	38.12	0	8.92	0	3.61	11.77			0.58	0.58	0.68	Biotite
KPF-5	*14*	*111*	0.29	16.77	12.37	39.11	0	9.07	0	2.8	9.78			0.71	0.55		Biotite
KPF-5	*15*	*118*	0.3	0	0	0.76	37.99	0.18	51.29	0	0.47	2.41					Apatite

Table 4, con't.

KPF-5	***17***	***129***	**0.38**	**17.07**	**10.92**	**39.08**	**0**	**9.02**	**0**	**3.71**	**11.92**		**0.44**	**Biotite**
KPF-5	*17*	*130*	0	18.18	11.05	39.51	0	9.54	0.16	1.79	11.37		0.68	Biotite

Sample	***Site***	***Spectra***	**Na_2O**	**MgO**	**Al_2O_3**	**SiO_2**	**P_2O_5**	**K_2O**	**CaO**	**TiO_2**	**FeO**	**ZrO_2**	
KPF-5	*12*	*98*	0	0	0.22	32.87	0	0	0	0	0.46	64.39	zircon